SYNTHESIS AND CHARACTERIZATION OF FUNCTIONALIZED BIO-MOLECULAR SURFACES WITH SELF-ASSEMBLED MONOLAYERS AND BIOREACTIVE LIGANDS FOR NANO/BIOTECHNOLOGICAL APPLICATIONS

By

Lian Wang

A Dissertation Submitted to the Faculty of the

DEPARTMENT OF CHEMICAL AND ENVIRONMENTAL ENGINEERING

In Partial Fulfillment of the Requirements
For the Degree of

DOCTOR OF PHILOSOPHY
WITH A MAJOR IN CHEMICAL ENGINEERING

In the Graduate College

THE UNIVERSITY OF ARIZONA

2008

THE UNIVERSITY OF ARIZONA

GRADUATE COLLEGE

As members of the Dissertation Committee, we certify that we have read the dissertation prepared by Lian Wang entitled Synthesis and Characterization of Functionalized Bio-Molecular Surfaces with Self-Assembled Monolayers and Bioreactive Ligands for Nano/Biotechnological Applications and recommend that it be accepted as fulfilling the dissertation requirement for the Degree of Doctor of Philosophy

_____Date: 11/13/08
Roberto Z. Guzman

_____Date: 11/13/08
A. Eduardo Sáez

_____Date: 11/13/8
Paul Blowers

Final approval and acceptance of this dissertation is contingent upon the candidate's submission of the final copies of the dissertation to the Graduate College.

I hereby certify that I have read this dissertation prepared under my direction and recommend that it be accepted as fulfilling the dissertation requirement.

_____Date: 11/13/08
Dissertation Director: Roberto Z. Guzman

STATEMENT BY AUTHOR

This dissertation has been submitted in partial fulfillment of requirement for an advanced degree at The University of Arizona and is deposited in the University Library to be made available to borrower under rules of the Library.

Brief quotations from this dissertation are allowable without special permission, provided that accurate acknowledgement of source is made. Request for permission for extended quotation from or reproduction of this manuscript in whole or in part may be granted by the head of the major department or the Dean of the Graduate College when in his or her judgment the proposed use of the material is in the interests of scholarship. In all other instances, however, permission must be obtained from the author.

SIGNED: _____*Lian Wang*____

TABLE OF CONTENTS

LIST OF FIGURES

LIST OF FIGURES--CONTINUED

LIST OF FIGURES--CONTINUED

LIST OF FIGURES--CONTINUED

LIST OF FIGURES--CONTINUED

LIST OF TABLES

ABSTRACT

In this work, the synthesis and characterization of functionalized biosurfaces that can be used for bioseparations and bio-nanotechnology are reported. A novel protein purification technique that incorporates chelating ligands and polymers onto the same chromatographic matrix is explored. A polysaccharide based gel, agarose, was modified systematically with hybrid ligands of the chelator iminodiacetic acid (IDA) and the polymer polyethylene glycol (PEG). The PEG molecule acts as a blocking polymer that can allow only small proteins to permeate onto the matrix surfaces and form conventional immobilized metal ion affinity chromatographic (IMAC) interactions with the chelators. Kinetic studies of chelator and polymer attachment were performed in order to effectively control the chelator and polymer densities on the matrix. Studies with different PEG surface densities and their effects on the adsorption of several proteins (e.g. myoglobin, lysozyme and bovine serum albumin (BSA)) were evaluated to characterize these new hybrid size exclusion IMAC (SEIMAC) matrices. An exclusion effect was observed while adsorption as observed in IMAC systems took place.

Functionalization schemes and procedures were extended in the activation and incorporation of affinity ligands on inorganic surfaces such as gold surfaces. Functional gold platforms were explored for development of nano-interconnects via functionalized self assembled monolayers (FSAMs) on gold to attach specific affinity ligands as linkers to immobilize biomolecules, such as microtubules (MTs). MTs eventually could be utilized as self assembling structures and templates for fabrication of nano-scale bio-

interconnect arrays and networks. In this work, different organothiols were used to form FSAMs and anti-glutathione S-transferase was attached as a linker to utilize the attachment of MT cap proteins, γ-tubulin. The γ-tubulin could recognize specifically a heterodimer of the MTs and can provide a nucleation center for MT growth. Several methodologies were employed including photolithographic methods and the use of photoreactive compounds for proper micro/nano scale dual protein functionalization of surfaces with homogeneous affinity ligands and with heterogeneous ligands as well.

CHAPTER 1 INTRODUCTION

Recent progress in molecular biology, biotechnology, and medicine brings forward demands of much improved separation methods for handling natural, synthetic, and semi-synthetic protein and peptide mixtures. This is true for all scales: from ultra micro-analysis to protein and peptide drug production. Despite the many efforts for developing efficient protein purification techniques, the purification of peptides and small proteins on a larger than analytical scale still is a significant challenge.

The development of protein separation techniques based on immobilized metal affinity chromatography (IMAC) is quite significant. IMAC is one of the affinity adsorption techniques introduced by Porath et al. (1975) and has the advantages of low cost, high capacity, and high efficiency. IMAC is an extremely versatile technique for protein separations based on different affinities of proteins to the metal ions immobilized on a matrix. IMAC has become almost synonymous with chromatographic isolation of histidine tagged recombinant proteins on immobilized nickel or copper ions (Chaga, 2001). By and large, the use of other metal ions has been limited. In this work, the copper ion was used to demonstrate the biomaterial separation using IMAC.

The work in our laboratory in separation of amino acids and small proteins has shown that it is possible to obtain separations of high efficiency by combining various different fractionation principles based on molecular sizes and specific chemical affinities in rationally applied adsorption procedures.

In IMAC, metal ions are immobilized by the chelators anchored on the matrix and

can form coordination interactions with the different amino acid side chains, such as histidine, cysteine, and tryptophan, which are exposed on the surfaces of proteins (Porath, 1992; Winzerling et al., 1992). IMAC is also a group selective technique since all proteins having histidine, cysteine, or tryptophan groups on the surface can be immobilized by the immobilized metal ions (Porath, 1992). Other highly specific affinity ligands such as antibodies, inhibitors, and any proteins with these amino acid groups on the surface can be adsorbed onto IMAC gels.

In this study, in order to enhance the selectivity of IMAC, the size exclusion effect used in chromatography was combined with the immobilized metal ion affinity to form a novel bioseparation method that relies on size exclusion and immobilized metal ion affinity, a process we denote as Size Exclusion Immobilized Metal Ion Affinity Chromatography (SEIMAC). A large polymeric ligand, PEG was attached to the IMAC gel and worked as a space blocking arm. This space arm polymer provided a hindrance effect to reduce or prevent large molecules access to the immobilized metal ions on the surface, so small proteins would have more affinity than larger ones.

In this work, polysaccharide agarose gels were chosen as chromatographic matrices. A covalent bound tridentate chelator, iminodiacetic acid (IDA) was used for immobilizing metal ions through its nitrogen atom and two carboxylate oxygen atoms, and a hydrophilic linear polymer, methoxyl polyethylene glycol amine (M-PEG-NH_2, or CH_3O-PEG-NH_2, MW: 5000) was used as the space arm for size exclusion.

New SEIMAC gels were synthesized and characterized by attaching IDA and different degrees of PEG to the agarose based matrices in a batch reaction system at room

temperature. Frontal analysis using different proteins was performed in order to characterize the hybrid SEIMAC and the PEG variations to assess its size exclusion effect on protein adsorption. This work is presented in chapter 3.

Since each IDA molecule forms only one complex with one metal ion, the IDA density on the surface can be indirectly obtained by measuring adsorption capacity of metal ions (i.e. Cu^{2+}). Using high performance liquid chromatographic (HPLC) frontal analysis, the coupling kinetics of IDA to the chromatographic matrices was obtained and a mathematical model was developed. The IDA attachment kinetics can be used to predict and control the desired IDA coupling density in the adsorbents. This work is presented in chapter 4 of this dissertation.

Similarly, the attachment kinetics of polyethylene glycol to the chromatographic matrices was obtained and a similar mathematical model adapted to the process. By using kinetic data and the theoretical model, the desired amount of PEG can be attached to the matrices for controlling the size exclusion effect. This work is presented in chapter 5 of this dissertation.

The protein modification of gold surfaces with self assembled monolayers (SAMs) is described in chapter 6. On the gold surfaces, SAMs of the organothiol compound, 16-mercaptohexadecanoic acid (MHA) were used to introduce reactive groups to the surface, and then several biomolecules and affinity ligands were immobilized on the surface. The immobilization of biomolecules on the different self assembled monolayers was studied using fluorescent microscopy and X-ray photoelectron spectroscopy (XPS).

In chapter 7, the anti-glutathione S-transferase (anti-GST) functionalized gold

surfaces have been used to attach a fusion protein, GST-γ-tubulin. The γ-tubulin is a MT nucleating and capping protein, and the surface bound γ-tubulin retains its biological ability to nucleate MTs is proven. MTs nucleated from functionalized gold surfaces have been observed using fluorescent microscopy. MTs grown from functionalized surface are often long (many exceed 20 μm in length) and definitely with one end anchored onto the surface.

The surface functionalization by photoreactive compounds, such as 4-[p-azidosalicylamido] butyl amine (ASBA) through the MHA SAMs provides a useful approach of micro patterning multiple active biomolecules on surfaces. By covalently attaching ASBA to the MHA SAMs modified gold surface using condensation reaction, different proteins can be bound to specific locations on a patterned substrate via photo lithographic methods. The patterning of heterogeneous biomolecules on two micro-scale gold surfaces separated by a few microns was successfully obtained and verified by fluorescent microscopy. This work is presented in chapter 8.

In Chapter 9, a general description and general conclusions together with the significance of this work are presented.

CHAPTER 2 LITERATURE REVIEW

A brief summary of the state of art of the material and research background for this work is presented in this chapter. The characterization and analysis of several bio-separation methods, biomolecule surface immobilization methods, specific ligands and polymer, and micro-scale protein patterning are described.

When producing antibodies, enzymes, and other biologically active biomolecules in ordinary or genetically engineered cell cultures, the desired product is normally at a dilute concentration in complicated broth solutions. The recovery and purification of the desired product is a major task and usually requires several time consuming steps. According to Bonnerjea et al., (1986), an average of 6-7 different steps is required to achieve the desired purity level. Since these biomolecules can also be very delicate, the isolation methods need to be relatively mild to produce biomolecules with the desired biological activity. The highest average purification achieved by affinity chromatography is over 100-fold, while other techniques such as precipitation, ion exchange chromatography, gel filtration, inorganic adsorption and hydrophobic chromatography have average purifications of only 12-fold. A short introduction about the affinity chromatographic separation is presented next.

Affinity Chromatography Separations

Affinity chromatography is a chromatographic separation method based on the selective adsorption of a biological compound from the solution onto a solid packing matrix. This matrix has been modified by covalent coupling of a chemical ligand that has

a specific affinity to the desired product (Scouten, 1981; Turkova, 1978; Lowe et al., 1974). Normally, a spacer molecule is used as a linker between the matrix and the ligand to reduce steric hindrances to the binding of the protein. The purification of enzymes involves chemical modifications that attach a specific inhibitor or cofactor to a solid matrix. Specific protein-protein interactions have also been used to purify antigens and antibodies (Cuatrecasas et al., 1971; Jacoby et al., 1974). Once the desired material has been adsorbed to the affinity adsorbents in a column, it may be desorbed by changing the pH, ionic strength, or temperature in the column, or by the addition of a stronger ligand or a substrate to the solution. The principle of the chromatographic method is presented in Figure 2.1.

The major advantage of this technique is the selectivity, since the affinity material associated with the matrix specifically binds to the desired biomolecule in the presence of a wide variety of biological compounds. The speed and ease of the single-step separation procedure leads to ready resolution of the desired biomolecule from contaminants. In principle, virtually any specifically interacting system composed of two or more species can be purified by this method.

Among affinity chromatographic separation methods, immobilized metal ion affinity chromatography (IMAC) is one of the most commonly used. This method is described in more detail in the following section.

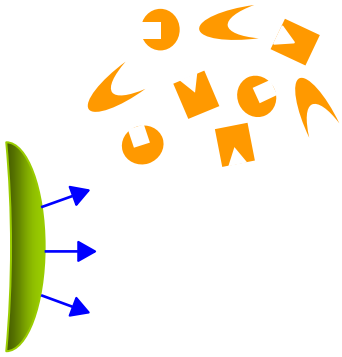

a) Proteins sieve through matrix of affinity beads

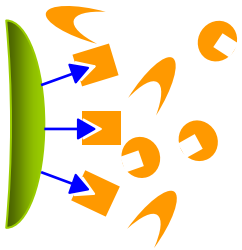

b) Proteins interact with affinity ligand with some binding tightly and other loosely

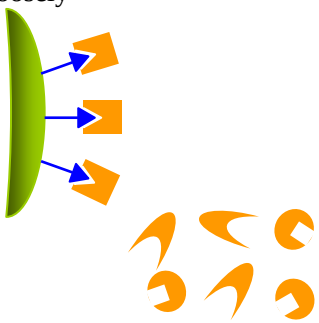

c) Wash off proteins that do not bind or bind loosely.

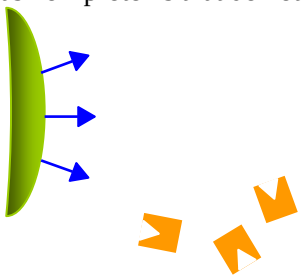

d) Elute proteins that bind tightly to ligand and collect purified protein of interest.

Figure 2.1 Schematic of affinity chromatographic method

Immobilized Metal Ion Affinity Chromatography (IMAC)

Among the affinity adsorption techniques, immobilized metal ion affinity

chromatography (IMAC) is an extremely versatile technique that takes the advantage of the specific interaction of chelated metal ions with histidine, cysteine, and tryptophan residues on the surfaces of proteins. Immobilized metal ion affinity chromatography has been extensively used for the purification of proteins and peptides (Sulkowski, 1989; Porath, 1988a; Porath, 1992; Goubran-Botros et al., 1991) and discrimination between cells of different species (Vijayalakshmi, 1989). In some cases, the performance of this technique is superior to that of bio-specific affinity based adsorbents. Selectivity of this method can be varied by the choice of type of chelator-ligand and metal ion as well as by varying the manners of elution.

To understand the interaction of metal ions with other chemical substances, the concept of Lewis Acid-Base theory will help. Lewis acids and bases can be further subdivided into hard/soft acids and hard/soft bases according to hard/soft acid/base (HSAB) principle (Pearson, 1973). In addition to “hard” and “soft” categories, there are two additional categories: borderline acids (BA) are intermediate between hard and soft acids, and borderline bases (BB) are intermediate between hard and soft bases. The basic idea of HSAB theory is simple: hard acids prefer hard bases; soft acids prefer soft bases. Similarly, borderline acids prefer borderline bases. Because the hard acids and bases tend to be highly charged and are non-polarizable, the interaction between them is largely ionic. Their small sizes allow the acid and base to get close enough together so that the ionic interaction is quite strong. In contrast, soft acids and soft bases have covalent interactions because their electron clouds are polarizable.

Typically, IMAC is divided into four components: the matrix (such as agarose and

silica beads) to which various chelators can be linked via spacer arms; chelators (such as iminodiacetic acid, IDA) which can effectively capture metal ions; metal ions (such as Cu^{2+}); and biomacromolecules (such as proteins) possessing specific groups which can coordinately interact with immobilized metal ions (Porath, 1992; Winzerling, 1992). A schematic illustration of an IMAC system is shown in Figure 2.2.

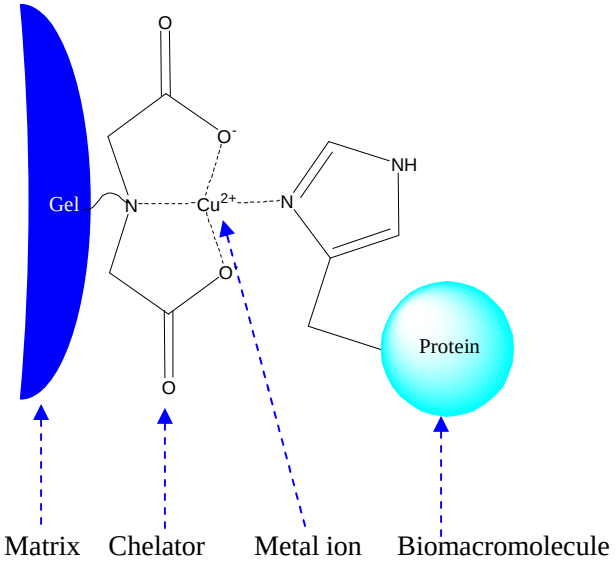

Figure 2.2 Schematic of an IMAC system

In this work, the matrices used are polysaccharide agarose gels which molecular structure is presented in Figure 2.3. Agarose has a structure consisting of alternating residues of D-galactose and 3-anhydrogalactose. The gel network of agarose contains double helices formed from left-handed threefold helices. These double helices are stabilized by water molecules bound inside the double helical cavity (Labropoulos et al., 2002). Exterior hydroxyl groups allow aggregation of up to 10,000 of these helices to form superfibers. The primary and secondary hydroxyl groups in agarose gel make it cross-linkable and activatable to immobilize the specific ligands onto the surfaces. The

cross-linking of agarose enhances the structure strength of the gel and results in some loss (30-50%) of activatable hydroxyl groups that are consumed in the chemistry of cross-linking (Labropoulos et al., 2002). A scanning electronic microscopic (SEM) image of 1% agarose gel is shown in Figure 2.4.

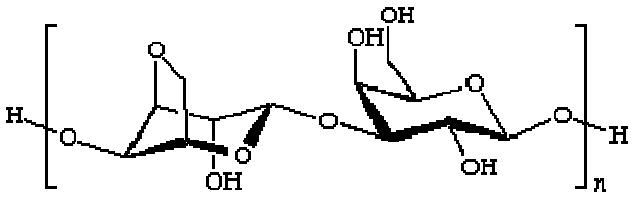

Figure 2.3 Molecular structure of agarose

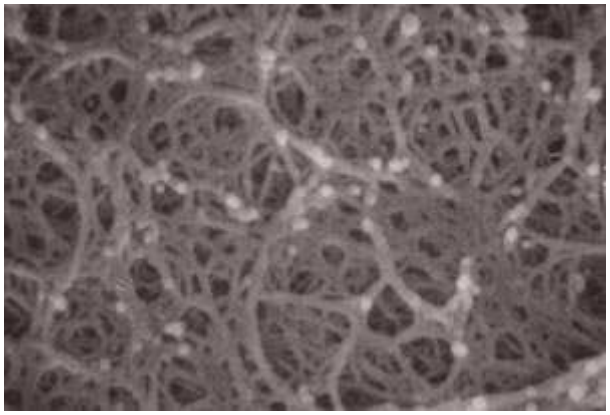

Figure 2.4 SEM image of 1% agarose gel with 22 kX magnification

The second component of an IMAC system is a chelator (or chelating ligand). Chelators are used in IMAC to bind metal ions, producing a polydentate chelate. Such chelators have a net charge and are highly soluble in an aqueous medium (Vijayalakshmi, 1989). Table 2.1 lists some commonly used chelators that usually contain N, O, S, or P (Porath, 1992; Winzerling, 1992) and their structure formulas are shown in Figure 2.5. In an IMAC system, the adsorption sites for biomolecules are the remaining coordination sites of the bound metal, and they are normally occupied by solvent molecules or by

weakly bound anions. Thus, the chelating ligand immobilized on the matrix should exhibit a compromise between a stable chelate complex and availability of free metal coordination sites. The influence of the chelating ligands has been reviewed by Porath (1988 b) and Fanou-Ayyi et al. (1983). Carboxymethylated amines, such as iminodiacetic acid (IDA), are usually chosen as chelating ligands.

Table 2.1 Commonly used chelators

Type	Chelator	Abbreviated Name
Bidentate	Ethylene diamine	En
Tridentate	Iminodiacetic Acid	IDA
Tetradentate	Carboxymethylated Aspartic acid	CM-Asp
	Nitrilo triacetic acid	NTA
	Tris (2-amino ethyl) amine	TREN
Pentadentate	Tris-carboxymethylated ethylene diamine	TED
Hexadentate	Ethylenediamine tetraacetic Acid	EDTA

The stronger the chelator is, the weaker the interactions of the immobilized metal ions with proteins are. Usually, it is advisable to select a chelator that can form a maximum number of 5- or 6- member ring systems while leaving a sufficient number of coordination sites on the immobilized metal ions available for interaction with proteins (Wong et al., 1991).

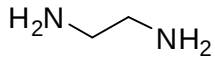

Ethylene diamine

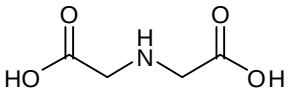

Iminodiacetic acid

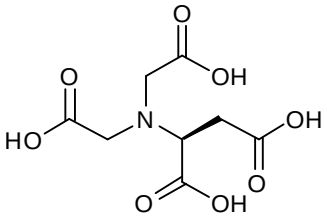

Carboxymethylated aspartic acid

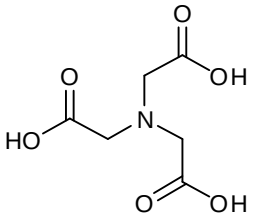

Nitrilo triacetic acid

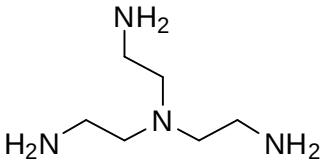

Tris (2-amino ethyl) amine

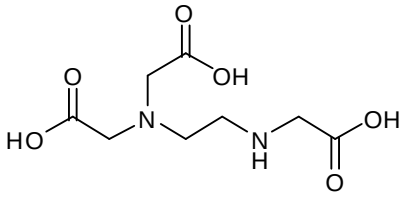

Tris-carboxymethylated ethylene diamine

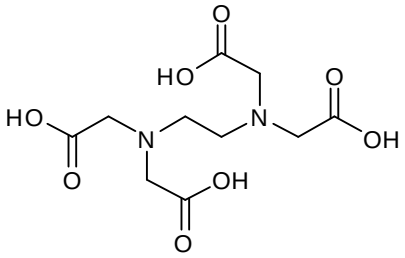

Ethylene diamine tetraacetic acid

Figure 2.5 Structural formulas of common used chelators

In IMAC, since reversible and rapid kinetics are of primary importance, the borderline acids (metal ions) have been extensively studied (Pearson, 1973). The strength of protein adsorption for commonly used immobilized metal ions increases in the following order: $Co^{2+} < Zn^{2+} < Ni^{2+} < Cu^{2+}$.

Different metal ions prefer to react with different amino acids. For example,

histidine, containing the imidazole group, or cysteine, containing the thiol group, can form a strong bond with some transition metal ions such as Cu^{2+}. Sulkowski (1987) concluded that the presence of one histidine residue is sufficient for protein retention and multipoint attachment to ligands results in a stronger retention (Chaga, 2001). Copper ion (Cu^{2+}), the most used metal ion in IMAC has a coordination number of 6 and, 4 of them can form a strong chelating complex. Thus, 4 donor atoms can be bound to Cu^{2+} to form a chelate. The chelator IDA forms a double five-membered ring chelate with Cu^{2+}, leaving one chelating site to bind other donor atom. An illustration of the chelate complex formed with IDA-Cu^{2+}-Histidine is presented in Figure 2.6. Thus, the immobilized Cu^{2+} on the polymer matrix can be used to separate proteins with histidine or cysteine from crude extracts (Porath et al., 1975). Thereby, the purpose of IMAC is to balance all factors for achieving optimal chromatographic efficiency. When the proteins with histidine or cysteine groups pass near the immobilized metal ions, they will bind to metal ions through either the imidazole ring of histidine moieties or the sulfur on the cysteine moieties. A column with bound proteins can then be recovered by eluting proteins by competition with another electron-donating species, such as imidazole or a soluble chelator. Elution can also be performed by protonation of the electron-donating groups on the protein, i.e., lowering the pH (Porath, 1992). In this dissertation, the work in IMAC was performed using mainly the chelator IDA.

Some of the work performed in this dissertation involved the use of polyethylene glycol (PEG) as a polymeric derivative to develop hybrids of IDA/PEG. Thus, a synopsis of some aspects of PEG is given here to provide an understanding of its relevance to the present research.

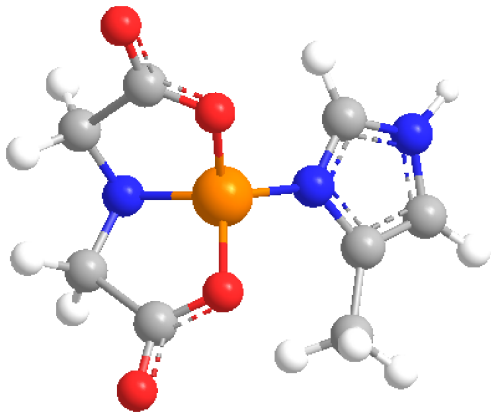

IDA Cu^{2+} Imidazole ring of histidine

Figure 2.6 Chelate complex of IDA-Cu^{2+}-Histidine

Polyethylene glycol (PEG)

Polyethylene glycol (PEG) is a neutral, crystalline, thermoplastic polymer which is highly soluble in both water and organic solvents (Harris, 1992). The chemical structural formulas of methoxyl PEGs are shown in Figure 2.7. Polyethylene glycol surface grafts have gained considerable attention as being stable films that provide resistance to non-specific protein adsorption (Porath, 1988a; Elbert et al., 1996; Harris et al., 1997; Harris, 1992). This protein resistance is of practical importance for a number of surface engineering applications including developing of biomaterials, in drug delivery, or in biosensors (Kingshott et al., 1999; Lee et al., 1998). In this work, some of these properties associated with PEG were used to enhance the separation of protein of certain molecular weight. Chromatographic matrices of agarose were modified both with chelating agents and with PEG to form hybrid IMAC-PEG affinity separation beads.

The protein repelling property of PEG has been credited to many molecular mechanisms. Two different aspects are usually considered: first, the brush-induced

"steric" repulsion that prevents the direct contact between proteins and the underlying surface (Jo and Park, 2000); and second, hydration shells, which suppress adsorption of proteins onto the PEG layer. It has been argued that the protein resistance also observed on well ordered model systems of self assembled monolayers of poly (ethylene glycol) may alternatively be due to charging effects (Jo and Park, 2000; Szleifer, 1997; Herrwerth et al., 2003).

Several research groups have explored the use of model solid surfaces for mechanistic studies on the protein resistance of PEG coatings. The use of these model interfaces makes it possible to apply a range of surface and thin-film characterization techniques. Prime et al. (1993) and Harder et al. (1998) studied the correlation of protein resistance with the molecular conformation of polyethylene glycol terminated self assembled monolayers (SAMs) of thiolates on metal surfaces. Some studies showed the effects of molecular length and chain density on protein adsorption properties (Sofia et al., 1998a; Malmsten et al., 1998; Papra et al., 2001).

a) M-PEG b) M-PEG-NH_2

Figure 2.7 Chemical structural formula of a) M-PEG and b) M-PEG-NH_2

The PEG-water interaction is commonly understood as PEG being an amphiphilic polymer, which is only structurally soluble in water. The hydrated PEG prefers staying in polar *gauche*-conformations that closely match the structure of water (Björling et al.,

1991). It is also recognized that there must be a particularly enhanced water structure around PEG chains (Müller et al., 1991). Based on thermodynamic considerations, a widely cited hydration model was proposed by Kjellander et al., (1981). This model described a helical PEG conformation encaged into a surrounding water structure. A minimum of about 2–3 water molecules per PEG monomer seems to be required to complete basic hydration (Maisano et al., 1993).

Polyethylene glycol in its hydroxylated form (HO-PEG-OH) does not readily adsorb onto surfaces. It must be grafted to the surface to form a brush layer with sufficiently high surface density to achieve protein resistance. Common grafting approaches include the use of block copolymers (Costello et al., 1993), surface induced polymerization (Ma et al., 2004), cross-linking of star-shaped PEG (Groll et al., 2004), covalent grafting of PEG chains to phospholipids (Tirosh et al., 1998), or chemical functionalization (Prime et al., 1993; Himmelhaus et al., 2003). The last one is used in this work to obtain PEG grafted surfaces.

In our work, functionalization scheme and procedures were extended to the activation and incorporation of biomolecules onto inorganic surfaces such as gold surfaces. In order to immobilize biomolecules onto surfaces, the surfaces must be functionalized first with a specific ligand or biomolecule layer. The uses of self assembled monolayers (SAMs) are commonly used methods for functionalization of surfaces. SAMs can be prepared in different fashions, and here we use derivatives of alkanethiol compounds to activate gold surfaces. A brief description of these systems is given here.

Self Assembled Monolayers (SAMs)

Immobilization of biomolecules to solid surfaces, such as silanized layers (König et al., 1994), polymer membranes, (Nakanishi et al., 1996; Wong et al., 2002) Langmuir-Blodgett films, (Pathirana et al., 2000) and self assembled monolayers (SAMs) (Ben-Dov et al., 1997; Park and Kim, 1998; Fung et al., 2001) is crucial in the development of solid-phase bio-analytical techniques, biosensors and biocompatible materials. The current immobilization methods based on SAM techniques offer some of the simplest ways to provide reproducible, ultrathin, and well-ordered layers suitable for further modification with biomolecules, and the potential in improving detection speed, sensitivity, and reproducibility (Whitesides et al., 2001; Wolfe et al., 2005). The self assembly method with alkanethiols can be used with a wide arrange of metal substrates such as Au (Park and Kim, 1998; Fung et al., 2001; Patel et al., 1997; Levicky et al., 1998), Ag (Harder et al., 1998; Walczak et al., 1991), Cu (Laibinis and Whitesides 1992), and Pt. (Hickman et al., 1992). The Au surfaces are the most studied as a promising substrate for biomaterial immobilization. That is in fact the material used in this work.

Currently, the most efficient approach to manufacture biomaterial layers onto a gold surface is to adsorb appropriate organothiols onto a gold substrate. As shown in Figure 2.8, the most ordered structures are formed from compounds with the structure HS-(CH_2)n-X, where n =16–18 and X is a small, organic functional group (Wolfe et al., 2005). These SAMs are highly ordered and densely packed assemblies of linear alkane molecules that are thermodynamically driven to form high coverage films of molecular dimensions (Nealey et al., 1997). The functional terminal group of the molecules from

which SAMs are formed determines the surface chemistry after modification. Physical interaction or chemical binding can be used to bind biomolecules to the SAM modified surfaces. An important requirement of biomolecule immobilization is the high bioactivity after the immobilization via SAMs (Williams et al., 1994). The physical adsorption is regarded as a mild method that preserves protein activity. However, it can be reversible; moreover, it does not provide as high a surface loading of protein as covalent coupling. Lower surface loading implies a decreased initial sensitivity relative to a sensor with covalent immobilization; desorption would further reduce the sensitivity over time. The chemical covalent binding is a stronger linkage between the biomolecules and substrate that can provide long-term usage. A reactive terminal group can also be chemically modified after deposition of the SAM to obtain a more diverse set of surface chemistries, which can be used for anchoring precursor molecules. The terminal groups now used most frequently are amino groups, carboxyl groups, and NHS groups (Levicky et al., 1998; Patel et al., 1997; Caruso et al., 1997; Aguilar et al., 2002, Huang et al., 2001).

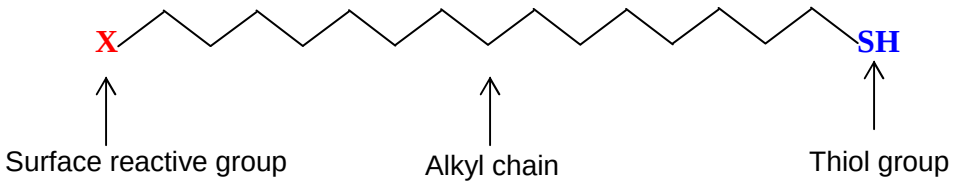

Figure 2.8 Illustrative representation of an organothiol compound

In this work, biomolecules were immobilized onto SAM functionalized surfaces. Specific biomolecule structures, microtubules (MTs) were utilized as self assembling structures and templates for fabrication of nano-scale bio-interconnect arrays and

networks. A brief introduction of MTs is presented.

Microtubules (MTs)

Microtubules (MTs) shown in Figure 2.9 are naturally formed tubular structures with an outer diameter of 24 nm and a length up to many microns (Schuyler et al., 2001). Microtubules are biopolymers assembled from protein heterodimers containing both α- and β-tubulins. The structure of α-and β-tubulin heterodimer is presented in Figure 2.10. The MTs' aspect ratio, chemical polarity, reversibility in assembly, and ability to be metalized by electroless plating (Yang et al., 2004) make them good candidates to serve as templates for the fabrication of metallic nanowires and other nano-scale systems (Mertig et al., 1998). In addition, microtubules can provide biological interactions with a native high specificity (Sarikaya et al., 2003; Antikainen et al., 2005). The exposure of different tubulin regions at either end of a microtubule (plus/minus end) makes it possible to control MT attachment to substrates in a specific orientation. For instance, Limberis et al. (2001) took advantage of the polarity and specificity of biological interactions of MTs to flow-align pregrown MTs. In this work, MTs were immobilized onto a gold patterned silica substrate using a single-chain antibody that binds only to a portion of α-tubulin exposed at the MT minus end.

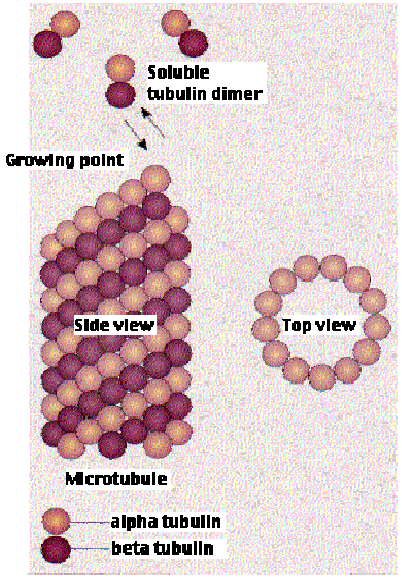

Figure 2.9 Illustrative representation of a microtubule

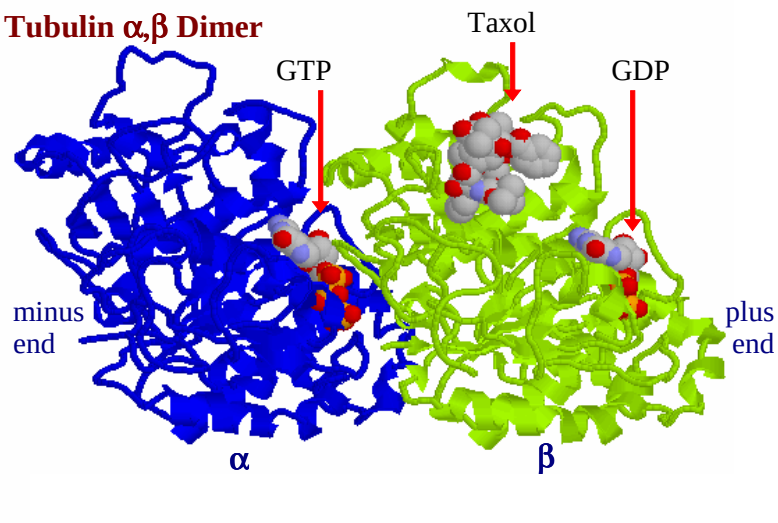

Figure 2.10 Illustrative structure of an α and β tubulin heterodimer

In order to form a controlled and aligned MT nano-scale bio-interconnects on a designed surface with micro features, a micro/ nano patterning approach must be applied to form hetero ligand or protein patterns on surfaces. In this work, hetero protein patterns

were prepared using self assembled monolayers functionalized with photoreactive derivatives and photolithographic methods.

Micro/ Nano Protein Patterning Development

Several techniques have been developed to generate patterns of functional biomolecules onto artificial surfaces to be used for biosensors, for cell studies and tissue engineering applications, for actuation of microelectromechanical systems (MEMS), as well as for proteomics and pharmacology, and basic biological research (Ito, 1999; Singhvi et al., 1994; MacBeath et al., 2000). However, both the study and application of proteins patterning have been challenged by the inherent difficulties associated with positioning these substances. Thus, a primary enabling technology is the ability to precisely immobilize biomolecules in well-defined patterns while maintaining their native functionality. Methods used for protein patterning include photolithography as in photochemical structuring (Nicolau et al., 1999; Clemence et al., 1995), deep UV lithography (Lom et al., 1994), and dip-pen lithography (Liu et al., 2002), as well as micro contact printing (Kovacs et al., 1998; Xia et al., 1998; Losic et al., 2001).

Currently, one of the most popular techniques is micro contact printing (“soft lithography”) (Kane et al., 1999; Mrksich et al., 1995). In this method, a polymer printing stamp is cast using a master which is produced with photolithography and silicon etching techniques. However, problems may arise when a precise alignment to prefabricated microstructures is required and when precise immobilization of different proteins on the same chip is intended. Dip-pen lithography (Lee et al., 2002; Liu et al., 2002) is capable

of nano-scale resolution, but it includes relatively delicate serial processes and thus lacks scalability.

Photolithographic techniques are well established for mass production of silicon chips with a pattern resolution and alignment precision of less than 1 μm on silicon, glass and metal substrates. The use of photolithography for protein micro patterning offers several advantages over micro contact printing (Veiseh et al., 2001; Sorribas et al., 2002), including higher resolution, straightforward scalability and its broad acceptance as a standard industrial technique. Photolithographic methods are used to create micro patterns by means of coating the silicon surfaces with a photoresist, masking, and then exposing the photoresist to UV light, chemical development, high vacuum vapor phase metal deposition and lift-off (Bushan, 2004). This results in micro patterned metal (in this work, gold) on a silicon wafer substrate. The resulting gold pattern is then available for functionalization by attachment of an alkanethiol self assembling monolayer and subsequent protein attachment using standard bio-conjugation chemistries (Whitesides et al., 2004; Hermanson, 1996; Duesman et al., 2004). Most of the work in this dissertation was carried out on gold and with MHA SAMs as the reactive linker.

Based on the above information, the study of synthesis and characterization of functionalized biosurfaces for bioseparations and bio-nanotechnology applications were performed and explored in this research work.

CHAPTER 3 SYNTHESIS AND CHARACTERIZATION OF NOVEL ADSORBENTS FOR PROTEIN AFFINITY CHROMATOGRAPHY

Abstract

The work presented here explores the feasibility of a new IMAC chromatographic approach. The concept involves the simultaneous specific adsorption of proteins and size exclusion effects. The concept is based on the principle of polymer modulated permeation control and the ability of introducing selected hydrophilic polymers and chemically bound affinity ligands in size exclusion gel matrices used in protein purifications. The resulting hydrogel consists of a layer of a polymer which acts as an obstacle to the permeation of molecules present in the surrounding liquid and specific ligands attached to the surface of the gel.

These matrices with selected hydrophilic polymers allow apparently sharper molecular size exclusion limits where only "selected" permeated biocompounds (of specific molecular size) are able to penetrate and interact with the chemically bound ligands on the gel surface. Soluble molecules will permeate to a certain extent or they may be excluded dependent on the dimensional relations between the modified voids of the matrix and the molecular size and shape of the solute. This sieving effect is the basis for the proposed size exclusion chromatographic effect in this concept.

As a first suitable polymer to test for size controlled permeation, methoxyl polyethylene glycol amine (M-PEG-NH_2) was used. The specific adsorption groups introduced in this work were chelating ligands, specifically the chelator iminodiacetic

acid (IDA).

The research performed in this work has shown evidence of success of the proposed protein purification concept with the model proteins lysozyme, myoglobin and bovine serum albumin (BSA). Once these derivatives adsorptive and methodology are further characterized, the concept can be extended to more complex systems.

Introduction

The overall objective of this research is to synthesize and explore new chromatographic methods that involve simultaneous specific adsorption, and size exclusion by controlled permeation of biomolecules, size controlled affinity chromatography (SCAC). In this research, immobilized metal ion affinity chromatography (IMAC) was used to test the concept. The soluble multifunctional polymeric derivatives, methoxyl-polyethylene glycol amine (polyalkylene derivatives) will be used as surface blocking arms to achieve sharp size exclusion limits. The method might allow for 1) concentration and separation of proteins in a single operation using a specified affinity to proteins and other macromolecular substances and particles, 2) isolation of small size solutes, such as peptides, amino acids, inorganic ions (metal ions) etc., and 3) at the same time avoid clogging of chromatographic columns, facilitate adsorbent regeneration and increase adsorption capacity at higher flow rates.

Size exclusion immobilized metal ion affinity chromatography will be accomplished by incorporating in a chromatographic matrix two types of multifunctional ligand derivatives, one that permits the permeation of only certain molecular size range compounds, and a second one that specifically binds target biomolecules among the

compounds of that specific molecular size range. In this study, we have attached M-PEG-NH_2 as the size exclusion polymer and iminodiacetic acid (IDA) as the affinity ligand (L) to the surface of agarose, a polysaccharide gel matrix. As hydrogels conditioned by controlled permeation, the resulting product will have a schematic structure as presented in Figure 3.1.

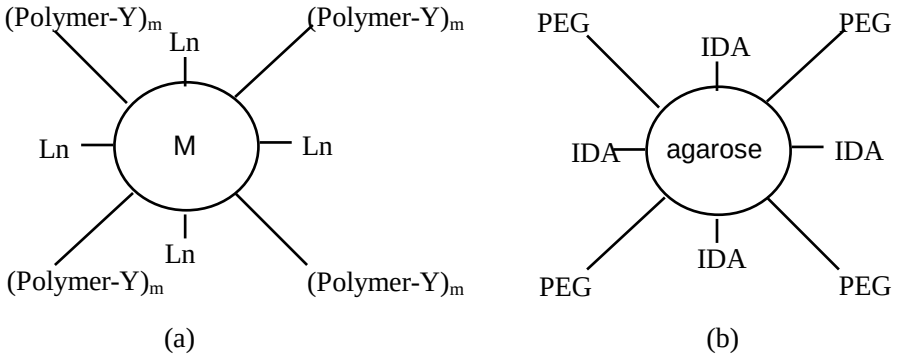

Figure 3.1 Schematic of (a) Size Controlled Affinity Chromatography (SCAC) and (b) Size Exclusion Immobilized Metal ion Affinity Chromatography (SEIMAC)

In Figure 3.1a, **M** is a solid phase matrix, and **L** represents an affinity ligand such as a metal ion chelator, ion exchanger or specific group that binds a specific solute to the matrix surface. The n and m represent the ratio of the ligand (L) and the polymer chain (Polymer-Y), respectively. Y represents a functional enhancing group that can be used to couple other chemical derivatives in order to increase the controlled permeation effects to the biomolecules. Figure 3.1b presents a specific case of size controlled affinity chromatography (SCAC), size exclusion immobilized metal ion affinity chromatography (SEIMAC) in which the matrix used is an agarose gel, the ligand is IDA, and the polymer is PEG without other enhancing group Y except the methoxyl group. This technique appears to be of particular interest for separation of low molecular weight biomolecules,

such as peptides.

The traditional size exclusion chromatography (SEC) can separate the samples depending on their size, but its sample volume is limited. Only a sample size corresponding to a small fraction of the chromatographic bed volume can be processed in a single operation. It also has problems when a low concentration sample solution is used. On the other hand, adsorption chromatographic methods can process large volumes of samples when the adsorbate is present in low concentrations.

It is possible to combine the desirable features of adsorption chromatography and size exclusion chromatography by the use of adsorbents with limited and well defined permeation properties. Conventionally (and commercially) this is done by selecting gels with varying degrees of gel density. Up until recently, this has been the only way available to control permeation. Adsorbents of such a kind suffer from certain disadvantages due to the fact that, for example, the size exclusion upper size limit is not well defined and a strong tendency for clogging due to adsorption of high molecular weight substances at, and close to, the particle surface.

The proposed chromatographic affinity adsorbents might be capable of protein and peptide separations with higher size selectivity than commercially available separation media. Their applications in chromatography have potential advantages for operations to be carried out on extreme scales. The immediate and future applications deal with separations of proteins and peptides based on controlled permeation and affinity adsorption of biomolecules.

This technology has great potential to decrease the problems of clogging of

chromatographic supports, thus increasing the possibility of using higher flow rates in chromatographic separations. This technology eliminates competition for adsorptive sites on the matrix surface between large and small molecules, thus increasing the adsorption rate and capacity of desired biomolecules. This proposed process is schematically shown in Figure 3.2.

In this work, several polysaccharide adsorbents (Novarose and Sepharose gels) were modified with IDA to obtain constant chelator density. After that, PEG was attached to the adsorbents to different degrees by reacting with the gels at different reaction time periods. All the coupling experiments with PEG and IDA were performed in batch systems at room temperature. Frontal analysis of protein adsorption was done with a Gilson HPLC to reveal the size exclusion effects of attached PEG on the different proteins.

Materials and Methods

Materials

Methoxyl polyethylene glycol amine (MW, 5000) (M-PEG-NH_2, 5000), imino diacetic acid (IDA), epichlorohydrin (EPI), cupric sulfate, sodium hydroxyl, sodium carbonate and bisodium phosphate were purchased from Sigma (St. Louis, MO, USA). Novarose Activated 300/40 gels were from Inovata (Bromma Sweden), and Sepharose 6B gels were from Pharmacia (Uppsala, Sweden). All proteins (myoglobin, BSA, and lysozyme) and the amino acid tryptophan were from Sigma (St. Louis, MO, USA). All materials were used as arrived.

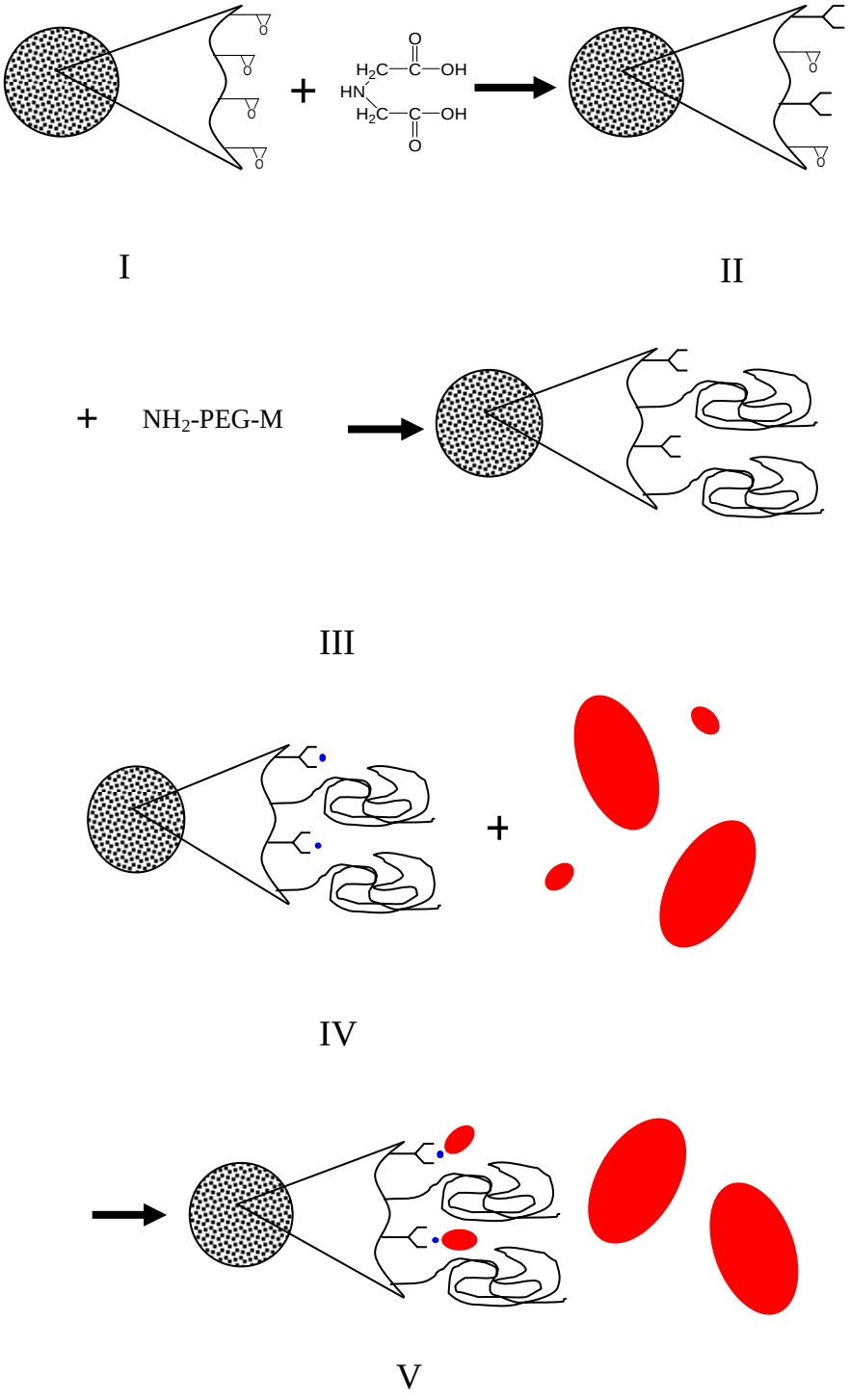

Figure 3.2 Schematic of SEIMAC process: synthesis steps (I, II, III) and operation steps (IV, V)

Activation of Chromatographic Matrices

In order to attach IDA and PEG to the matrices, the Sepharose 6B gels were first activated with epichlorohydrin. The gels were rinsed with D.I. water in a glass filter to remove the storage solution (22% ethanol aqueous solution). A mass of 16 g suction dried Sepharose 6B gels were then mixed with 0.25 g sodium borohydrin, 7.5 mL of epichlorohydrin and 70 mL of 2.0 M NaOH. While continuously stirring the gel suspension, another 70 mL of 2.0 M NaOH and 34 mL of EPI were added in small portions over a period of 1.5 hr. Afterwards, the gel suspension was kept well mixed and left reacting overnight on a shaker. Finally, the mixture was filtered in the glass filter and washed 4 times with 50 mL of each: 0.1 M hydrochloride acid, D.I water, 0.1 M Sodium carbonate, and then D.I water. The activated gels were kept in 22% ethanol aqueous solution at 4 ºC for further use.

Synthesis of IDA-PEG Hybrid SEIMAC Gels

The agarose-based IDA-PEG hybrid SEIMAC gels were prepared with activated Sepharose 6B gels and Novarose Activated 300/40 gels.

Sepharose-IDA/PEG Hybrid Preparation

A mass of 14 g of EPI modified Sepharose 6B gel was rinsed with D.I. water in a glass filter to remove the storage solution and then divided evenly into seven 20-mL vials. To one vial, an excess of IDA was added and exhaustively reacted for at least 24 hours. In each of the other 6 vials, 1.0 g M-PEG-NH_2 was added and reacted for different time periods. After washing, the 6 PEG modified gels were exhaustively reacted with an

excess of IDA (0.7 g) and 20 mL 1.0 M Na_2CO_3, and the mixtures were well shaken for 24 hours on a shaker. The mixture was then filtered and washed. The remaining active sites on the gels were neutralized by reacting the gels with 0.1 M ethanol amine in 1.0 M sodium carbonate for 1.0 hour. Finally, the mixture was filtered in the glass filter and washed 4 times with 50 mL of each: 0.1 M hydrochloride acid, D.I water, 0.1 M Sodium carbonate, and then D.I water. This synthesized Sepharose-based hybrid SEIMAC gel was kept in 22% ethanol aqueous solution at 4 ºC for further characterization and use. In this case, we expect to have gels with changing surface densities of PEG and IDA.

Novarose-IDA/PEG Hybrid Preparation

For the Novarose activated 300/40 gel, a mass of 16 g of gel was mixed with 10 mL 6% IDA (wt %) including 1.0 M Na_2CO_3 (pH 12) and the mixtures were shaken for 30 minutes at a temperature of 25°C. Then the gels were washed thoroughly with DI water and were split into 8 vials. 2.0 g of M-PEG-NH_2 and 1.0 M Na_2CO_3 were added to each vial and reacted for different times at room temperature. After that, the gels were washed thoroughly with DI water. The remaining active sites on the gels were eliminated by reacting the gels with 0.1 M ethanol amine in 1.0 M sodium carbonate for 1.0 hour. Finally, the mixture was filtered in the glass filter and washed 4 times with 50 mL of each: 0.1 M hydrochloride acid, D.I water, 0.1 M Sodium carbonate, and then D.I water. The Novarose-based hybrid SEIMAC gels were kept in 22% ethanol aqueous solution at 4 ºC for further characterization.

Characterization of IDA-PEG Hybrid SEIMAC Gels

IDA-PEG hybrid SEIMAC gels were characterized by measuring copper and protein capacities with chromatographic frontal analysis using a Gilson FPLC system.

In all the experiments, 10.00 mM of cupric sulfate solution prepared in D.I. water was used to measure the copper capacity and form the chelating complex with IDA. BSA, myoglobin, and lysozyme were chosen as model proteins. All protein solutions with a concentration of 1.00 mg/mL were prepared in a phosphate buffer (20 mM sodium phosphate, 0.5 M NaCl, pH 7.0). In addition, adsorption experiments were conducted with the amino acid tryptophan as well, known for its interaction with immobilized copper. The last experiments were conducted to assess the adsorption and permeation of small adsorptive molecules.

A glass chromatographic column from Pharmacia with an internal diameter of 5 mm and length of 10 cm was used in chromatographic analysis. The gel packed bed height was around 3 cm and the flow rate used in all the experiments was 0.2 mL/min.

Results and Discussion

Sepharose 6B-IDA/PEG Gel Analysis

The SEIMAC gels prepared with Sepharose 6B showed changing copper capacity in all the gels after reaction with PEG derivatives, and the results for surface densities of PEG equal to zero showed a maximum copper capacity of the gel of 20 μmol/mL. These results are presented in Figure 3.3. The maximum density of PEG was obtained after a reaction time of 16 hours. At this PEG density on the gel surface, the immobilized copper concentration was found to be only 4 μmol/mL. The gels prepared here exhibited

practically no protein adsorption, since at this immobilized copper capacity, the amount of protein adsorbed (myoglobin) was practically zero (from 0 to 0.01 μmol/mL of gel). Further PEGylation was not performed after 16 hours.

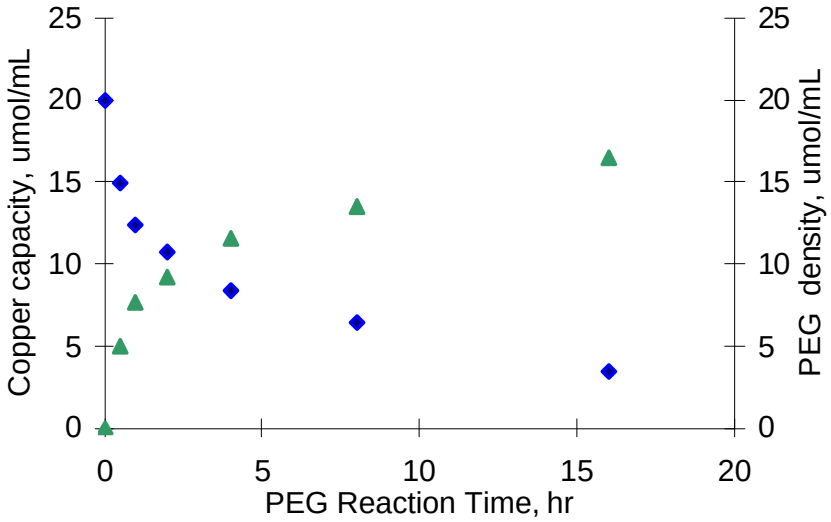

Figure 3.3 Copper ion capacities of Sepharose-PEG/IDA gel with varying surface densities of PEG and IDA.
▲: PEG surface densities; ♦: copper capacities

For each gel with different IDA and PEG surface density, protein adsorption experiments were conducted with myoglobin as in a typical immobilized metal ion affinity chromatographic system. The gels were packed in an IMAC column (internal diameter of 0.5 cm and length of 10 cm). All experiments were performed at a flow rate of 0.2 mL/min with the myoglobin concentration of 1.0 mg/mL in phosphate buffer. The results with the Sepharose-IDA/PEG gel with myoglobin are presented graphically in Figures 3.4 and 3.5. The myoglobin protein capacity with the classical IMAC gel

(without PEG attached) was measured as 1.34 μmol/mL of gel, with only copper metal ions loaded onto the column.

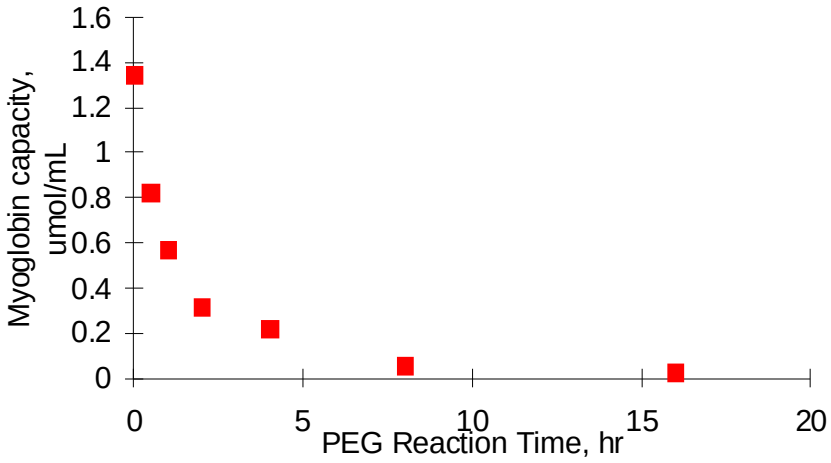

Figure 3.4 Myoglobin capacities of Sepharose-PEG/IDA gel with varying surface densities of PEG and IDA.

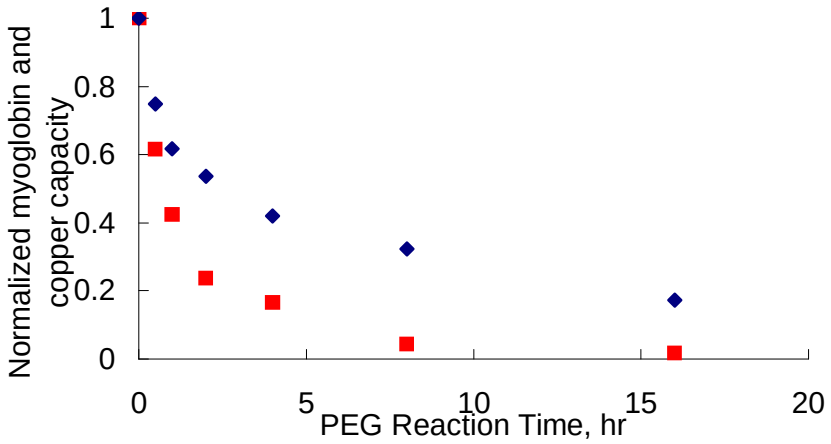

Figure 3.5 Normalized copper and myoglobin capacities of Sepharose-PEG/IDA gel with varying surface densities of PEG and IDA.
■: myoglobin capacities; ♦: copper capacities

From Figure 3.4, it is clear that the protein capacities decrease with increasing PEG surface density. But since in these experiments the IDA density was also varied, the

effect of permeation itself was difficult to elucidate. The normalized copper and myoglobin capacities are shown in Figure 3.5. It appears however that since the capacity for myoglobin decreases sharper than the capacity of IDA, a possible PEG permeation effect is present, but the evidence is not convincing, as yet. In order to elucidate such effects, experiments were designed in a different form, as described in the next section with PEG/IDA hybrid Novarose 300/40 gels.

Novarose 300/40-IDA/PEG Gel Analysis

Copper Adsorption Analysis

In this scheme, Novarose 300/40 Activated High gels, they were prepared in a way such that the capacity for metal ions was kept constant. This was accomplished by first reacting the gels with a given concentration of the chelator IDA and for a given specific reaction time according to standard curves and kinetic studies described in chapter 4. This was effectively done and all the gels prepared had a copper capacity of ~20 µmol/mL of gel. The maximum possible copper capacity of 110 µmol/mL for this gel was determined by reacting the gel beads exhaustively with IDA for 24 hours. These partially carboxymethylated gels afterwards were also effectively modified with PEG by reacting with a M-PEG-NH_2 solution for varying time periods. After PEG attachment to the matrix, possible remaining reactive groups on the matrix were neutralized by reaction with amino ethanol. The entire process was apparently successful and a constant capacity of copper was always observed for all the IDA/PEG hybrid gels. Frontal analysis for copper results are shown in Figure 3.6, where it can be seen that PEG does not have any effect on the retention of copper in these gels, at least under the working conditions

described here. Protein adsorption experiments were carried out with these new gels where the permeation effect could readily be seen. The copper capacity independent of PEG density is presented graphically in Figure 3.7.

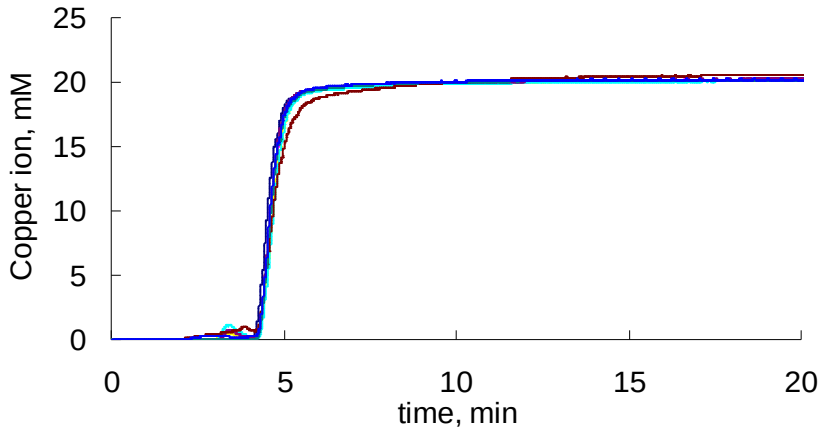

Figure 3.6 Frontal analysis of copper ion in Novarose 300/40- PEG/IDA gels with constant IDA and different PEG surface densities
—: 0 µmol/mL; —: 11.6 µmol/mL; —: 19.4 µmol/mL; —: 24.0 µmol/mL; —: 31.0 µmol/mL; —: 41.2 µmol/mL; —: 63.6 µmol/mL

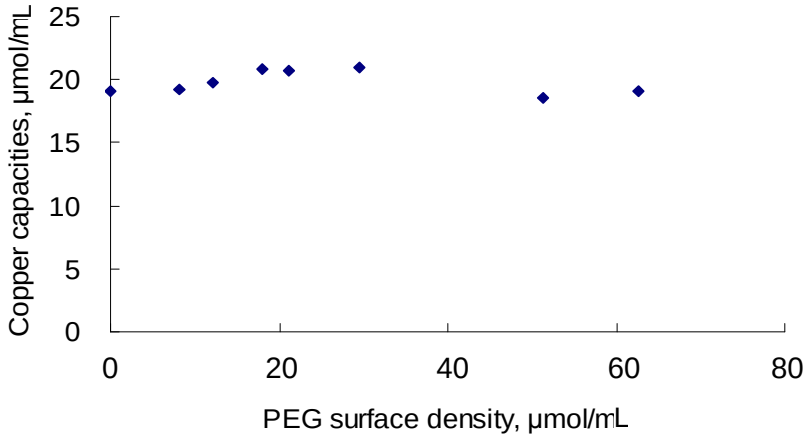

Figure 3.7 Copper ion capacities of Novarose 300/40- PEG/IDA gel with constant IDA density and different PEG surface densities.

Amino Acid (Tryptophan) Adsorption Analysis

The adsorption analysis of tryptophan with gels with constant IDA and varying density of PEG resulted in adsorption capacities of the amino acid corresponding to the copper chelated on the matrices. Apparently, for this small molecule, the effect of the permeating polymer PEG was negligible. The average tryptophan capacity for all the experiments conducted was around 17 µmol/mL of gel. This is very promising evidence that small molecules (copper, tryptophan) can penetrate the polymer barrier and interact with chelator ligands bound to the surface of the matrix. The results are presented graphically in Figure 3.8 and the frontal analysis data in Figure 3.9.

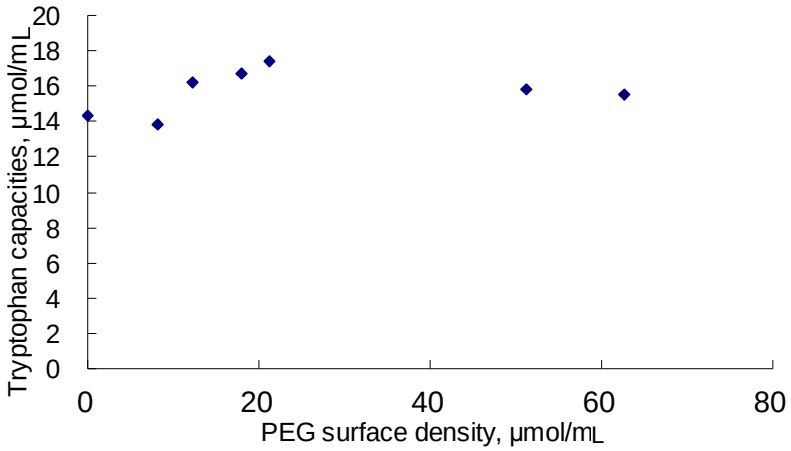

Figure 3.8 Amino acid (tryptophan) adsorption capacities in Novarose 300/40- PEG/IDA gel with constant IDA density and different PEG surface densities

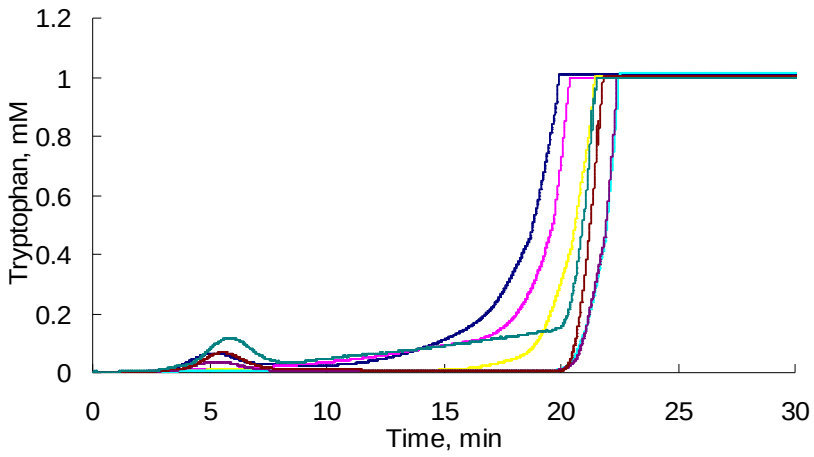

Figure 3.9 Frontal Analysis of tryptophan adsorption in Novarose 300/40- PEG/IDA gels with constant IDA density and different PEG surface densities
—: 0 µmol/mL; —: 11.6 µmol/mL; —: 19.4 µmol/mL; —: 24.0 µmol/mL; —: 31.0 µmol/mL; —: 41.2 µmol/mL; —: 63.6 µmol/mL

Protein Adsorption Analysis

Protein adsorption experiments with the proteins BSA (MW: 64 kDa) and lysozyme (Lys, MW: 15 kDa) were carried out with the SEIMAC hybrid gels of constant IDA and variable PEG. For both proteins, the capacity of the gel with no PEG attached was determined by traditional IMAC where the adsorption was based only on the interaction with immobilized copper ions on IDA. The capacities by frontal analysis were 11.0 mg/mL gel and 103 mg/mL gel for BSA and Lysozyme, respectively.

The adsorption capacities of both proteins of the hybrid gels decreased dramatically with increasing of PEG densities. The results are presented in Figures 3.10 and 3.11. The frontal analysis experimental data are presented in Figures 3.12 and 3.13 for lysozyme and BSA, respectively. From these data, it can be appreciated that there is a much sharper decrease in adsorption for BSA than for lysozyme. The BSA adsorption capacity dropped from 11 mg/mL to 0 mg/mL, while the lysozyme adsorption capacity dropped from 103

mg/mL to 0 mg/mL. From the results, the protein capacities drop to zero quickly with increasing PEG attachment. The lysozyme capacity decreased to 0 when the PEG density was larger than 30 µmol/mL, while the larger protein, BSA dropped its capacity to 0 when the PEG density is only 19 µmol/mL. This means the high PEG surface density will block proteins from the chelator and the larger protein requires less PEG on surface to fully block. The permeation effects of PEG as a space arm were proven here and the concept of SEIMAC was proven to work well. At the same time, the amino acid adsorption experiments show that very small molecules can permeate through the PEG layer and be adsorbed to chelators even if the PEG density is as high as 64 µmol/mL (see Figure 3.8). No trend is shown that the amino acid adsorption capacity decreases with increasing PEG surface density.

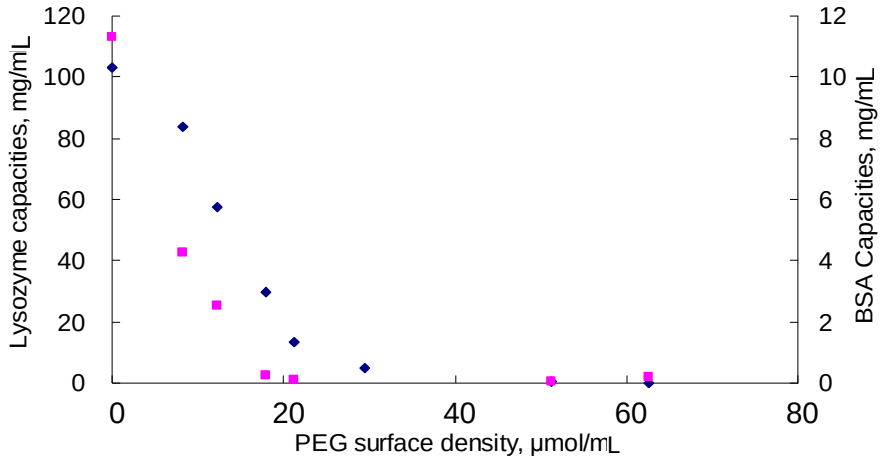

Figure 3.10 Proteins adsorption capacities in Novarose 300/40- PEG/IDA gel with constant IDA density and different PEG surface densities
■: BSA; ♦: lysozyme

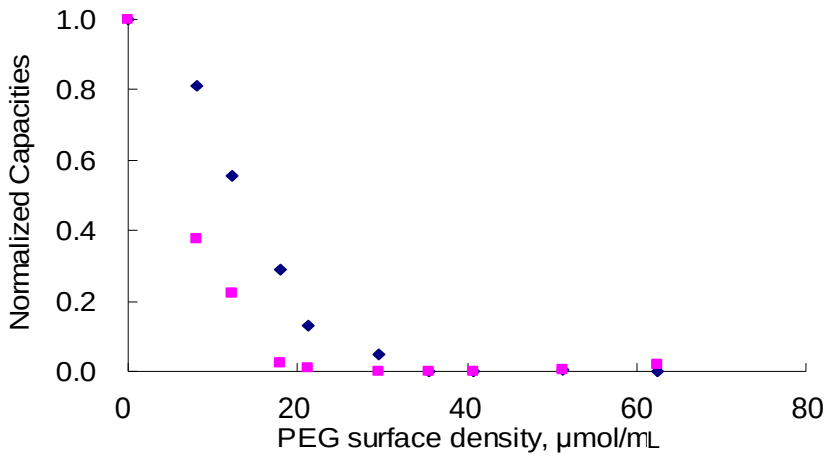

Figure 3.11 Normalized proteins adsorption capacities in Novarose 300/40- PEG/IDA gel with constant IDA density and different PEG surface densities
■: BSA; ♦: lysozyme

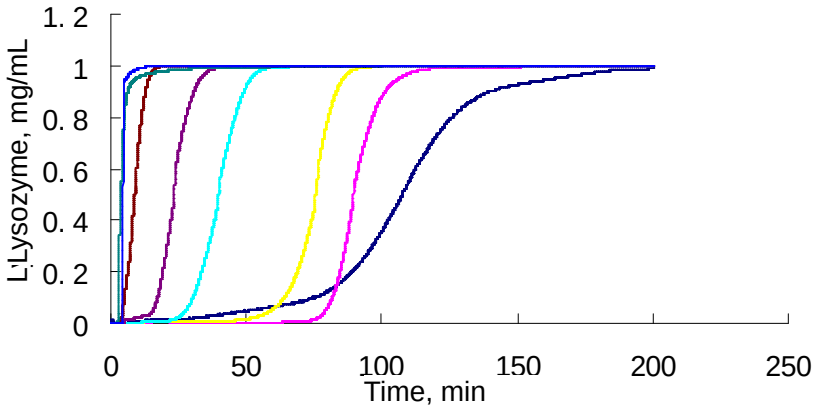

Figure 3.12 Frontal analysis of lysozyme in Novarose 300/40- PEG/IDA gels with constant IDA density and different PEG surface densities
—: 0 μmol/mL; —: 11.6 μmol/mL; —: 19.4 μmol/mL; —: 24.0 μmol/mL; —: 31.0 μmol/mL; —: 41.2 μmol/mL; —: 63.6 μmol/mL

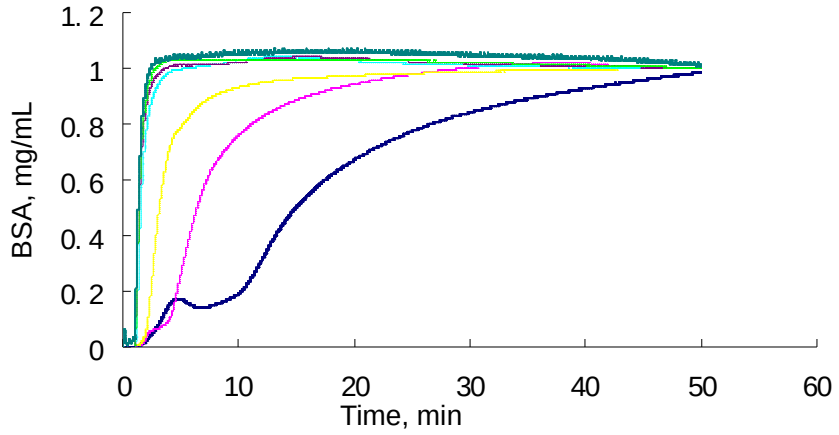

Figure 3.13 Frontal analysis of BSA in Novarose 300/40- PEG/IDA gels with constant IDA density and different PEG surface densities
—: 0 µmol/mL; —: 11.6 µmol/mL; —: 19.4 µmol/mL; —: 24.0 µmol/mL; —: 31.0 µmol/mL; —: 41.2 µmol/mL; —: 63.6 µmol/mL

The data show that lysozyme adsorbs proportionally less with the increase of PEG on the matrix. From Figure 3.11, the permeation effect seems very clear, when for example at a PEG density of around 24 µmol/mL gel the adsorption of BSA is practically zero while the adsorption of lysozyme is still quite significant. These results are clear evidences of the permeation effect. The frontal analysis presented in Figure 3.12 for lysozyme adsorption shows a typical IMAC adsorption scheme when no PEG is present and also how the adsorption decreases as the PEG density increases. The gel with high PEG density shows a typical behavior of gel size exclusion where PEG completely blocks the access to the IDA groups.

The frontal analysis for BSA presented in Figure 3.13 shows a similar behavior, even though BSA does not really adsorb effectively in IMAC columns. The adsorption usually observed in IMAC systems also decreases with the increase in PEG density, as in the case of lysozyme, upon the incorporation of PEG. Thus it is very clear that effective

polymer blocking has prevented the interaction of the proteins with the IDA groups on the agarose surface.

Conclusions

Novel hybrid chelating-polymer adsorbents were prepared and characterized for their selectivity to adsorb proteins of different molecular weights. This concept for protein adsorption presented here that combines affinity adsorption and polymer permeation was demonstrated using the chelator IDA as the affinity adsorbing ligand and the polymer PEG as the permeating polymer. Several hybrid IDA/PEG gels were synthesized on agarose based Sepharose and Novarose gels. Hybrid adsorbents with constant IDA density and variable PEG densities were effectively prepared. The adsorption and exclusion effect of the gels was successfully demonstrated with myoglobin (MW 17 kDa), BSA (MW 64 kDa) and lysozyme (MW 15 kDa). Adsorption experiments with these proteins show a remarkable decrease in adsorption with increased density of PEG on the gel surfaces. Selective permeation was observed with these proteins when BSA was excluded more effectively compared with the exclusion of lysozyme. The gels at all PEG densities show no permeation exclusion to small molecules as observed with constant adsorption capacities of tryptophan and copper. To increase the effectiveness of this approach, the systematic incorporation of both the ligand (in this case IDA) and the polymer (in this case PEG) will be essential to engineer adsorbents with specific and clear molecular weight cut-offs for proteins and other biomolecules. Theoretical models and/or experimental standard curves for the controlled coupling of IDA and PEG will help advance this new technique. In the next chapters, we

have performed kinetic studies and present results of the work to accomplish the development of adsorbents with specific IDA and PEG densities.

CHAPTER 4 KINETIC ANALYSIS OF GRAFTING OF CHELATORS ON CHROMATOGRAPHIC ADSORBENTS

Abstract

Chelating chromatographic techniques have been widely used in several research areas. One of their main applications is in protein separation technology and is the basis for Immobilized Metal ion Affinity Chromatography (IMAC). This work describes the coupling kinetics of a trident chelator, imino diacetic acid (IDA) to an epoxy activated chromatographic matrix. All the coupling studies were performed in a batch system at constant temperature, pH, and volume.

To assess the kinetics, HPLC frontal analysis of metal ion (i.e. Cu^{2+}) adsorption were performed that allowed for the indirect determination of the amount of IDA bound. The matrix was an epoxy activated polysaccharide agarose gel. The IDA coupling kinetics experimental data were used to propose a descriptive mathematical model of the IDA immobilization. The binding process apparently follows a reaction controlling process. The kinetic model can be used in our work to predict and control the desired amount of IDA density on adsorbents used in protein and metal ion separations..

Introduction

Among the affinity adsorption techniques, immobilized metal ion affinity (IMAC) is one of most important and widely used affinity chromatographic methods. IMAC utilizes the differential affinity of proteins for immobilized metal ions bound to a metal-chelating substance which is immobilized on a chromatographic matrix. After being

introduced by Porath et al. in 1975, IMAC, initially as a protein separation method, has been used in many other areas. The application of histidine tags for isolation of recombinant proteins and polypeptides is the best known improvement of this technique (Flaschel et al., 1993). Histidine and other metal affinity tags have made IMAC a powerful tool for protein and peptide purifications (Enzelberger et al., 2000).

The majority of the chelating groups used in IMAC are multidentate chelating agents. These multidentate chelators provide enough strength for the complex formed by the chelator, metal ion, and protein side chain. The more dentates the chelator has, the stronger the interaction between the chelator and the metal ion is, which causes a weaker interaction between the metal ion and the protein. This requires a balance between the two interactions in order to obtain optimized protein separation results.

The tridentate ligand, iminodiacetic acid (IDA), is the most commonly used metal chelator in IMAC separations. IDA is an N-substituted glycine derivative and its degree of coordination is used as a model for understanding the different conformations stabilized by the metal ions interacting with biological molecules. IDA interaction with a metal ion involves binding to the nitrogen atom and to two oxygen atoms of the carboxylic groups, thus leaving three chelating sites for protein or solvent molecules. In this research, copper (II) was used.

Normally, during the synthesis of chelating gels, they are fully coupled to the active sites of the matrix to obtain the highest capacity. There are not many references, if any, in the literature dealing with the kinetics of immobilization of chelators. This work describes the coupling kinetics of the iminodiacetic acid (IDA) chelating agent to epoxy

activated chromatographic matrix derivatives of Novarose and Sepharose.

To assess the coupling kinetics, experimental work was carried out using HPLC frontal analysis of metal ions (i.e. Cu^{2+}) adsorption, which allowed the determination of the amounts of IDA bound in a batch process. The matrix under study was an epoxy activated polysaccharide agarose gel schematically shown in Figure 4.1. The IDA coupling kinetics data obtained were analyzed by a simple mathematical model. The data thus obtained has been used in our work to control and prepare chromatographic adsorbents with specific amounts of IDA densities. To the best of our knowledge, no literature about the kinetics of immobilization of chelators has been reported.

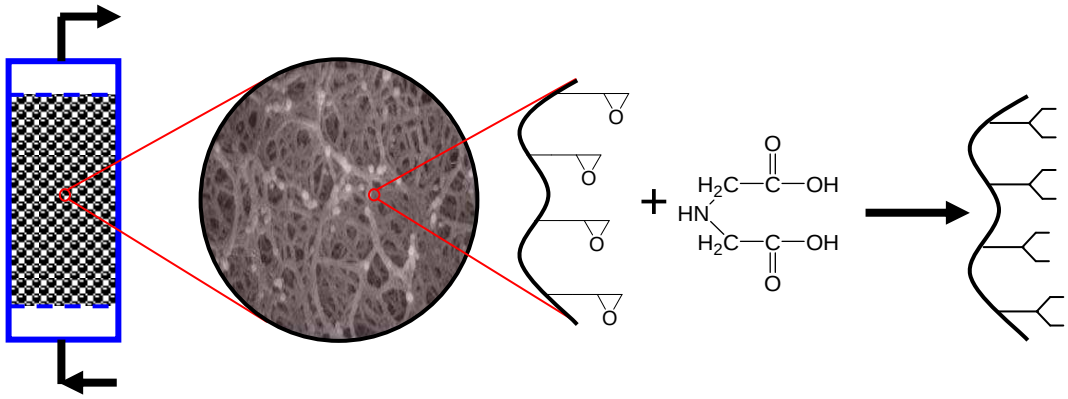

Figure 4.1 Schematic of IDA attachment onto epoxy activated agarose beads

Materials and Methods

The agarose gel matrix used in this work was Novarose Act high 300/40 gels from Inovata (Bromma, Sweden). Imino diacetic acid (IDA), cupric sulfate, sodium hydroxyl, sodium carbonate and hydrochloride acid (HCl) were from Sigma Company (St. Louis, MO, USA) and used as received. All chemicals utilized were of analytical or reagent grade.

Matrix (agarose) Activation

These Novarose gels are cross-linked agarose beads activated according to the bromohydrin method shown in Figure 4.2. Briefly, this method involved reacting the hydroxyl groups of the matrix with 3-bromo-1-propene, and then the resulting bromohydrin (4.2a) being treated with a high concentration of sodium hydroxide to form the epoxy groups (the active sites). This method gives a spacer arm with 4 to 16 atom lengths between the agarose backbone and the attached chelator.

IDA Coupling

The IDA coupling procedure is presented in Figure 4.3. Before reacting with the ligand IDA, the gel was thoroughly washed with DI water to remove the aqueous ethanol solution that is used as a preservative in these gels and suction dried in a sintered glass filter using vacuum.

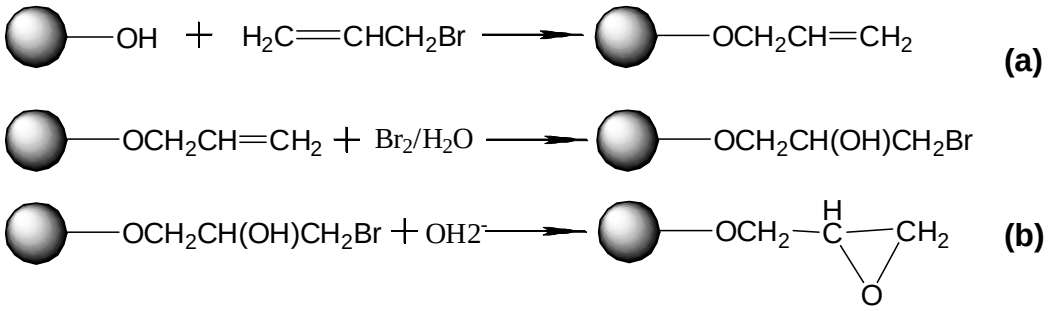

Figure 4.2 Activation procedure of agarose using bromohydrin method

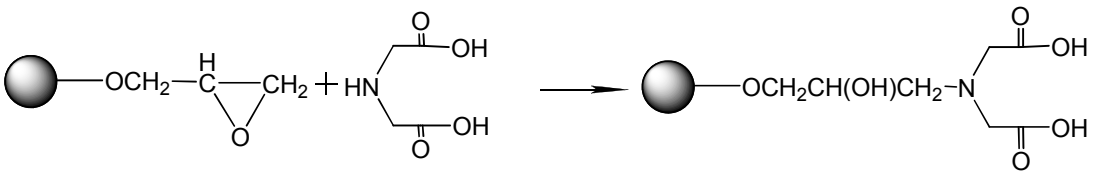

Figure 4.3 Coupling procedure of IDA to the epoxy activated agarose gel

This particular gel, Novarose 300/40, has an average size of 40 µm and a pore size

that corresponds to a molecular weight cut off of 300 kDa.

Experiments

A mass of 16 g of activated gel was evenly divided into eight 2.0 g fractions and transferred each to a 20-mL vial. A specified concentration of IDA and 1.0 M Na_2CO_3 were added to these vials and left to react for different time periods from 0 to 50 hours on a shaker at room temperature. Afterwards, the gel fractions were washed thoroughly with 0.1 M HCl, DI water, 0.1 M Na_2CO_3, and DI water again. The concentrations of IDA used in these experiments were 1%, 3%, and 6 % by weight. The pH value was maintained throughout the reactions at 11 in the 1.0 M Na_2CO_3 buffer.

In all the IDA modified gels, their copper ion capacities were measured by frontal analysis with a Gilson HPLC system using a 0.5-cm (i.d.) column that was packed with the IDA modified agarose gel beads. Steps of adsorption, washing, desorption, and regeneration of the adsorbent were executed by a programmable HPLC. In all the experiments, a flow rate of 0.2 mL/min was used to avoid back pressure problems. For the copper binding experiments, the column was first rinsed thoroughly with water equaling 20 times the column volume at pH 5.5. The copper solution was prepared at a concentration of 20 mM in water at pH 5.5. The unbound copper ions were removed with water using 10 column volumes. Afterwards, the chelating bound copper ions were eluted with a 0.1 M HCl solution with 10 column volumes followed with water until the pH was back to 5.5. Once the column was regenerated, the same procedure was repeated in triplicate for reproducibility.

Since IDA and copper ions complex theoretically with a 1:1 stoichiometry, the

moles of copper ion adsorbed onto the gel was assumed to be the same as the moles of IDA coupled onto the gels after saturation. This was the basis to evaluate the coupling kinetics of IDA onto the agarose gel surfaces.

Results and Discussion

IDA coupling

The reaction process in batch proceeded without major variations. The pH value in the reaction suspension always remained at 11 with the carbonate buffer. And the temperature was, for practical purposes, constant at around 25°C. The different concentrations of IDA did not add volume or viscosity to the reacting suspensions.

The removal of excess reagents (practically only IDA) was effective in the washing process. The IDA modified gel fractions were of a soft white color consistency. In addition, once the IDA modified gel was packed in the chromatographic columns, before the copper loading step, it was thoroughly washed with water until reaching a pH of 5.5. This step would further remove any non-covalently bound IDA molecules.

Copper Binding

The copper solution was fed to the column at a constant slow rate of 0.2 mL/min and the copper was clearly retained by the IDA modified gels. The color change on the gel was evident, from a soft white to a sky blue color, reflecting the effective binding of copper ions to the IDA-agarose gels. It was also observed in these experiments, that there was a difference in the blue color for the gels with different IDA densities, being deeper for the high IDA density gels, as expected. The feeding of the copper ions was continuously monitored by frontal analysis all the way until a breakthrough occurred.

This allows us to estimate the dynamic capacity of each IDA modified gel for copper. Such copper capacity was the one used to evaluate the amount of IDA bound to the agarose gels. The bound copper ions were eluted very effectively with 0.1 M HCl solution, followed by D.I water until the blue color clearly disappeared. In all the desorption experiments, a fine front of the desorbed copper was always observed. The elution continued until the pH value returned to 5.5. After this step, the analysis was repeated 3 times without major difference in the process.

The 24 gels synthesized with different initial concentrations of IDA and 8 different reaction times (the 24^{th} gel with no IDA bound to the matrix was used as a control), were all analyzed for copper capacity under the same condition using HPLC frontal analysis. These results are presented in Table 4.1 and in Figures 4.4-4.6 for copper capacities.

Table 4.1 Experimental conditions and analysis results

Run	Initial IDA concentration, %	Reaction time, hr	Copper capacities, μmol/mL
1	1%	0.25	2.0
2	1%	0.5	5.3
3	1%	1	12.0
4	1%	2	18.1
5	1%	4	32.4
6	1%	18	77.1
7	1%	26.25	87.4
8	1%	50.25	98.3
9	3%	0.25	10.4
10	3%	0.5	16.5
11	3%	1	31.6
12	3%	2	41.2
13	3%	4	47.8
14	3%	17	95.6
15	3%	27	109.5
16	3%	48	110.5
17	6%	0.25	10.8
18	6%	0.5	23.4
19	6%	1	42.0
20	6%	2	52.8
21	6%	17	103.2
22	6%	26	108.9
23	6%	48	109.8

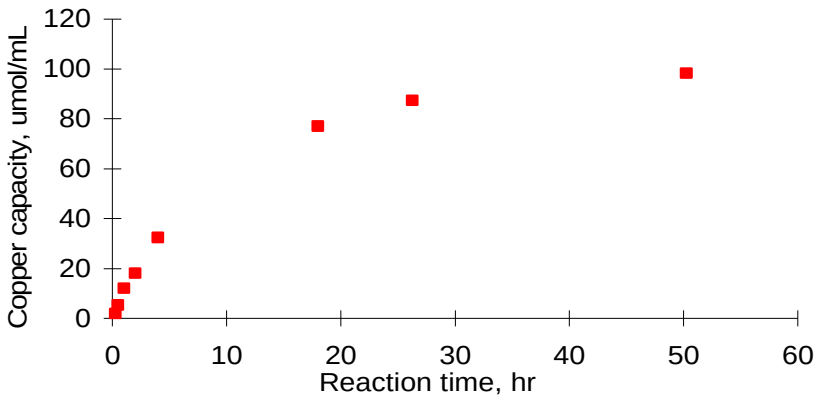

Figure 4.4 Copper capacities of gel for initial IDA reaction concentration of 1%

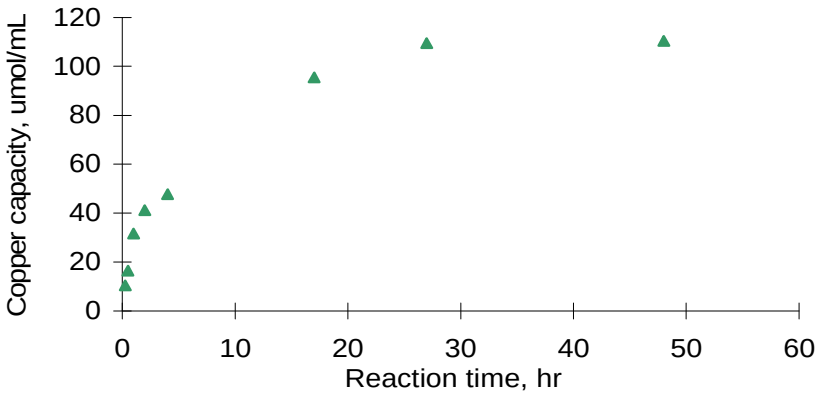

Figure 4.5 Copper capacities of gel for initial IDA reaction concentration of 3%

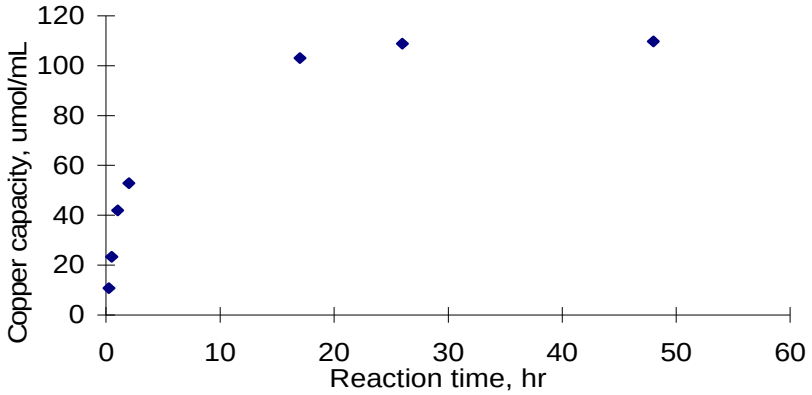

Figure 4.6 Copper capacities of gel for initial IDA reaction concentration of 6%

IDA Density Analysis

The amount of IDA immobilized onto the gel was determined indirectly based on the copper capacity for each IDA modified gel.

The experimental maximum copper capacity was 110 µmol of copper per mL gel and was obtained with the gels reacted with IDA at concentrations of 1%, 3% and 6%, and after exhaustive reaction periods (reaction times longer than 24 hours). After reaching this maximum capacity of copper, the assumption here is that all gel active sites have been modified with the chelator IDA.

In this analysis, we consider the manufacturer specifications (Inovata Company), where the copper capacity for the gel Novarose 300/40 is 111 µmol/mL gel and equivalent to the number of active sites substituted with IDA. Thus, with these characteristics, a ratio of moles of IDA and copper ion system can be considered of 1 to 1 at maximum capacity. Thus, for practical purposes, the IDA density on the gels was evaluated based on the copper capacity obtained by frontal analysis for each of the 24 gel

derivatives. It is important to consider however, that if this turns out not to be the case and the ratio is different than 1 to 1, it is still possible to consider the maximum capacity of copper bound to correspond to a normalized maximum density of IDA attached to the gel. Ultimately, the relevance of this work is that with these results, one could able to evaluate and control the amount of copper bound to a specific IDA-gel.

For practical purposes and commensurate with our goal, we can relate the copper capacity measurements to the IDA derivative reacted and attached to the surface. The IDA density on the gel as a function of time is presented in Figures 4.7-4.9 for the 3 initial IDA reaction concentrations.

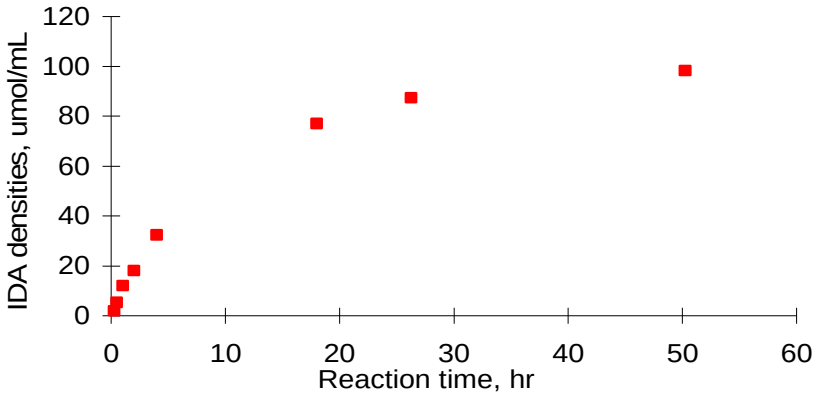

Figure 4.7 IDA surface densities of gel for initial IDA reaction concentration of 1%

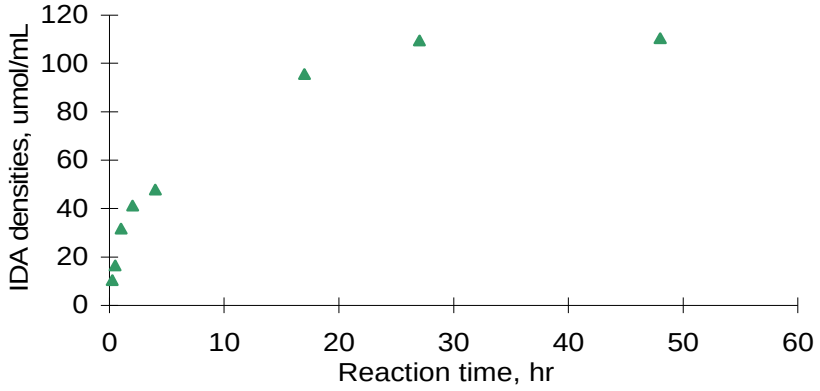

Figure 4.8 IDA surface densities of gel for initial IDA reaction concentration of 3%

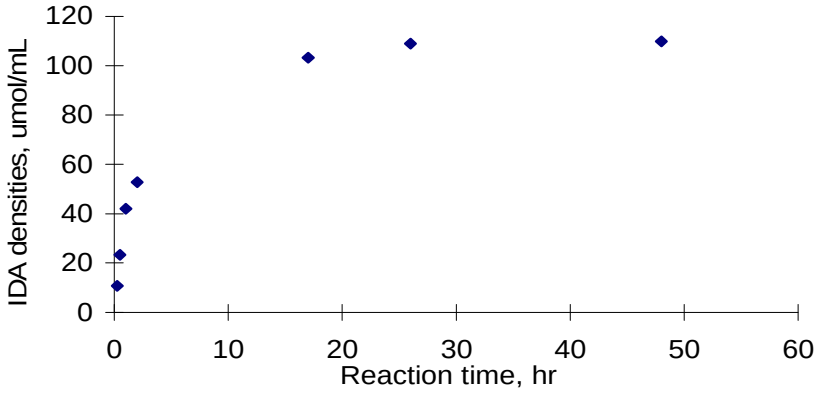

Figure 4.9 IDA surface densities of gel for initial IDA reaction concentration of 6%

The trend of the kinetic behavior for the 3 initial IDA concentrations is observed in Figure 4.10, which is a summary of the 3 previous Figures 4.7-4.9. Again, as an observation, each point represents an average value of 3 measurements. These results in terms of IDA kinetics reflect in fact, that the reaction of IDA with the active sites on the gel occurs irreversibly and at 100% IDA derivatization.

Here, the reaction between the active sites or epoxy groups on the matrix with the

IDA derivatives can be considered a nucleophilic substitution of a combination of second and first order irreversible reactions, this assumption is based on the analysis presented in the literature by Bruice (2004). These types of reactions involve several molecular rearrangements and therefore take a long time to proceed. The shape and behavior in Figures 4.7-4.9 with these reactions support this possible scenario.

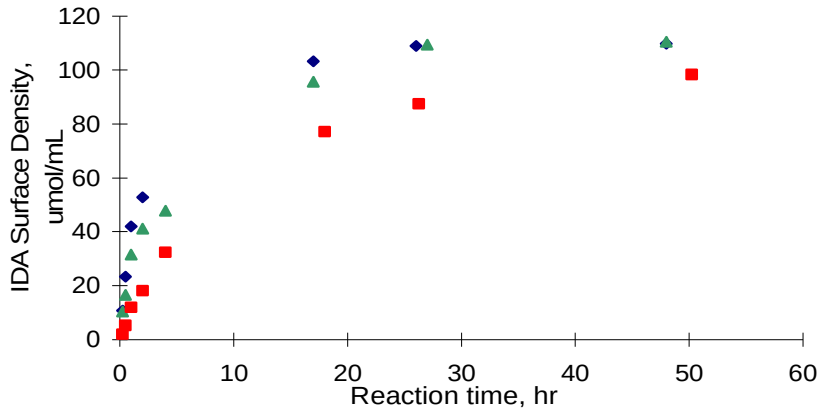

Figure 4.10 IDA attachment kinetics at room temperature with different IDA initial concentration ■: 1%; ▲: 3%; ♦: 6%

However, in order to assess and develop a quantitative model for these surface chemical reactions, all the possible steps involved in the coupling process, when carried out in a batch system will be considered. That is, (1) transport from the bulk phase to the gel particles, (2) film transport around the particles, (3) pore diffusion, and (4) chemical reaction and coupling with active sites on the gel internal surface.

The experimental maximum attachment density of IDA of 111 μmol/mL gel represents the maximum active site capacity of the gel. It is comparable to the amount of reactive sites given by the manufacturer. As mentioned, the IDA bound to the beads was

considered, for practical purposes, equal to the amount of copper ions bound. The maximum IDA density capacity for all the gel was then considered to be 111 μmol/mL and in this analysis will be denominated q_m.

Physical and Mathematical Modeling

The objective in this analysis is to present a model that would help elucidate and predict conditions (time and concentration) to obtain a desired ligand (chelator) density on chromatographic matrices.

The experimental results obtained in this work will be used to determine (1) how many of the reactive active sites on the matrix have been used; (2) how much chelator should be used in an attachment cycle; (3) the process time for a desired chelator density on the matrix. In an attempt to design and scale-up ligand immobilization in a systematic way, a mathematical model to predict the dynamic behavior of the coupling process was considered.

Physical Model

In this study, the kinetic model is based on the isothermal heterogeneous chemical reaction of a single chelator, IDA, to a porous spherical adsorbent particle, agarose beads with an average radius, r_m, and a porosity, ε_i, on which the reactive groups are epoxy derivatives grafted on the matrix. The reaction is performed in a well mixed flask with a total system volume, V. The volume of liquid external beads is $\varepsilon_b V$ and the bead volume is $(1-\varepsilon_b)V$. The initial and the transient chelator concentrations in the liquid are c_0 and c_i, respectively. The chelator concentrations in the liquid and solid phase of the agarose beads are c_i and q_i, respectively.

The conceptual physical model for the agarose beads with mass transfer and chemical reaction involves these four consecutive mass transport steps associated with the chemical binding of the solute IDA and represented in Figure 4.11. The first step involves bulk transport of the chelator in the solution phase. This is usually a rapid step because of the control exerted over the mixing intensity in the bulk solution and the convective flow. The second step, film transport, involves diffusion of the chelator through a hypothetical "stagnant film" which is the hydrodynamic stagnant boundary layer around the bead, characterized by the film coefficient, k_f and the radius of the stagnant film r_m. In the third step, pore diffusion, where the chelator is transported through the bead pores, which involves diffusion of the chelator within the pore network, characterized by a diffusion coefficient, D_i. The fourth step, the chemical reaction of the chelator onto the active sites of the beads, this involves the nucleophilic substitution reaction between the epoxy groups on the bead inner surface and the imino groups of IDA proposed in the literature. (Bruice, 2004; Horstmann et al., 1989)

Transport Model

The chemical reaction process in this work seems to be described best by rate theories. This process involves the use of conservation equations, kinetic laws of transport and chemical reaction, with appropriate initial and boundary conditions. For this analysis, the following steps are considered:

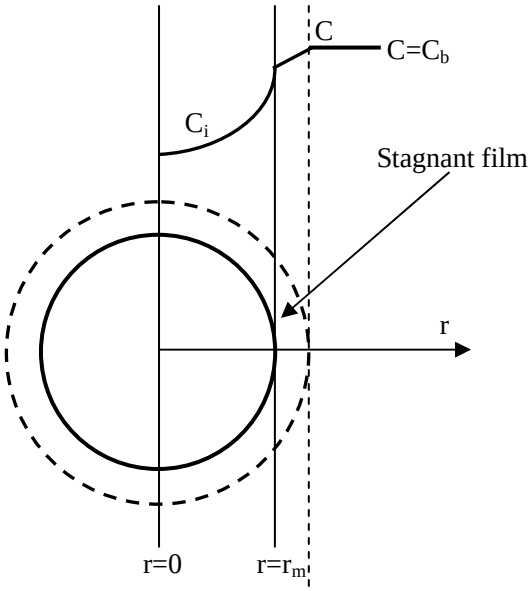

Figure 4.11 Schematic of consecutive steps of IDA transport and reactions in activated agarose beads

a) To describe the chelator concentration change with time in the bulk solution, and with resistance to mass transfer through the stagnant film from the bulk solution to the surface of the agarose beads, a mass balance based on a total batch volume, gives the following equation,

$$\frac{dc}{dt} = -\frac{3(\varepsilon_b)}{r_m(1-\varepsilon_b)} k_f (c - c_i)\Big|_{r=r_m} \tag{1}$$

where

k_f : Film mass transfer coefficient,

c : IDA concentration in the bulk,

c_i : IDA concentration inside of the pores,

ε_b : Bead volume ratio to batch total volume,

r_m : Radius of bead

Since this process takes place in a well mixed batch reactor system, we can assume

that no concentration gradients exist in the bulk solution:

$$\frac{\partial c}{\partial r} = 0 \qquad \text{for} \qquad r \geq r_m \tag{2}$$

b) the change of the chelator concentration in the fluid inside the pores can be derived by a mass balance of the chelator inside a spherical particle as,

$$\varepsilon_i \frac{\partial c_i}{\partial t} + \frac{\partial q_i}{\partial t} = \varepsilon_i D_i \left(\frac{\partial^2 c_i}{\partial r^2} + \frac{2}{r}\frac{\partial c_i}{\partial r}\right) \tag{3}$$

Where,

ε_i: Bead porosity,

q_i: IDA attached on the surface inside the pores base on bead volume,

D_i: Diffusion coefficient of IDA inside of the pores,

c) To describe the chemical reaction between the chelator and the active sites on the surface of the beads, a nucleophilic substitution reaction is considered between the epoxy group on the gel and the imino group of IDA. The structure of the epoxy groups allows it to undergo both an S_N1 (first order) reaction and an S_N2 (second order) reaction, where both reactions take place simultaneously (Bruice, 2004).

Thus, the total overall chemical reaction on the inner surface of the beads can be treated as a sum of a second and a first order irreversible reaction, as follows,

For the second order reaction: $A + S \longrightarrow P$ (4)

For the first order reaction: $A \xrightarrow{Slow} B^+ + S \xrightarrow{Fast} P$ (5)

Here,

A: Chelator agent, IDA,

S: Epoxy groups, (activated sites on the surface),

B^+: Intermediate compound

P: Products representing the attached IDA, (S-IDA)

The reaction rate for these surface reactions could be represented by an expression with contributions by both the S_N1 and S_N2 reactions according to Bruice (2004), thus, for the kinetics of IDA on the surface, one can write:

$$\frac{dq_i}{dt} = r_{S_N 2} + r_{S_N 1} = k_2 c_i (q_m - q_i) + k_1 (q_m - q_i) \tag{6}$$

Here,

q_m: Maximum (all active sites are used up) attached IDA on the surface of the beads,

$q_m - q_i$: Remaining free active sites in the interior of the beads.

Initial and Boundary Conditions:

d) At the beginning of the reaction, the chelator concentration in the bulk solution is c_0 and there is no chelator attached inside the beads, thus

$$\text{at } t = 0, \qquad c = c_0; \tag{7}$$

$$\text{at } t = 0, \qquad c_i = 0, \qquad 0 \le r \le r_m \tag{8}$$

$$\text{at } t = 0, \qquad q_i = 0, \qquad 0 \le r \le r_m \tag{9}$$

e) Considering that the beads are spherical and symmetric,

$$\text{at } r = 0, \qquad \frac{\partial c_i}{\partial r}\Big|_{r=0} = 0 \tag{10}$$

f) At the entrance of the pores, the following boundary condition applies:

$$\text{at } r = r_m, \qquad k_f (c - c_i)\Big|_{r=r_m} = \varepsilon_i D_i \frac{\partial c_i}{\partial r}\Big|_{r=r_m} \qquad t > 0 \tag{11}$$

Using the following dimensionless variables:

$$C = \frac{c}{c_0} \tag{12}$$

$$C_i = \frac{c_i}{c_0} \tag{13}$$

$$R = \frac{r}{r_m} \tag{14}$$

$$\tau = \frac{D_i t}{r_m^2} \tag{15}$$

$$\phi = \frac{q}{q_m} \tag{16}$$

The corresponding equations 1, 3, and 6 can be written as:

$$\frac{dC}{d\tau} = -\frac{3\varepsilon_b r_m}{(1-\varepsilon_b)D_i} k_f (C - C_i)\Big|_{R=1} \tag{17}$$

$$\frac{\partial C_i}{\partial \tau} + \frac{q_m}{\varepsilon_i c_o}\frac{\partial \phi_i}{\partial \tau} = (\frac{\partial^2 C_i}{\partial R^2} + \frac{2}{R}\frac{\partial C_i}{\partial R}) \tag{18}$$

$$\frac{d\phi_i}{d\tau} = \frac{r_m^2}{D_i}\left[k_2 c_0 C_i (1-\phi_i) + k_1 (1-\phi_i)\right] \tag{19}$$

And the initial conditions and boundary conditions become:

$$\tau = 0, \qquad C = 1; \tag{20}$$

$$\tau = 0, \qquad C_i = 0, \qquad 0 \le R \le 1 \tag{21}$$

$$\tau = 0, \qquad \phi_i = 0, \qquad 0 \le R \le 1 \tag{22}$$

$$R = 0, \qquad \frac{\partial C_i}{\partial R}\Big|_{R=0} = 0 \qquad \tau > 0 \tag{23}$$

$$R = 1, \qquad \frac{\partial C_i}{\partial R}\Big|_{R=1} = \frac{k_f r_m}{\varepsilon_i D_i}(C - C_i)\Big|_{R=1} \qquad \tau > 0 \tag{24}$$

Thus, the general model can be represented by equations 17 - 24. This is a set of nonlinear partial differential equations, and the solution can be obtained by numerical techniques. The question here is under what conditions this model can be simplified and

if the conditions used in this work would help produce such a simplified model. To assess this possibility, a reaction and transport time analysis was performed.

Time Scale Analysis

In order to obtain a practical assessment of the relevant steps on the kinetics of IDA coupling, we performed a simple time scale analysis considering that the total time t_{TOTAL} effectively determines the rate controlling steps in our system. Thus, the total time for the reaction and coupling of IDA involving the following time steps can be written as

$$t_{TOTAL} = t_B + t_F + t_D + t_R \tag{25}$$

t_{TOTAL}: Total time for solute transport from the bulk solution into the bead's inner surface and covalent binding to the surface,

t_B: Time for solute transport from the bulk solution to the stagnant film around the beads,

t_F: Time for solute transport through the stagnant film around the bead,

t_D: Time for solute diffusion inside the bead's pores,

t_R: Time for solute covalent binding to the bead's inner surface.

Bulk Mass Transfer Time Determination

In the present experiments, the reactions were performed in a well mixed batch reactor, thus, the time t_B was practically 0.

Film Mass Transfer Time Determination

The characteristic times for film mass transfer and for diffusion were estimated using empirical correlations, for instance, the characteristic film mass transfer time t_F of a solute within a stagnant film outside a gel particle, according to Geankopolis, (1983), can be approximated and calculated by the expression

$$t_F = \frac{r_m \varepsilon_b}{3k_f (1-\varepsilon_b)} \tag{26}$$

Here,

k_f: film mass transfer coefficient,

ε_b : Ratio of bead volume to batch total volume,

r_m : Radius of bead

The film mass transfer coefficient k_f for a solute like IDA stirred in a tank can be calculated by the following expression according to Geankopolis, (1983)

$$k_f = \frac{D_i}{r_m} + 0.31\left(\frac{\mu}{\rho D_i}\right)^{-\frac{2}{3}}\left(\frac{\Delta\rho\mu g}{\rho^2}\right)^{\frac{1}{3}} \tag{27}$$

Where

ρ: Particle density

Δρ: Density difference between the adsorbent particle and the liquid,

μ: Liquid viscosity

g: Gravitational constant

D_i: Diffusion coefficient of IDA

r_m : Bead radius

The particle density of agarose beads has been reported as 1100 kg/m^3 by Chase and Draeger (1992). From the Handbook of Chemistry and Physics (2007), the viscosity and density of water used here was obtained, where at 25 °C, the viscosity μ is 0.890 x 10^{-3} Pa·s and the density is 997 kg/m^3. Thus, the density difference Δρ is equal to 103 kg/ m^3.

Thus, for the system under consideration the k_f was calculated as 4.2 x 10^{-5} m/s using equation 27.

In the present experimental system, the bead volume ratio ε_b is 0.1. Thus, taking

these parameters into consideration using equation 26, the time t_F for chelator transport through the film outside bead surface can be calculated as 0.017 s.

Since in the laboratory, the experimental attachment of IDA to reach 50% bind takes more than 1 hour, one can consider that the stagnant film mass transfer of IDA is infinitely fast and offer no resistance to the transport process. This means the concentration c, in the bulk solution, for practical purposes, is equal to the concentration c_i, at the particle solution interface.

$$c = c_i \qquad \text{at} \quad r = r_m \tag{28}$$

Intraparticle Mass Transfer Time Determination

According to Champluvier and Kula (1992), the average diffusion time of a solute within a gel particle can be approximately determined by the following expression

$$t_D = \frac{L_D^2}{D_i} \tag{29}$$

Where

t_D: Average diffusion time,
L_D: Diffusion path
D_i: Diffusion coefficient of solute (IDA),

In this work, L_D can be approximately regarded as the bead radius r_m of the beads, in this case 20 μm. The pore diffusion coefficient D_i of IDA considered before is 8.4×10^{-10} m^2/s at 23ºC (Benjamin et al., 1999). Accordingly, taking these parameters into equation 29, the average intrapore diffusion time of IDA in the agarose beads is estimated as 0.5 s.

With the same constraints mentioned before, the experimental attachment of IDA took more than one hour to reach 50 % conversion. Thus, it seems that the intrapore diffusion step of IDA is considered also infinitely fast compared to the overall IDA binding process and the diffusion resistance is considered negligible as well.

Thus, considering the experimental data from this research and the empirical data for similar systems from the literature, we proceeded to develop a simplified model that accordingly can represent the overall IDA coupling process by considering the reaction of IDA from the inner particle fluid to the inner surface (surface reaction) as the overall rate controlling step. That is, the external mass transfer, film mass transfer, and intraparticle diffusion resistances become negligible.

With this physical evidence, we model and explain our experimental results with a simplified overall process that accordingly reduces equation 3 to the following expression, without considering the diffusion term.

$$\varepsilon_i \frac{dc}{dt} + \frac{dq_i}{dt} = 0 \tag{30}$$

This equation considers only the bead volume, to account for the overall batch volume in the system and again under the assumption that the IDA concentration is uniform in the liquid continuous phase, the above equation can be written as:

$$(1 - \varepsilon_b + \varepsilon_b \varepsilon_i) V \frac{dc}{dt} + \varepsilon_b V \frac{dq_i}{dt} = 0 \tag{31}$$

Where the term $(1 - \varepsilon_b + \varepsilon_b \varepsilon_i)$ is the ratio of the total liquid volume including pore volume and external volume to the system's batch total volume.

As stipulated before, the reaction between the epoxy groups of the gels and the

imino groups of IDA on the surface can be represented by the expression presented by Bruice, (2004):

$$\frac{dq_i}{dt} = k_2 c(q_m - q_i) + k_1(q_m - q_i) \tag{6}$$

Thus, equation 31 can be written as

$$(1 - \varepsilon_b + \varepsilon_b \varepsilon_i)\frac{dc}{dt} = -\varepsilon_b \left[k_2 c(q_m - q_i) + k_1(q_m - q_i)\right] \tag{32}$$

Here,

c : IDA concentration in the bulk phase based on the total volume of the system

c_0 : Initial IDA concentration based on the total volume,

q_i : Attached IDA density on the surface of the pores based on bead volume

q_m : Maximum attached IDA density bound to the surface of the beads

k_1 : First order reaction constant

k_2 : Second order reaction constant

The stoichiometric ratio between free IDA and attached IDA in this reaction is 1:1 as described below,

$$IDA + S \longrightarrow S - IDA, \tag{33}$$

Here S is an active site (epoxy group) on the gels.

Considering the overall mass balance and the stoichiometric ratio, one can write the change in concentration of IDA in the system as a function of the amount of IDA bound to the surface, that is, since

IDA moles in liquid = Initial IDA moles in liquid - IDA moles attached to the surface (34)

Thus, the IDA concentration in the solution can be written as a function of the IDA bound to the surface, q_i, as

$$c = c_0 - \frac{\varepsilon_b}{(1-\varepsilon_b+\varepsilon_b\varepsilon_i)} q_i \tag{35}$$

When c is substituted in equation 6 as c_i, the expression reduces to the following equation with q_i as the dependent variable as a function of time, or

$$\frac{dq_i}{dt} = k_2[c_0 - \frac{\varepsilon_b}{(1-\varepsilon_b+\varepsilon_b\varepsilon_i)} q_i](q_m - q_i) + k_1(q_m - q_i) \tag{36}$$

This equation is a first order ordinary differential equation that can be solved analytically with the initial condition:

$$\text{at } t = 0, \qquad q_i = 0 \tag{37}$$

Separating variables, integration gives the following equation,

$$\ln\left(\frac{k_2c_0 + k_1 - k_2\frac{\varepsilon_b}{(1-\varepsilon_b+\varepsilon_b\varepsilon_i)} q_i}{q_m - q_i}\right) = \left(k_2c_0 + k_1 - k_2\frac{\varepsilon_b}{(1-\varepsilon_b+\varepsilon_b\varepsilon_i)} q_m\right)t + \ln(\frac{k_2c_0}{q_m}) \tag{38}$$

This equation thus provides the coupling density of the chelator IDA as a function of time for the entire coupling process, from $q_i = 0$ to $q_i = q_m$.

However, to determine an estimate of the reaction rate constants k_1 and k_2 we consider the experimental values at the beginning of the coupling reaction when the amount of bound IDA is relatively small compared to the bulk concentration c_i or (c_0). Thus for short time binding, equation 36 can be written as

$$\frac{dq_i}{dt} = k_2c_0(q_m - q_i) + k_1(q_m - q_i) \tag{39}$$

Integration of this equation and using the same initial condition (equation 37) gives the following simplified result

$$\ln(q_m - q_i) = \ln(q_m) - (k_2 c_0 + k_1)t \tag{40}$$

This equation can be used now to obtain the reaction rate constants k_1 and k_2 by plotting $\ln(q_m - q_i)$ versus t. Thus with at least two sets of experimental data, one can obtain k_1 and k_2. In this case, 3 sets of data points were considered. The experimental data for this purpose was obtained using different values of the initial IDA concentration. Linear regression was used to calculate these values.

In Table 4.2, the corresponding c_0 (the IDA initial concentrations) and the value of the maximum active site capacity q_m are given.

Table 4.2 Experimental conditions of IDA attachment

IDA concentration	1%	3%	6%
C_0, base on total volume, µmol/mL	75.0	225.1	450.1
q_m, µmol/mL	111	111	111

In this approach, the first 4 data points (low q_i values) were used together with linear regression to obtain the slopes from equation 40. The results are given in Figure 4.12.

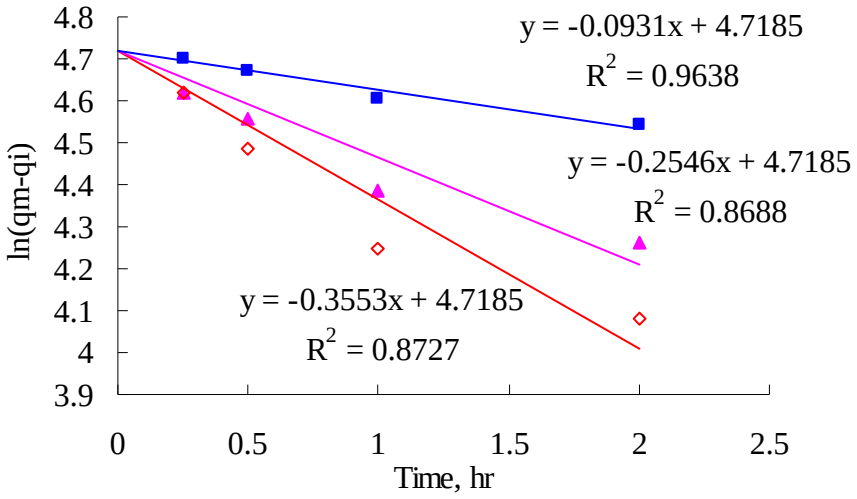

Figure 4.12 Plot to determine slopes using linear regression based on initial reaction data. Experiments were performed with different IDA initial concentrations.
■: 1%; ▲: 3%; ◊: 6%

The value of the slopes $-(k_2 c_0 + k_1)$ obtained here by linear regression are summarized in Table 4.3

Table 4.3 Slopes calculated using linear regression

IDA concentration	1%	3%	6%
Slope, $-(k_2 c_0 + k_1)$	0.0931	0.2546	0.3553

The term $-(k_2 c_0 + k_1)$ from Table 4.3 is a linear function $y(c_0)$, $[y = -(k_2 c_0 + k_1)]$. By plotting this function $y(c_0)$ versus the initial concentration c_0 and linear regression, the slope gives the reaction rate constant k_1 and the intercept gives the reaction rate constant k_2. The resulting values are presented in Table 4.4

Table 4.4 Reaction rate constants k_1 and k_2

k_1, hr^{-1}	6.45×10^{-2}
k_2, $mL \cdot \mu mol^{-1} \cdot hr^{-1}$	6.79×10^{-4}

Once the reaction rate constants k_1 and k_2 are determined, Equation 38 can now be used to calculate the complete IDA coupled (q_i) onto the matrix as a function of time. The resulting calculations with this model are plotted in Figure 4.13 (solid line) together with the experimental data at different initial IDA concentrations. The experimental data fit relatively well into the model considering the given conditions. For practical purposes, the model provides a good guide for the control of the chelator density on this type of gel matrices.

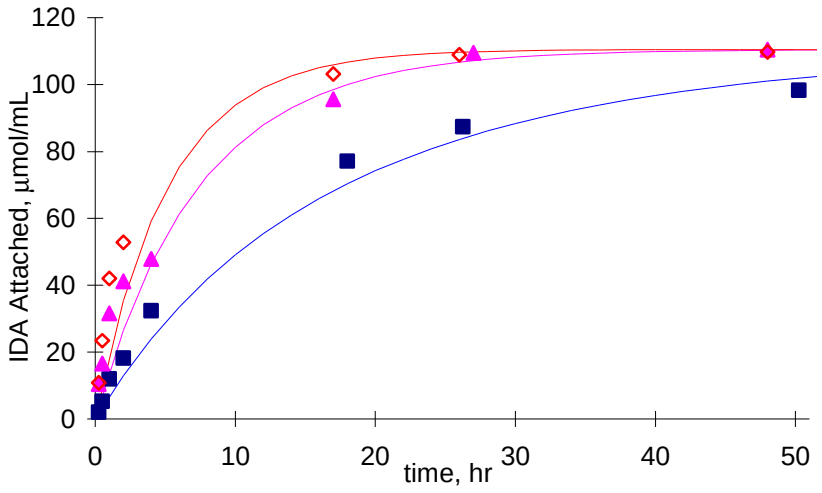

Figure 4.13 IDA attachment kinetics at room temperature with different IDA concentrations
■: 1%; ▲: 3%; ◊: 6%

Conclusions

Kinetic experiments of the attachment of the chelator IDA onto agarose activated

matrices were performed at different initial IDA concentrations as a function of binding reaction time until saturation of all active sites in the matrix was obtained.

A mathematical model was considered in order to obtain theoretical standard curves for IDA coupling. The effort to incorporate a theoretical aspect to the immobilization of affinity ligands to chromatographic matrices seems, according to this first attempt, to be in the right direction. The model proposed here, when mass transfer limitations do not control the overall attachment of ligands, appears to be surface reaction controlled only. This model can help predict chelator loading densities and thus provides the means to prepare affinity matrices with the desired amount of ligands in general for specific protein chromatographic applications. The physical model seems to be accurate with respect to the behavior of chelating ligand attachment to the agarose matrices used here. The mathematical model gives practical estimates of the amount of material bound to matrices as a function of time. This modeling effort will provide an approximated scheme to incorporate IDA densities that allows other ligand attachments such as polymers, and will help optimize metal ions and protein binding.

CHAPTER 5 KINETIC ANALYSIS OF IMMOBILIZATION OF POLYMERS ON CHROMATOGRAPHIC ADSORBENTS

Abstract

The attachment kinetic analysis of a hydrophilic polymer, polyethylene glycol (PEG) to chromatographic matrices is described in this work. PEG was incorporated in these matrices to assess its affect as an adsorption controlling agent. By coupling different degrees of PEG onto surfaces, different blocking arm densities controlled, for example, proteins and metal ions access to ligand groups on such surfaces. By controlling the degree of PEG on the surface, agarose gels seems to have a size exclusion effect on proteins in a new bioseparation scheme under development.

To measure the kinetics and degree of modification of PEG on the gels, an indirect method was used to determine the PEG attachment. After each PEG attachment, the remaining non occupied active sites in the gels were reacted with a functional chelator, iminodiacetic acid (IDA), which, upon incorporation on the surface, can bind metal ions. Frontal analysis of the copper binding capacity on IDA was monitored at different times and degrees of PEG attachment, this approach allowed for the effective determination of PEG on the surface. The binding of PEG was used to control the size exclusion effect on IMAC adsorption of proteins or peptides to surfaces. In this work, the adsorbents under study were polysaccharide agarose based chromatographic matrices. Epichlorohydrin (EPI) was chosen as the active bifunctional linker on the gels and M-PEG-NH_2 with a molecular weight of 5000 was used as the blocking permeating agent. The results of PEG

coupling kinetics data suggests a physical scheme based on chemical diffusion and second order reaction.

Introduction

It is well known that a grafted hydrophilic, nonionic polymer chain can reduce protein adsorption on surfaces (Stolnik et al., 1995). Polyethylene glycol (PEG) or sometimes called polyethylene oxide (PEO) is synthetic, nontoxic, and water-soluble and is one of the most used polymers for preventing protein non-specific adsorption. PEG is hydrophilic and uncharged and it can form highly hydrated polymer coils on biomaterial surfaces, which effectively repel proteins. The energy to remove bound water molecules makes the process of protein adsorption extremely unfavorable for thermodynamic reasons (Gombotz et al., 1992).

PEGylation of a surface can be achieved in different ways, for example, by adsorbing PEG-containing block copolymers on the surface (Stolnik et al., 1997), by surface grafting using established strategies (Sofia et al., 1998b), by depositing PEG-like coatings using a radiofrequency glow discharge technique (Shen et al., 1993) or by forming self assembled monolayers (Prime et al., 1993).

The physical adsorption of PEG-containing copolymers has the disadvantage of possible desorption from the surface during protein separation operations. On the other hand, chemical covalent grafting of PEG via functional groups present on the surface is well controllable in terms of PEG length, density, and orientation (Harris and Zalipsky, 1997). This is the approach used in this work.

In this work, the attachment kinetics of PEG to chromatographic matrices is

described in terms of coupling different degrees of PEG onto agarose gel surfaces to provide different block arm densities to possibly control protein access to IDA groups or surfaces. The degree of PEG on the gel surface provides size exclusion effects for protein adsorption. This behavior will be used to explain and explore a new bioseparation scheme.

The reaction scheme of PEG attachment to gel porous beads is presented in Figure 5.1. The gel activated with EPI reacts with the primary amino groups of amino-PEG derivatives to form a structure resembling a PEG shield on the surface. Figure 5.2 describes schematically the reaction between the epoxy group of EPI and the amino group of M-PEG-NH_2.

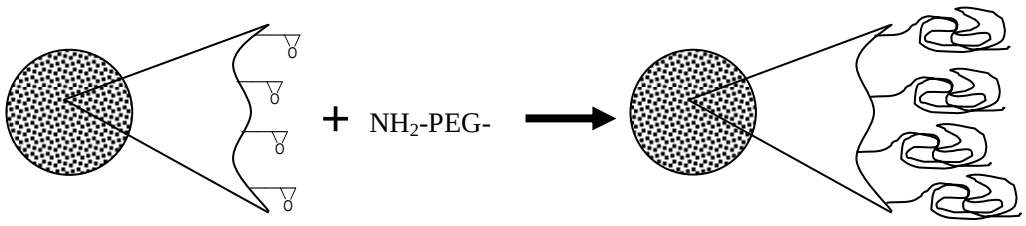

Figure 5.1 Schematic of M-PEG-NH_2 grafting and structure on activated agarose beads

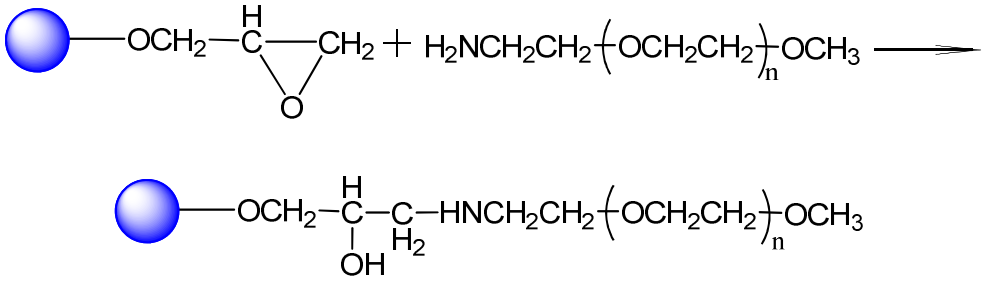

Figure 5.2 Coupling reaction scheme of amino PEG to EPI activated agarose gels

Materials and Methods

The chromatographic matrices were Novarose and Sepharose gels. Novarose gels

were obtained from Inovata Company (Bromma, Sweden) and Sepharose gels were purchased from Pharmacia Company (Uppsala, Sweden). Methoxyl-polyethylene glycol amine (MW: 5000), imino diacetic acid (IDA), epichlorohydrin (EPI), sodium hydrogen boride ($NaBH_4$), cupric sulfate, sodium hydroxyl, sodium carbonate and concentrated hydrogen chloride acid (HCl) were purchased from Sigma (St. Louis, MO, USA). All chemicals utilized were of analytical or reagent grade and used as they arrived.

Activation of Agarose Gels

The activation procedure of the gel is shown schematically in Figure 5.3. For each experiment, before use, a given amount gel was thoroughly washed with deionized water (DI) to remove the storage preservative (ethanol) and suction dried in a sintered glass filter using vacuum. In a typical set of experiments, a mass of 14 g of the suction dried gel was measured into a beaker. To this beaker, 7.5 mL of epichlorohydrin, 20 mL of 0.6 M NaOH, and 30 mg of $NaBH_4$ were added. The mixture was continuously stirred at room temperature. Afterwards, other 20 mL of 0.6 M NaOH and 7.5 mL of EPI were added in small portions over a period of 1.5 hours. This mixture was stirred for 24 hours at room temperature and then washed thoroughly on a sintered-glass filter with 0.1 M HCl, deionized (DI) water, 0.1 M Na_2CO_3, and DI water, in succession.

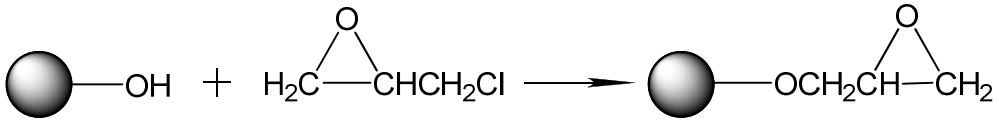

Figure 5.3 Activation reaction scheme of agarose with epichlorohydrin

Coupling and Determination of PEG and IDA in Agarose Gels

The previously activated gel was evenly divided into seven 2.0 g fractions and

transferred into seven 20-mL vials. To one vial, sample 1, an excess of IDA was added and exhaustively reacted to determine its maximum active site capacity as assessed by its chelating interaction to copper ions, and to the other 6 vials, a uniform initial concentration of M-PEG-NH_2 5000 and 2.0 M Na_2CO_3 were added and reacted for different time periods (from 0 to 70 hours) at room temperature. After that, each sample of reacted gel was washed thoroughly with 0.1 M HCl, DI water, 0.1 M Na_2CO_3, and DI water, in succession.

Following the PEG attachment, the gels were exhaustively reacted with IDA and resulting IDA densities on the gel were measured via copper ion binding. The PEG densities grafted on the gel were thus calculated by subtracting the amount of IDA bound from the total active group capacity previously determined with IDA saturated gels when no PEG was used (gel sample 1).

The 6 PEG modified gel fractions were exhaustively reacted with an excess of IDA after each PEG attachment experiments as follows: 0.7 g of IDA and 15 mL of 1.0 M Na_2CO_3 were added to each vial and the mixtures were shaken for 24 hours to assure that all remaining active sites reacted with IDA. The procedure was repeated in general with varying initial concentrations of PEG from 0.2 g/mL to 0.7 g/mL.

Copper Capacity Measurement for All Agarose Gels

Copper capacities of IDA and PEG modified gels were measured by frontal analysis using a Gilson HPLC system. In all these experiments, a 0.5-cm (i.d.) chromatographic column was packed with the hybrid PEG and IDA modified agarose gel beads. A program for adsorption, desorption, and regeneration of the adsorbent was executed by a

programmable HPLC. A flow rate of 0.2 mL/min was used to avoid back pressure problems.

The matrices used and activated in this work included (only reported here) Novarose 1000/40 gel and Sepharose 6B gel. The activation of these gels was performed with EPI in 2.0 M Na_2CO_3 for 24 hours. Novarose 300/40 Activated High gel which was already activated by the manufacturer (Inovata) was also used. Different initial concentrations of PEG were used with the reaction on the Novarose 1000/40 and Novarose 300/40 gels.

Results and Discussion

Copper and PEG Binding Density of Sepharose-PEG Gels

For the coupling reaction on Sepharose 6B gels with an initial PEG solution concentration of 1.0 g/mL, the maximum density of active sites was 20 µmol/mL gel as assessed by measuring the copper capacity using frontal analysis as described before. The copper capacities for the gels with different densities of PEG attached are given in the Table 5.1, the values obtained were from 19.9 µmol/mL gel to 3.42 µmol/mL gel, corresponding to values of PEG attached from 0 to 16.5 µmol/mL, respectively. The corresponding reaction times were from 0 to 16 hours. In graphical form, the resulting PEG density on the gel versus time is given in Figure 5.4.

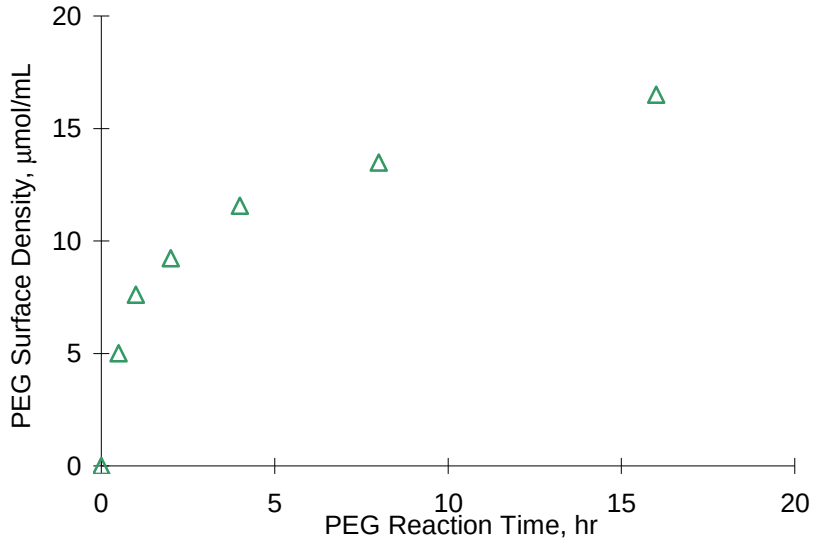

Figure 5.4 PEG coupled density versus reaction time on Sepharose 6B gels

Table 5.1 PEG density on Sepharose gel determined by copper capacities measurement

PEG Reaction Time, hr	Copper capacity, µmol/mL	PEG Density, µmol/mL
0	19.92	0
0.5	14.91	5.01
1	12.31	7.61
2	10.68	9.24
4	8.36	11.56
8	6.43	13.49
16	3.42	16.50

From Figure 5.4, it can be seen that the PEG density on the gels increases monotonically with reaction time and tends to reach a maximum value of about 20 µmol of active sites per mL gel. In these experiments with Sepharose gel, the largest experimental reaction time was only 16 hours, and this gel was not completely saturated with PEG.

Novarose 1000/40-PEG Gels *(Low Copper Capacity Gels)*

For the coupling reaction on Novarose 1000/40 gels, the maximum active site density was 21 µmol/mL gel assessed by copper capacity measured by frontal analysis. The copper capacities for the gels with different densities of PEG attached are given in Tables 5.2 - 5.4. The reaction time for these modifications ranged in this case from 0 to 64 hours and PEG initial concentrations ranged from 0.2 g/mL to 0.7 g/mL

The results for these PEG densities are plotted in Figure 5.5. The PEG densities on these gels, as with the Sepharose gels, increase monotonically and tend to also reach the maximum density corresponding to the copper maximum capacity as well.

Table 5.2 PEG density on Novarose gel determined by copper capacities measurement with initial PEG solution concentration of 0.2 g/mL

PEG reaction time, hr	PEG initial concentration, 0.2 g/mL	
	Copper capacity, µmol/mL	PEG density, µmol/mL
0	20.66	0
0.25	20.25	0.41
1	19.37	1.30
4	17.37	3.29
16	12.61	8.05
64	6.04	14.62

Table 5.3 PEG density on Novarose gel determined by copper capacities measurement with initial PEG solution concentration of 0.4 g/mL

PEG reaction time, hr	PEG initial concentration, 0.4 g/mL	
	Copper capacity, µmol/mL	PEG density, µmol/mL
0	20.66	0
0.25	20.48	0.19
1	19.95	0.71
4	15.61	5.05
16	10.86	9.80
64	4.55	16.12

As seen in Table 5.2, the initial PEG solution concentration was 0.2 g/mL, the copper capacities ranged from 20.66 to 6.04 µmol/mL gel corresponding to values of attached PEG from 0 to 14.6 µmol/mL. The reaction time corresponding to these modifications were from 0 to 64 hours

For the initial PEG solution concentration of 0.4 g/mL, the copper capacities ranged from 20.66 to 4.55 µmol/mL gel corresponding to values of PEG density from 0 to 16.1 µmol/mL presented in Table 5.3. The reaction time were the same from 0 to 64 hours

For the initial PEG solution concentration was 0.7 g/mL, the copper capacities ranged from 19.09 to 2.18 µmol/mL gel corresponding to values of PEG from 1.6 to 18.5 µmol/mL. The same reaction times from 0 to 64 hours were used as shown in Table 5.4.

In graphical form, the PEG densities on the gel surface versus reaction time with different initial PEG concentrations are plotted in Figure 5.5. Similarly to the Sepharose PEG system, the PEG densities increased with reaction time with a tendency to reach the maximum value of about 20 µmol/mL gel. From Figure 5.5, it can be seen that the kinetics of binding is a function of the initial PEG concentration as in the case of IDA kinetics previously described. From here, the idea that the kinetic model of PEG attachment might follow the same physical model proposed for IDA kinetics was developed. In this case, however, the maximum value for coupled PEG on the surface was never equal to the maximum capacity of total active sites, even after 64 hours of reaction. It appears that since PEG is a much larger molecule than IDA, that after it is bound to the surface, the steric effects might play a role in the last stages of coupling when saturation was approaching.

Table 5.4 PEG density on Novarose gel determined by copper capacities measurement with initial PEG solution concentration of 0.7 g/mL

PEG reaction time, hr	PEG initial concentration, 0.7 g/mL	
	Copper capacity, µmol/mL	PEG density, µmol/mL
0	19.09	0
0.25	18.80	1.86
1	16.32	4.34
4	13.82	6.84
16	6.43	14.23
64	2.18	18.48

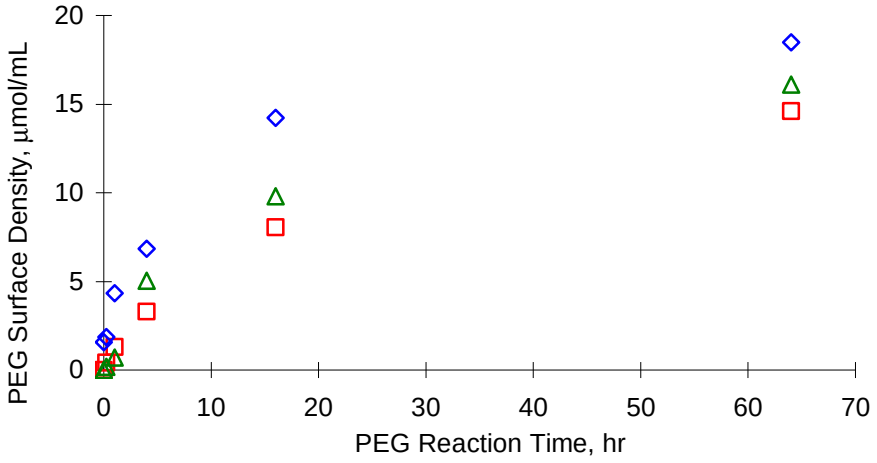

Figure 5.5 PEG attachment kinetics on Novarose 1000/40 gels activated by EPI with different initial PEG concentrations
□: 0.2 g/mL; Δ: 0.4 g/mL; ◊: 0.7 g/mL

Novarose 300/40-PEG Gels (High Copper Capacity Gels)

For the coupling reaction on Novarose 300/40 Activated High gels, the maximum active site density was 104.6 µmol of copper per mL gel as assessed by copper capacity determined by frontal analysis. The copper capacities for the gels with different densities of PEG attached are given in Table 5.5 ranging from 104.6 to 60 µmol/mL of gel, corresponding to values of PEG attached from 0 to 43.6 µmol/mL. The reaction time

corresponding to these modifications were from 0 to 25.5 hours.

In graphical form, the PEG densities on these gel surfaces versus reaction time are plotted in Figure 5.6.

Table 5.5 Copper capacities of the Novarose 300/40 Activated High gels

PEG reaction time, hr	IDA density, µmol/mL	PEG density, µmol/mL
0	104.6	0
0.5	99.6	11.6
1	91.9	19.4
3	87.6	24.0
5	73.6	31.0
18.5	63.4	41.2
25.5	60.0	43.6

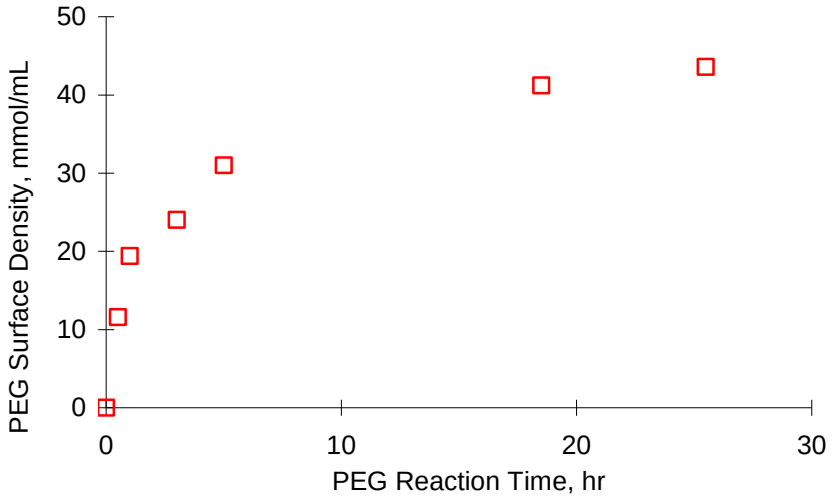

Figure 5.6 PEG attachment kinetics on Novarose 300/40. Activated High gel with PEG-NH_2 concentration of 0.2 g/mL

In this gel, the PEG density increased with reaction time and approaches a maximum value of about 44 µmol/mL gel compared to the maximum active site density of about 110 µmol/mL gel. Obviously, in this case not all the binding sites on the matrices

were able to react with PEG molecules even after exhaustive PEGylation. In all the cases, after exhaustive PEG treatment, we could still observe binding of IDA groups onto the matrices. It appears that on these surfaces with high binding capacities, there are some relatively inaccessible reactive sites that do not allow the incorporation of large molecules such as PEG (MW 5000 Da) to interact on the activated surfaces compared with the IDA groups (MW 134 Da) which are smaller molecules. Still another reason might be that steric hindrance provided by the immobilized PEG molecules makes the path to the surface more difficult and inaccessible. This is an area of research that could be explored to further answer these questions.

The experimental data obtained from all these adsorbents was used to develop a physical and mathematical model for PEG attachment to chromatographic matrices. The resulting model can help systematically prepare new matrices in affinity chromatography and in enzyme immobilization systems as well as in development of smart surfaces for biosensor applications.

Physical and Mathematical Model

The objective in this analysis is to present a model that would help elucidate and predict conditions (time and concentration) to obtain a desired polymer density on chromatographic matrices. The experimental results obtained in this work will be used to determine (1) how many of the reactive active sites on the matrix have been used; (2) how much chelator should be used in an attachment cycle; (3) the process time for a desired polymer density on the matrix. In an attempt to design and scale-up ligand immobilization in a systematic way, a mathematical model to predict the dynamic

behavior of the coupling process was considered.

Physical Model

In this study, the kinetic model is similar to the previous IDA binding model based on the isothermal heterogeneous chemical reaction of a single polymer, PEG, to a porous spherical adsorbent particle, agarose beads with an average radius, r_m, and a porosity, ε_i, on which the active group, epoxy is immobilized. The reaction is performed in a well mixed flask with a total system volume, V. The volume of liquid external beads is $\varepsilon_b V$ and the bead volume is $(1-\varepsilon_b)V$. The initial and the transient polymer concentrations in the liquid are c_0 and c_i, respectively. The polymer concentrations in the liquid and solid phase of the agarose beads are c_i and q_i, respectively.

Mathematical Model

To obtain a mathematical description of a batch chemical reaction system, similar to the previous chapter, three consecutive transport rate resistances are considered: film mass transfer near the beads outside the surfaces, diffusion in the porous beads, and kinetic chemical reaction between the polymer (PEG) and the active site (epoxy). The same general governing equations were obtained. For stagnant film transport,

$$\frac{\partial c}{\partial t} = -\frac{3(\varepsilon_b)}{r_m(1-\varepsilon_b)} k_f (c - c_i)\Big|_{r=r_m} \tag{1}$$

and for intraparticle diffusion,

$$\varepsilon_i \frac{\partial c_i}{\partial t} + \frac{\partial q_i}{\partial t} = \varepsilon_i D_i \left(\frac{\partial^2 c_i}{\partial r^2} + \frac{2}{r}\frac{\partial c_i}{\partial r}\right) \tag{2}$$

Where,

k_f : Film mass transfer coefficient,

c : PEG concentration in the bulk,

c_i : PEG concentration in the pores,

ε_b : Bead volume ratio to batch total volume,

r_m : Bead radius,

ε_i : Bead porosity,

q_i : Attached polymer on the surface inside the pores,

D_i : Diffusion coefficient of PEG.

The chemical reaction between the amino groups of the polymer and the active sites, epoxy groups on the surface of the beads, is a nucleophilic substitution reaction. The reaction undergoes both a S_N1 reaction and a S_N2 reaction, both reactions take place simultaneously (Bruice, 2004).

Thus, the total overall chemical reaction on the inner surface of the beads can be treated as a sum of second and first order irreversible reactions. The overall reaction rate for this surface reaction could be represented by an expression:

$$\frac{dq_i}{dt} = r_{SN2} + r_{SN1} = k_2 c_i (q_m - q_i) + k_1 (q_m - q_i) \tag{3}$$

Here,

q_m : Maximum (all active sites are used up) attached IDA on the surface of the beads,

$q_m - q_i$: Remaining free active sites in the interior of the beads.

Similarly to the previous chapter, the boundary and initial conditions are as follows:

$$\text{at } t = 0, \qquad c = c_0; \tag{4}$$

$$\text{at } t = 0, \qquad c_i = 0, \qquad 0 \le r \le r_m \tag{5}$$

$$\text{at } t = 0, \qquad q_i = 0, \qquad 0 \le r \le r_m \tag{6}$$

$$\text{at } r = 0, \qquad \frac{\partial c_i}{\partial r}\Big|_{r=0} = 0 \tag{7}$$

$$\text{at } r = r_m, \qquad k_f (c - c_i)\Big|_{r=r_m} = \varepsilon_i D_i \frac{\partial c_i}{\partial r}\Big|_{r=r_m} \quad t > 0 \tag{8}$$

Using the following dimensionless variables, this chemical reaction model can be written in dimensionless form.

$$C = \frac{c}{c_0} \tag{9}$$

$$C_i = \frac{c_i}{c_0} \tag{10}$$

$$R = \frac{r}{r_m} \tag{11}$$

$$\tau = \frac{D_i t}{r_m^2} \tag{12}$$

$$\phi = \frac{q}{q_m} \tag{13}$$

The corresponding equations are:

$$\frac{\partial c}{\partial t} = -\frac{3(\varepsilon_b)}{r_m(1-\varepsilon_b)} k_f (c - c_i)\Big|_{r=r_m} \tag{14}$$

$$\frac{\partial C_i}{\partial \tau} + \frac{q_m}{\varepsilon_i c_o}\frac{\partial \phi_i}{\partial \tau} = \left(\frac{\partial^2 C_i}{\partial R^2} + \frac{2}{R}\frac{\partial C_i}{\partial R}\right) \tag{15}$$

$$\frac{\partial \phi_i}{\partial \tau} = \frac{r_m^2}{D_i} q_m \left(k_2 c_0 C_i (1-\phi) + k_1 (1-\phi)\right) \tag{16}$$

The initial conditions and boundary conditions become

$$\tau = 0, \qquad C = 1; \tag{17}$$

$$\tau = 0, \qquad C_i = 0, \qquad 0 \le R \le 1 \tag{18}$$

$$\tau = 0, \qquad \phi_i = 0, \qquad 0 \le R \le 1 \tag{19}$$

$$R = 0, \qquad \frac{\partial C_i}{\partial R}\Big|_{R=0} = 0 \quad \tau > 0 \tag{20}$$

$$R = 1, \qquad \frac{\partial C_i}{\partial R}\Big|_{R=1} = \frac{k_f r_m}{\varepsilon_i D_i}(C - C_i)\Big|_{R=1} \quad \tau > 0 \tag{21}$$

Thus, the general model for this batch chemical reaction problem can be represented by equations 14 - 21. This is a set of nonlinear partial differential equations, and the solution can be obtained by numerical techniques.

Under the working conditions of this research, these governing equations will be similarly simplified using the same approach described in the previous chapter so that a "practical" model can be obtained.

Time Scale Analysis

In order to obtain a practical assessment of the relevant steps on the kinetics of PEG coupling, we performed a simple time scale analysis considering that the total time t_{TOTAL} effectively determines the rate controlling steps in our system. Thus, the total time for the reaction and coupling of PEG involving the following time steps can be written as

$$t_{TOTAL} = t_B + t_F + t_D + t_R \tag{22}$$

t_{TOTAL}: Total time for solute transport from the bulk solution into the bead's inner surface and covalent binding to the surface,

t_B: Time for solute transport from the bulk solution to the stagnant film around the beads,

t_F: Time for solute transport through the stagnant film around the bead,

t_D: Time for solute diffusion inside the bead's pores,

t_R: Time for solute covalent binding to the bead's inner surface.

Bulk Mass Transfer Time Determination

In the present experiments, the reactions were performed in a well mixed batch

reactor, thus, the time t_B was practically 0.

Film Mass Transfer Time Determination

The characteristic times for film mass transfer and for diffusion were estimated using empirical correlations, for instance, the characteristic film mass transfer time t_F of a solute within a stagnant film outside a gel particle, according to Geankopolis, (1983), can be approximated and calculated by the expression

$$t_F = \frac{r_m \varepsilon_b}{3k_f(1-\varepsilon_b)} \tag{23}$$

Here,

k_f: film mass transfer coefficient,

ε_b: Ratio of bead volume to batch total volume,

r_m: Radius of bead

The film mass transfer coefficient k_f for PEG stirred in a tank experiment can be calculated by the following expression according to Geankopolis, (1983)

$$k_f = \frac{D_i}{r_m} + 0.31\left(\frac{\mu}{\rho D_i}\right)^{-\frac{2}{3}}\left(\frac{\Delta\rho\mu g}{\rho^2}\right)^{\frac{1}{3}} \tag{24}$$

Where

ρ: Particle density

Δρ: Density difference between the adsorbent particle and the liquid,

μ: Liquid viscosity

g: Gravitational constant

D_i: Diffusion coefficient of PEG

r_m: Radius of bead, 20 μm

The bead radius r_m of the beads is in 20 μm. The pore diffusion coefficient D_i of

PEG is 2.0 x 10^{-10} m^2/s at 23 ºC according to Arakali et al. (1995).The particle density of agarose beads has been determinated as around 1100 kg/m^3 by Chase and Draeger (1992). The viscosity and density of water was used here to calculate the film mass transfer coefficient k_f. From the Handbook of Chemistry and Physics (2007), at 25 °C, the viscosity μ is 0.890 x 10^{-3} Pa·s and the density is 997 kg/m^3. Thus, the density difference Δρ is equal to 103 kg/ m^3. Thus, for our system, the k_f was calculated as 1.0 x 10^{-5} m/s from equation 24.

In the present experimental system, the bead volume ratio ε_b is 0.1. Thus, taking these parameters into consideration using equation 23, the time t_F for chelator transport through the film outside bead surface can be calculated as 0.074 s.

Since the experimental attachment of PEG takes more than 1 hour to reach 50% binding, one can consider that the stagnant film mass transfer of PEG is infinitely fast and offer no resistance to the transport process. This means the concentration c, in the bulk solution, for practical purposes, is equal to the concentration c_i, at the particle solution interface

$$c = c_i \qquad \text{at} \quad r = r_m \tag{25}$$

Intraparticle Mass Transfer Time Determination

According to Champluvier and Kula (1992), the average diffusion time of a solute within a gel particle can be approximately determined by the following expression

$$t_D = \frac{L_D^2}{D_i} \tag{26}$$

Where

t_D: Average diffusion time,

L_D: Diffusion path

D_i: Diffusion coefficient of solute (PEG),

In this work, L_D can be approximately regarded as the bead radius r_m of the beads, in this case 20 μm. The pore diffusion coefficient D_i of PEG considered before is 2.0 x 10^{-10} m^2/s at 23 ºC (Arakali et al., 1995). Accordingly, taking these parameters into equation 26, the average intrapore diffusion time of PEG in the agarose beads is estimated as 2.0 s.

With the same constraints mentioned before, the experimental attachment of PEG took more than one hour to reach 50 % conversion. Thus, it seems that the intrapore diffusion step of PEG is considered also infinitely fast compared to the overall PEG binding process and the diffusion resistance is considered negligible as well.

Thus, considering the experimental data from this research and the empirical data for similar systems from the literature, we proceeded to develop a simplified model that accordingly can represent the overall PEG coupling process by considering the reaction of PEG from the inner particle fluid to the inner surface (surface reaction) as the overall rate controlling step. That is, the external mass transfer, film mass transfer, and intraparticle diffusion resistances become negligible.

With this physical evidence, we model and explain our experimental results with a simplified overall process that accordingly reduces equation 2 to the following expression, without considering the diffusion term.

$$\varepsilon_i \frac{dc}{dt} + \frac{dq_i}{dt} = 0 \qquad (27)$$

This equation considers only the bead volume. To account for the overall batch volume in the system and again under the assumption that the PEG concentration is uniform in the liquid continuous phase, the above equation can be written as:

$$(1-\varepsilon_b+\varepsilon_b\varepsilon_i)V\frac{dc}{dt}+\varepsilon_b V\frac{dq_i}{dt}=0 \tag{28}$$

The term $(1-\varepsilon_b+\varepsilon_b\varepsilon_i)$ is the ratio of the total liquid volume including pores' volume and external volume to the batch total volume.

As stipulated before, the reaction between the epoxy groups of the gels and the amino groups of PEG on the surface can be represented by the expression presented by Bruice, (2004):

$$\frac{dq_i}{dt}=k_2c(q_m-q_i)+k_1(q_m-q_i) \tag{3}$$

Thus, the equation 28 can be written as

$$(1-\varepsilon_b+\varepsilon_b\varepsilon_i)\frac{dc}{dt}=-\varepsilon_b\left[k_2c(q_m-q_i)+k_1(q_m-q_i)\right] \tag{29}$$

Here,

c : PEG concentration in the bulk based on total volume of the system

c_0 : Initial PEG concentration based on the total volume,

q_i : Attached PEG density on the surface of the pores based on bead volume

q_m : Maximum attached PEG density bound to the surface of the beads

k_1 : First order reaction constant

k_2 : Second order reaction constant

The stoichiometric ratio between free PEG and attached PEG in this reaction is 1:1

as described below,

$$PEG + S \longrightarrow S - PEG\,, \tag{30}$$

Here S is active site (epoxy group) on the gels.

Considering the overall mass balance and the stoichiometric ratio, one can get the change in concentration of PEG in the system as a function of the amount of PEG bound to the surface, that is, since

PEG Moles in liquid = Initial PEG moles in liquid - PEG moles attached to the surface (31)

Thus, the PEG concentration in the solution can be written as a function of the PEG bound to the surface, q_i, as

$$c = c_0 - \frac{\varepsilon_b}{(1-\varepsilon_b+\varepsilon_b\varepsilon_i)} q_i \tag{32}$$

When c is substituted in equation 3, the expression reduces to an equation with q_i as the dependent variable as a function of time, or

$$\frac{dq_i}{dt} = k_2[c_0 - \frac{\varepsilon_b}{(1-\varepsilon_b+\varepsilon_b\varepsilon_i)} q_i](q_m - q_i) + k_1(q_m - q_i) \tag{33}$$

This equation is a first order ordinary differential equation that can be solved analytically with the initial condition:

$$\text{at } t = 0, \qquad q_i = 0 \tag{34}$$

Separating the variables, integration gives the following equation,

$$\ln\left(\frac{k_2c_0 + k_1 - k_2\frac{\varepsilon_b}{(1-\varepsilon_b+\varepsilon_b\varepsilon_i)} q_i}{q_m - q_i}\right) = \left(k_2c_0 + k_1 - k_2\frac{\varepsilon_b}{(1-\varepsilon_b+\varepsilon_b\varepsilon_i)} q_m\right)t + \ln(\frac{k_2c_0}{q_m}) \tag{35}$$

This equation thus provides the coupling density of the polymer PEG as a function of time for the entire coupling process, from $q_i = 0$ to $q_i = q_m$.

However, to determine an estimate of the reaction rate constants k_1 and k_2 we consider the experimental values at the beginning of the coupling reaction when the amount of bound PEG is relatively small compared to the bulk concentration c_i or (c_0). Thus for short time binding, equation 33 can be written as

$$\frac{dq_i}{dt} = k_2 c_0 (q_m - q_i) + k_1 (q_m - q_i) \tag{36}$$

Integration of this equation and using the same initial condition (equation 34) gives the following simplified result

$$\ln(q_m - q_i) = \ln(q_m) - (k_2 c_0 + k_1)t \tag{37}$$

This equation can be used to obtain the reaction rate constants k_1 and k_2 by plotting the $\ln(q_m - q_i)$ versus the time, t. Thus, with at least two sets of experimental data, one can obtain the k_1 and k_2. In this case, 3 sets of data points were used. The experimental data for this purpose was obtained using different values of the initial M-PEG-NH_2 concentration. Linear regression was used to calculate these values.

In Table 5.6, the corresponding c_0 (the PEG initial concentrations) and the value of the maximum active site capacity q_m are given.

Table 5.6 Experimental conditions of PEG attachment

PEG initial concentration	0.2g/mL	0.4g/mL	0.7g/mL
C_0, base on total volume, μmol/mL	40.0	80.0	140
q_m, μmol/mL	20	20	20

In this work, the first 4 data points with low q_i values were used together with linear regression to obtain the slopes from equation 37. The results are given in Figure 5.7.

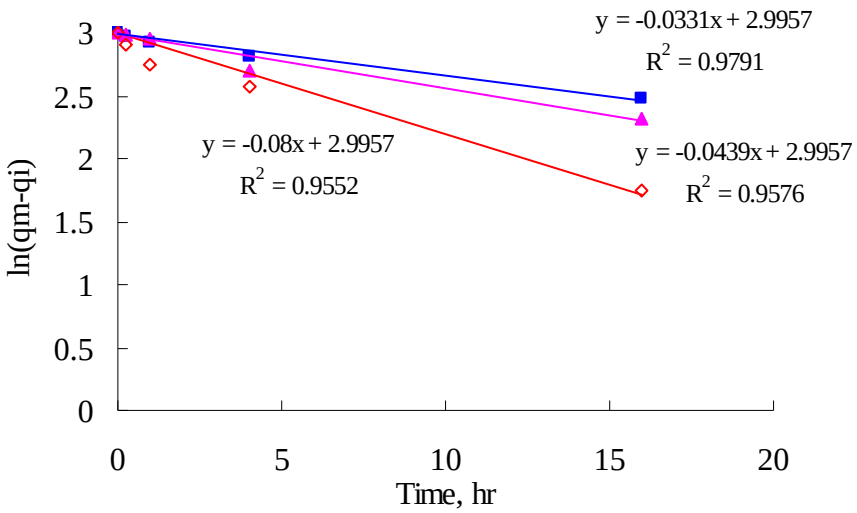

Figure 5.7 Slopes calculated using the linear regression based on initial reaction data. Experiments were performed with different PEG initial concentrations.
■: 0.2g/mL; ▲: 0.4 g/mL; ◊: 0.7 g/mL

The value of the slopes $-(k_2 c_0 + k_1)$ obtained here by linear regression are summarized in Table 5.7

Table 5.7 Slopes calculated using linear regression

PEG initial concentration	0.2g/mL	0.4g/mL	0.7g/mL
	40.0μmol/mL	80.0μmol/mL	140μmol/mL
Slope, $-(k_2 c_0 + k_1)$	-0.0331	-0.0439	-0.0800

The term $-(k_2 c_0 + k_1)$ from Table 5.7 is a linear function $y(c_0)$, $[y = -(k_2 c_0 + k_1)]$. By plotting this function $y(c_0)$ versus the initial concentration c_0 and linear regression,

the slope gives the reaction rate constant k_1 and the intercept gives the reaction rate constant k_2. The resulting values are presented in Table 5.8

Table 5.8 Reaction rate constants k_1 and k_2

k_1, hr^{-1}	2.04×10^{-2}
k_2, $mL \cdot \mu mol^{-1} \cdot hr^{-1}$	1.28×10^{-4}

Once the reaction rate constants k_1 and k_2 are determined, Equation 39 can now be used to calculate the PEG coupled (q_i) onto the matrix as a function of time. The resulting calculations of PEG attachment onto Novarose 300/40 and Sepharose 6B.with this model are plotted in Figures 5.8 (Novarose 300/40) and 5.9 (Sepharose 6B), respectively. The calculation from the model is presented with a solid line together with the experimental data. The experimental data fit relatively well into the model considering the given conditions. For practical purposes, the model provides a good guide for the control of the polymer density on this type of gel matrices.

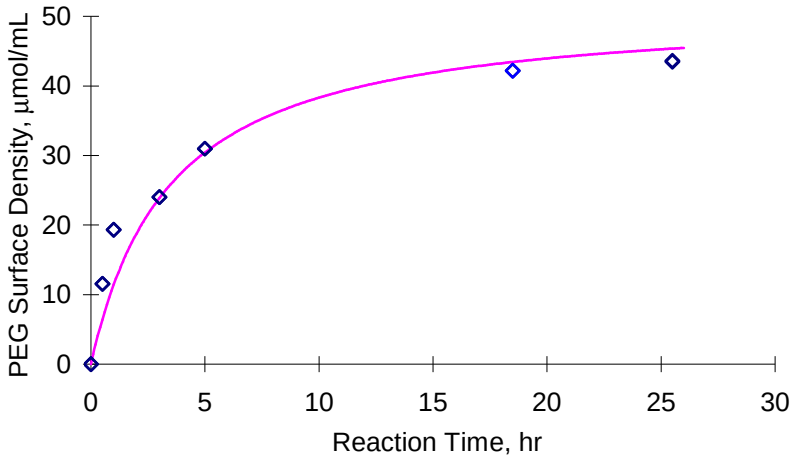

Figure 5.8 PEG attachment kinetics on Novarose Act-High 300/40 gel

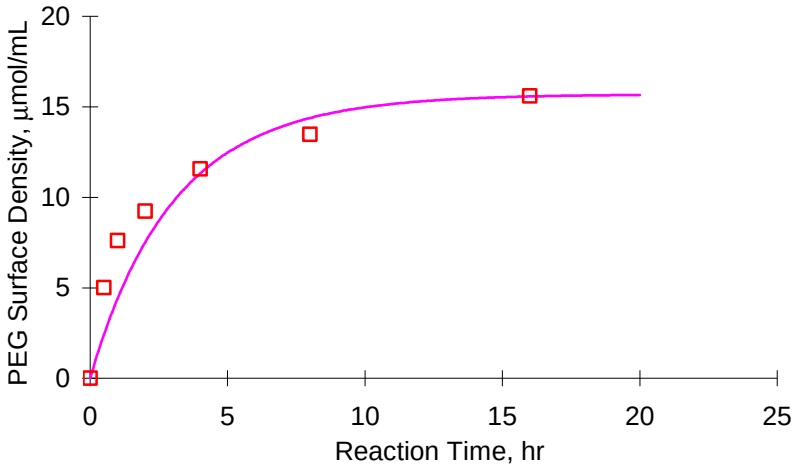

Figure 5.9 PEG attachment kinetics on epichlorohydrin modified Sepharose 6B gel

Comparing to the IDA attachment, the reaction rate constants of PEG to epoxy group are a little smaller. PEG is a much larger molecule than IDA, but the reactivity of the amino group of M-PEG-NH_2 is more reactive than the imino group of IDA. Thus, reaction rate constants of these two reactions are very close.

Conclusions

In this work, kinetic coupling experiments of the polymer PEG onto agarose activated matrices were performed as a function of binding reaction time until saturation of all active sites in the matrix was obtained.

A mathematical model was considered in order to obtain theoretical standard curves for PEG coupling. The efforts to incorporate a theoretical aspect to the immobilization of polymer ligands to chromatographic matrices seem, according to this first attempt, to be in the right direction. The model proposed here, when mass transfer limitations do not control the overall attachment of polymer ligands, appears to be surface reaction controlled only. This model can predict polymer coupling densities on different

chromatographic matrices and thus provides the means to prepare affinity matrices with the desired amount of ligands in general, for specific protein chromatographic applications. The physical model seems to be accurate with respect to the behavior of polymer attachment to the agarose matrices used here. The mathematical model gives practical estimates of the amount of material bound to matrices as a function of time. This modeling effort will provide an approximated scheme to incorporate PEG densities that allows other ligands attachments such as chelating agents and will help optimize metal ions and protein adsorption.

CHAPTER 6 IMMOBILIZATION AND CHARACTERIZATION OF ACTIVE BIOMOLECULES ON A GOLD SURFACE WITH SELF ASSEMBLED MONOLAYERS

Abstract

The main objective of this work was to study and characterize the preparation of affinity ligands or gold surfaces. The ligands can serve as linkers for MT binding and growth. The immobilization of biomolecules on different self assembled monolayers (SAMs) were studied by fluorescent microscopy and X-ray photoelectron spectroscopy (XPS). The organothiols used here were cysteamine, 3,3′-dithiodipropionic acid di(N-hydroxysuccinimide ester) (DTP) and 16-mercaptohexadecanoic acid (MHA). The long chain MHA SAMs show the capability of long-term stability in water solution, which makes it a good surface modification reagent for biomolecule immobilization. Different solvents and SAM formation times were studied until maximum plateaus were reached. These surfaces were characterized with several fluorescent tags, fluorescein isothiocyanate (FITC) and rhodamine bound avidin. The anti-glutathione S-transferase (anti-GST) ligand was coupled to these SAM modified gold surfaces, and then the GST-γ-tubulin fusion protein was attached to form a γ-tubulin coated gold surface providing an accessible nucleation center for microtubule growth.

Introduction

Biomolecule immobilization onto solid surfaces is crucial in the development of solid-phase bioanalytical techniques, biosensors and biocompatible materials. The

methods based on SAM techniques offer one of the simplest ways to provide a reproducible, ultrathin, and well-ordered layer suitable for further modification with antibodies, with potential to improve detection speed, sensitivity, and reproducibility. Currently, the most efficient approach to manufacture such layers onto a gold surface is to adsorb appropriate organothiols onto a gold substrate. The most ordered structures are formed from compounds with the structure $HS(CH_2)_nX$, where n =16–18 and X is a small, organic functional group (Whitesides and Gorman, 1995; Dubois et al., 1990). These SAMs are highly ordered and densely packed assemblies of linear alkane molecules that are thermodynamically driven to form high coverage films of molecular dimensions.

Carboxylic acid groups are some of the most interesting functional terminal groups. After Nuzzo (1990) first described this particular type of organothiol (MHA), there has been a wide range of applications in surface science (Fisher et al., 2000; Smith et al., 2000; Ashby et al., 2000; Kokkoli and Zukoski, 2001), electrochemistry (Sugihara et al., 2000; Boubour and Lennox, 2000), biology (Lahiri et al., 2000; Franco et al., 2000; Chapman et al., 2000; Whitesides et al., 2001), surface engineering (Lee and Laibinis, 2000 (a), (b); Huck et al., 1999; Xu et al., 1999), and nanoparticles (Auer et al., 2000). By using the carboxylic acid terminal organothiol MHA, $HS\text{-}(CH_2)_{15}\text{-}COOH$, a long-chain carboxylic acid terminating alkanethiol, can self assemble an ordered and oriented monolayer onto Au surfaces. The SAMs of MHA appear to be stable indefinitely in aqueous solutions at room temperature, and are thermally more stable than the SAMs from the short-chain disulfides or thiols (Bain et al., 1989; Mirsky et al., 1997). The condensation reaction between the carboxyl groups of MHA and the amino groups on

proteins in the presence of carbodiimides has been commonly used in immobilization on the MHA monolayer in the preparation of capacitive biomolecule monolayers (Fung and Wong, 2001; Williams and Blanch, 1994; Lahiri et al., 1999; Qian et al., 2002; Jung et al., 2000). The chemical reaction mechanism is shown in Figure 6.1.

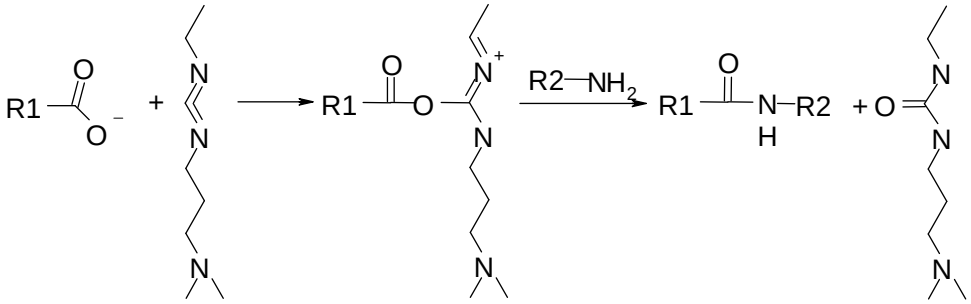

Figure 6.1 Chemical reaction mechanism of the condensation reaction between an amino group and a carboxyl group in the presence of carbodiimides

The avidin and biotin system is commonly used in bio-immobilizations. Avidin and biotin (Hermanson, 1996) have a high protein-ligand interaction with a $K_d=10^{-15}$ M^{-1}. The surface functionalization by avidin provides a useful approach of immobilization of many other biomolecules, such as antibodies, enzymes, and peptides that are available or can be prepared as biotinylated compounds. The avidin is composed of 4 nearly identical subunits, which can each bind a molecule of biotin. The avidin modified surface provides a coverage of free binding sites for biomolecules that give us a very high biomolecule binding capacity.

In this work, the immobilization of biomolecules on gold surfaces with different self assembled monolayers (SAMs) by covalent bonds was studied using fluorescent microscopy and X-ray photoelectron spectroscopy (XPS). The organothiols used in this

work were cysteamine, DTP, and MHA. The long chain MHA SAMs show the capability of long term stability in water solutions that made it a good surface modification reagent for the biomolecule immobilizations. Different solvents and SAM formation times were studied, the MHA SAMs coverage, for instance, reached a maximum plateau with water as a solvent in 48 hours immersion. Different fluorescent tagged proteins (FITC-avidin, and rhodamine-avidin) were immobilized to the SAM surfaces and verified by fluorescent microscopy. The anti-GST, a ligand for MTs was coupled to a SAM modified gold surface, then the GST-γ-tubulin fusion protein was attached to form a γ-tubulin protein coated gold surface to provide the accessible nucleation center for microtubules growth from the gold surface.

Materials and Methods

16-mercaptohexadecanoic acid (MHA) ($HS(CH_2)_{15}COOH$, 90%), 1-ethyl-3-(3-dimethylaminopropyl) carbodiimide hydrochloride (EDAC), 3,3′-dithiodipropionic acid di(N-hydroxysuccinimide ester) (DTP), FITC-avidin, rhodamine-avidin bovine serum albumin (BSA), NHS-biotin, DMF ethanol (200-proof) were purchased from Aldrich (Milwaukee, WI); sodium phosphate dibasic heptahydrate ($Na_2HPO_4 \cdot 7H_2O$, 98.0%), sulfuric acid (95%), and 30 % hydrogen peroxide were obtained from Fisher (Fairlawn, NJ). All these reagents were used without further purification. Anti-GST, IgG-Cy5 goat anti rabbit, IgG-Cy3 goat anti mouse, anti-γ-tubulin (from mouse), were supplied from Sigma–Aldrich (St. Louis, MO). GST-γ-tubulin fusion protein was provided by the Biomedical Engineering Department, University of Arizona (Tucson, AZ). Gold-patterned silicon dioxide wafers were prepared at the Micro/nano Fabrication Center,

University of Arizona (Tucson, AZ). The thickness of the Au(111) thin layer was 100 nm with a 0.75 nm chromium adhesion layer. Ultra pure water (18 MΩ·cm) produced by a Milli-Q system was used.

Experimental Methodology

Formation of Functional Self Assembled Monolayers (SAMs)

The gold patterned silicon dioxide chips with a gold area of ~0.13 cm^2 were cleaned using a piranha solution (95% H_2SO_4/30% H_2O_2, 70:30, v/v). The wafers were immersed in a freshly prepared piranha solution for 30 min in an ultrasonic bath, followed by washing thoroughly with M.Q. water.

Cysteamine, DTP and MHA SAMs were formed on Au (111) by immersing the freshly cleansed gold coated SiO_2 wafers for ~24 hrs at room temperature in a 1.0 mM corresponding thiol solution. The newly formed Au(111)/SAM specimens were successively rinsed with water before further use.

Coupling and Characterization of Avidin on Au/SAM surface

Cysteamine SAMs: There were 2 approaches used to verify protein binding by Fluorescent microscopy.

(A) The first approach consisted in adding 20 µl 0.1 M NHS-biotin DMF solution to the nearly prepared cysteamine modified chip's surface. After standing for 30 minutes, the modified wafer (electrode) was washed with M.Q. water by gently shaking for 30 seconds 3 times. Then 20 µl of 0.5 mg/mL FITC-avidin was added to the wafer surface and reacted for 30 minutes at 25 °C. Again, this new modified wafer was washed with

M.Q. water by gently shaking for 30 seconds 3 times and fluorescent images were immediately taken.

(B) The second approach was followed by immersing the nearly prepared cysteamine modified chips into 1.0 mL of 0.10 M phosphate buffer (pH 5), then adding 10 μL of 1.0 mg/mL FITC-avidin and 1.0 mg of EDAC. After gently shaking for 4 h, the modified wafer as before was washed with PBS buffer by gently shaking for 30 seconds 3 times and fluorescent images were immediately taken.

DTP SAMs:

The freshly prepared DTP modified chips were immersed into 1.0 mL of 0.10 M phosphate buffer (pH 5), then 10 μL of 1.0 mg/mL FITC-avidin was added together with 1.0 mg of the carbodiimide, EDAC. After gently shaking for 4 h, the modified wafer was washed with PBS buffer by gently shaking for 30 seconds 3 times and fluorescent images were immediately taken, as before.

MHA SAMs:

The freshly prepared MHA modified chips were immersed into 1.0 mL 0.10 M phosphate buffer (pH 5), then 10 μL of 1.0 mg/mL FITC-avidin were added together with 1.0 mg of EDAC. After gently shaking for 4 h, the modified wafer was washed with PBS buffer by gently shaking 30 seconds 3 times and fluorescent images were immediately taken. The analysis was very systematic for all cases and become the standard protocol for all similar prepared samples.

The general reaction coupling of avidin derivatives on the gold surfaces via SAMs of cysteamine, DTP, and MHA is shown schematically in Figure 6.2.

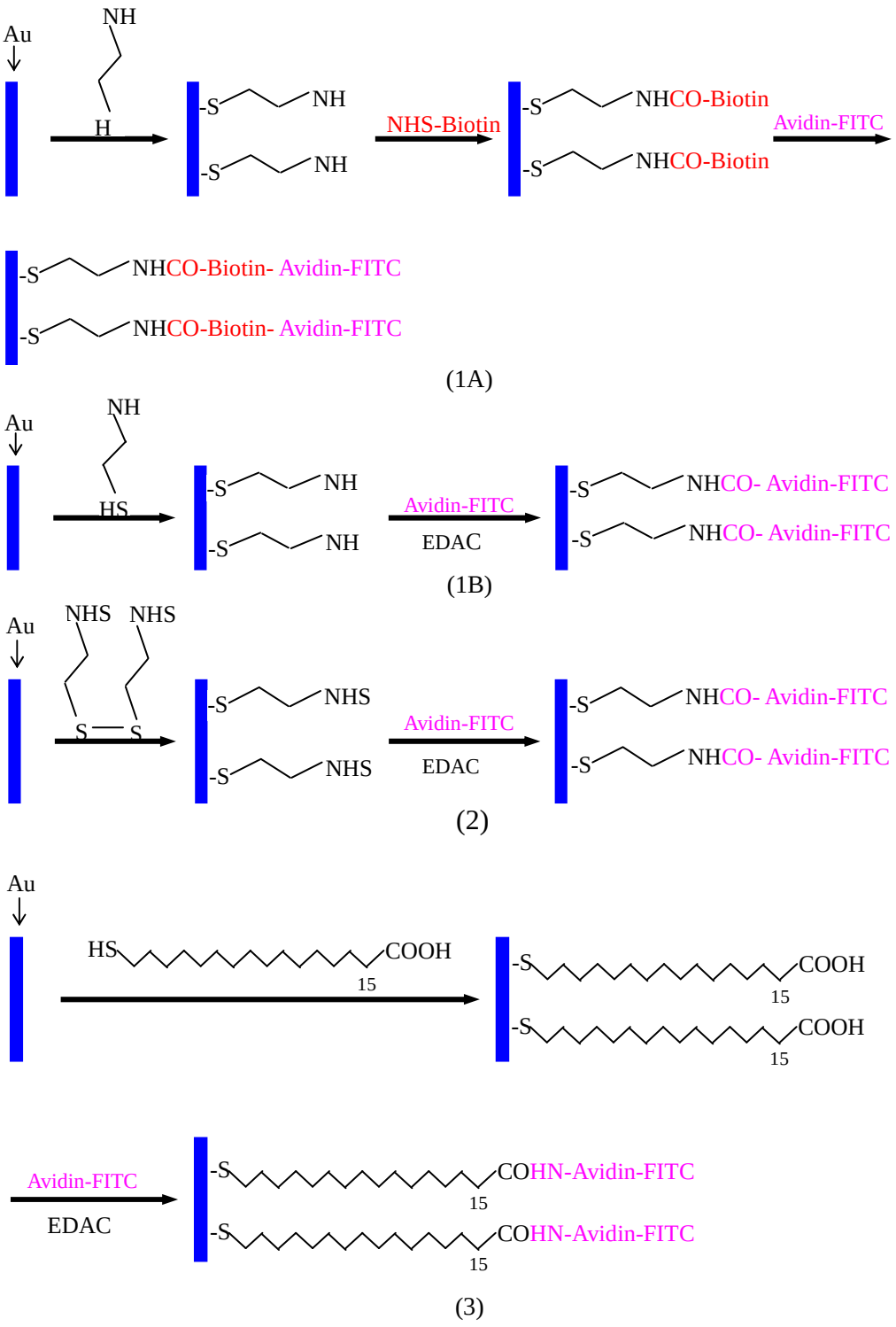

Figure 6.2 Schematic of Au surface modification with SAMs. (1A) cysteamine SAMs followed by NHS-Biotin coupling, (1B) cysteamine SAMs followed by EDAC mediated coupling, (2) DTP SAMs, (3) MHA SAMs

Coupling and Characterization of anti-GST on the Au (111)/SAM Surface

In the case of anti-GST immobilization, a thiol monolayer of MHA was chosen as a binding layer for anti-GST. The freshly prepared MHA modified chips were immersed into 1.0 mL of 0.10 M phosphate buffer (pH 5), then 5 µL of 1.0 mg/mL anti-GST/PBS solution were added together with 1.0 mg of EDAC. After gently shaking for 4 h, the modified wafer was washed with PBS buffer by gently shaking for 30 seconds 3 times. The process is shown in Figure 6.3.

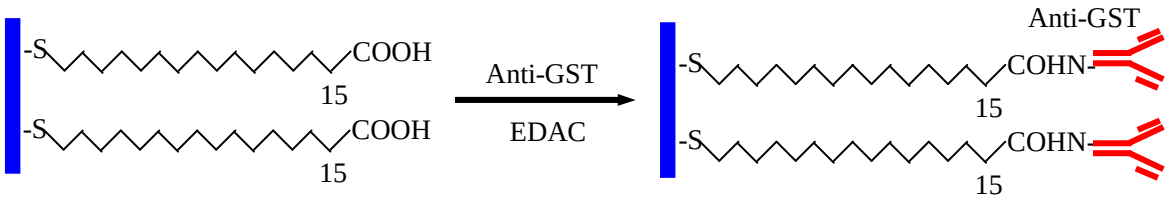

Figure 6.3 Schematic of attachment of anti-GST on Au surface via MHA SAMs

After coupling the anti-GST ligand, the wafer was immersed into a blocking solution (PBS buffer which contained 0.2% BSA and 0.2% dry milk powder) for 30 minutes. Afterwards the wafer was suction dried and 20 µl of 10 µg/mL IgG-Cy5 goat anti rabbit solution were added onto the chip surface. After standing for 30 minutes the chips were washed with PBS buffer by gently shaking for 30 seconds 3 times and Fluorescent images were taken immediately. The coupling process is shown in Figure 6.4.

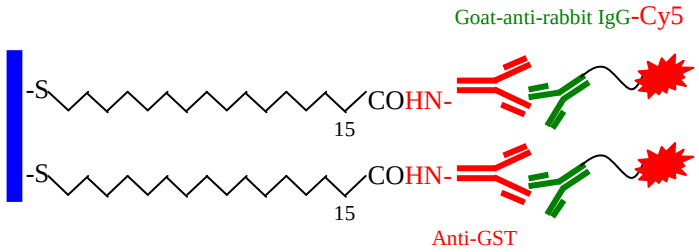

Figure 6.4 (a) Schematic of verification of anti-GST attachment onto MHA SAM modified surface using the labeled goat-anti-rabbit IgG-Cy5

Coupling and Characterization of γ-tubulin onto the anti-GST Functionalized Surfaces

After coupling of the anti-GST to the SAM modified gold surface, 20 µl of 0.3 mg/mL GST-γ-tubulin/PBS solution was added to the wafer and reacted for 30 minutes at 25°C. Then the wafer was washed with PBS buffer by gently shaking for 30 seconds 2 times. The coupling process scheme is presented in Figure 6.5.

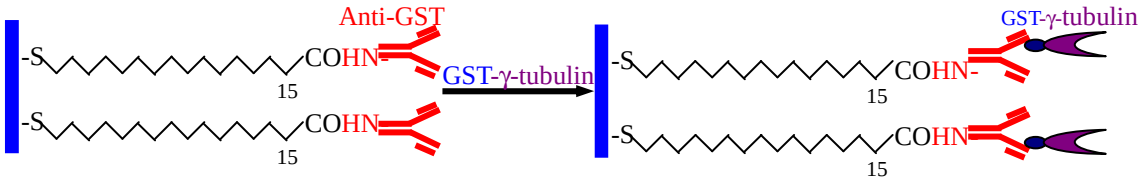

Figure 6.5 Schematic of affinity binding of GST-γ-tubulin onto an anti-GST modified surface

After binding of the GST-γ-tubulin, the wafer was immersed into the blocking solution (PBS buffer which contains 0.2% BSA and 0.2% dry milk powder) for 30 minutes. Then the wafer was suction dried and 20 µl of 10 µg/mL anti-γ-tubulin (from mouse) solution was added on the chip surface and let stand for 30 minutes. The chips were washed with PBS buffer by gently shaking for 30 seconds for 3 times. 20 µl of 10 µg/mL IgG-Cy3 goat anti mouse solution was added on the chip surface. After standing

for 30 minutes, the chips were washed with PBS buffer by gently shaking for 30 seconds 3 times and Fluorescent images were taken immediately. This binding process is presented in Figure 6.6.

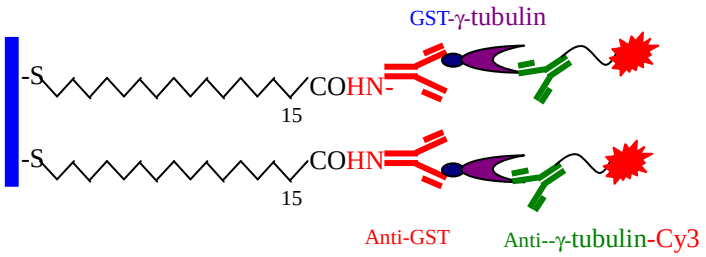

Figure 6.6 Schematic of verification of GST-γ-tubulin attachment on the anti-GST functionalized surface using the labeled anti-γ-tubulin-Cy3 antibody

X-ray Photoelectron Spectroscopy (XPS)

To ensure high quality of the thiol SAM layers formed on the surface of Au (111) for effective anti-GST attachment, XPS analysis to characterize the SAM surface was used. XPS spectra were obtained using a Kratos Axis 165 Ultra spectrometer. The spectra were accumulated at a take off angle of 70° relative to the surface at a pressure less than 1×10^{-8} Torr. In this analysis, the lens mode was hybrid; Pass Energy was 80 meV; Anode was Mono (Al) (300 W); Step was 1000.0 meV; Dwell was 100 ms; 3 Sweeps and Acquisition Time was 330s.

Fluorescent Microscopy

Fluorescent images were taken with a Nikon Optiphot-2 Fluorescent microscope (Nikon Instruments Inc., Melville, NY) and a Sony EKC 5000 digital camera after the fluorescent tagged protein were coupled to the SAM coated specimens.

Results and Discussion

Cysteamine SAM Modification

Figure 6.7 shows the resulting fluorescent images obtained after (a) the attachment of NHS-biotin followed by FITC-avidin; (b) the attachment of FITC-avidin via EDAC mediated condensation reaction onto the cysteamine modified Au surface. Both images show that there is fluorescence on gold area of the chips. This means that the SAMs are only formed on the gold region not on the silicon dioxide region of the wafer. Images (a) and (b) show very weak fluorescence of the FITC groups, most likely due to possible desorption of the cysteamine monolayer. According to Mirsky et al (1997), the short alkanethiol monolayers, like cysteamine, desorb in water very quickly while the longer alkanethiol monolayers (carbon number > 14) are very stable in water solutions. From the above observations, the quick desorption from the monolayer on the gold surface makes the short chain organothiol a poor SAM material for long-term biomolecule immobilization.

DTP SAM Modification

Figure 6.8 was taken after attaching the FITC-avidin to the NHS group of the DTP SAMs on the gold surface. The DTP has a disulfur group which breaks and forms 2 Au-S bonds with the gold surface. The terminal group of the DTP SAMs is an NHS group that can react quickly and effectively with amino groups at mild conditions. Similarly to cysteamine, DTP also has a very short alkyl chain (2 carbons), and the NHS group is much larger than the NH_2 group. So even in a very short period of time, about 30 minutes, the SAMs desorbed from the gold surface and no FITC-avidin was observed attached to

the gold surface afterwards. So we believe that using DTP is not suitable for long term immobilization of biomolecules in our work.

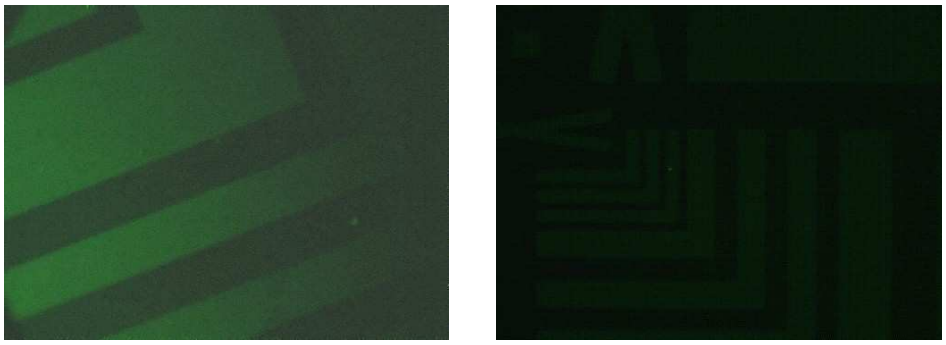

a b

Figure 6.7 Fluorescent images after the attachment of cysteamine modified Au surface with (a) FITC-avidin through NHS-biotin and (b) FITC-avidin through the EDAC mediated condensation reaction. The exposure times used were 4 s. The specimens were excited at λex ~495 nm and monitored at λem ~520 nm

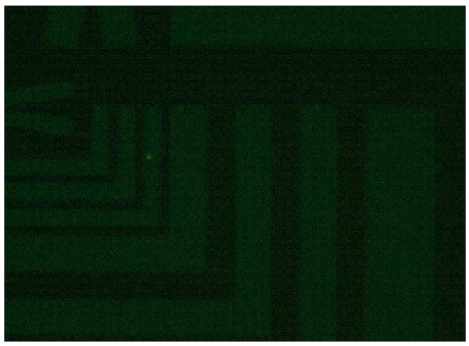

Figure 6.8 Fluorescent images obtained after the attachment of DTP modified Au surface with FITC-avidin through the EDAC mediated condensation reaction. The exposure times used were 4 s. The specimen were excited at λex ~495 nm and monitored at λem ~520 nm.

MHA SAM Modification

Figure 6.9 describes the fluorescent results of the coupling of FITC-avidin to the MHA SAM surfaces via EDAC. The results show that the FITC-avidin is coupled only on the gold region and not at all on the silicon dioxide region. The 16 carbon alkyl chain provides a strong van der Waals interaction between the alkyl chains and makes the

SAMs much more stable than the cysteamine or DTP systems. This is in accordance to observation in the literature (Jung and Campbell, 2000; Whitesides and Gorman, 1995). The SAM formation in general appears to be obtained in 2 steps: a fast adsorption step and a slow rearrangement step. The adsorption step takes just minutes to adsorb a loose single MHA monolayer to the gold surface. The latter step may take days to arrive to the final equilibrium of a densely, well ordered monolayer. In these results from the Fluorescent images, the fluorescent strength gets to a maximum plateau only after 48 hours of MHA SAM formation time.

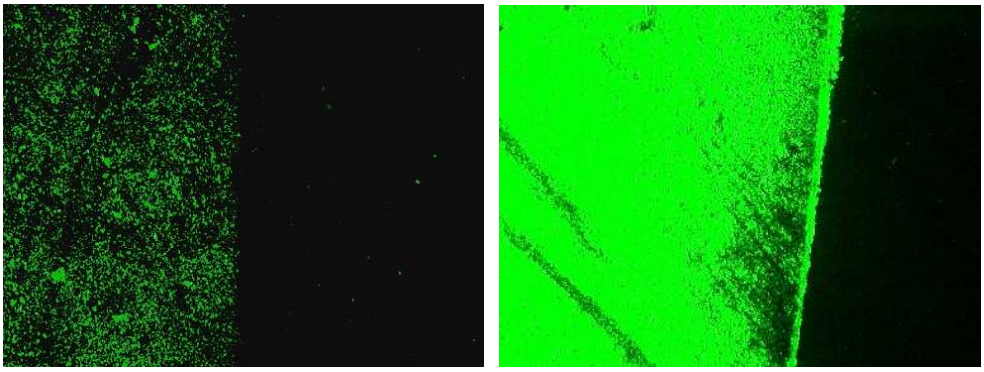

a b

Figure 6.9 Fluorescent images obtained after attachment of FITC-avidin to MHA modified Au surfaces which formation time is (a) 24 h and (b) 48 h. The exposure times used were 4 s. The specimens were excited at λex ~495 nm and monitored at λem ~520 nm.

In Figure 6.10, the MHA appears to form more dense and stable SAMs on the gold surface in water than in ethanol, so it seems the alkyl chain interaction of SAMs is stronger in the water solution. All the proteins were prepared in aqueous solution, the replacement of ethanol from water affected the SAMs and caused desorption of MHA from the SAM surfaces. Despite the lower solubility of MHA in water which slows down

the formation of SAMs, the systems with water seem to produce better results. In any case, fluorescence analysis showed effective immobilization of avidin in all the systems.

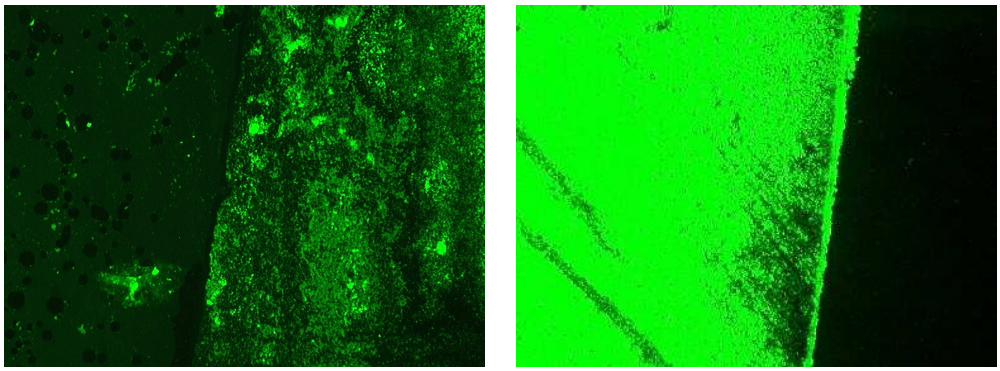

a b

Figure 6.10 Fluorescent images obtained after attachment of FITC-avidin to MHA modified Au surfaces with different solvents used: (a) Ethanol and (b) water. The SAM formation time is 48 hours. The exposure times used were 4 s. The specimens were excited at λex ~495 nm and monitored at λem ~520 nm.

Anti-GST Immobilization and Verification

Figure 6.11 describes the fluorescent results of the coupling of fluorescent tagged antibodies IgG-cy5 onto the anti-GST modified surfaces. The Fluorescent images show that the fluorescence is only on the gold region not on the silicon dioxide region demonstrating the specificity of binding. From the XPS spectrum given in Figure 6.12, it is observed that there is a large peak of N atom which most likely corresponds to the presence of the anti-GST protein. This verifies that the anti-GST is in fact attached onto the gold surface, and that in fact the anti-GST layer is formed on the gold surface through the MHA SAMs. This anti-GST layer provides an antibody monolayer that can now bind the GST-γ-tubulin fusion proteins by means of the high affinity antibody-antigen interaction between them. The immobilization of the antibody onto the gold surface

maintains high bioactivity as will be proved experimentally with binding of the GST-γ-tubulin.

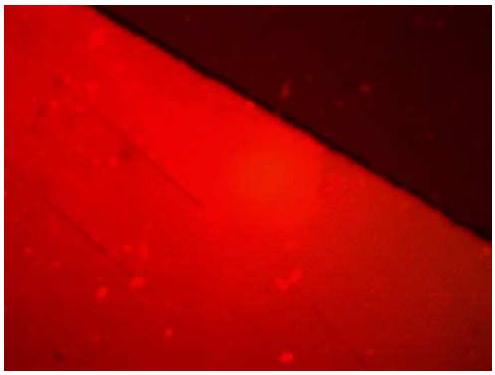

Figure 6.11 Fluorescent image obtained after the binding of Cy5 tagged goat-anti-rabbit IgG onto anti-GST modified Au surfaces. The exposure times used were 1 s. The specimens were excited at λex ~545 nm and monitored at λem ~610 nm

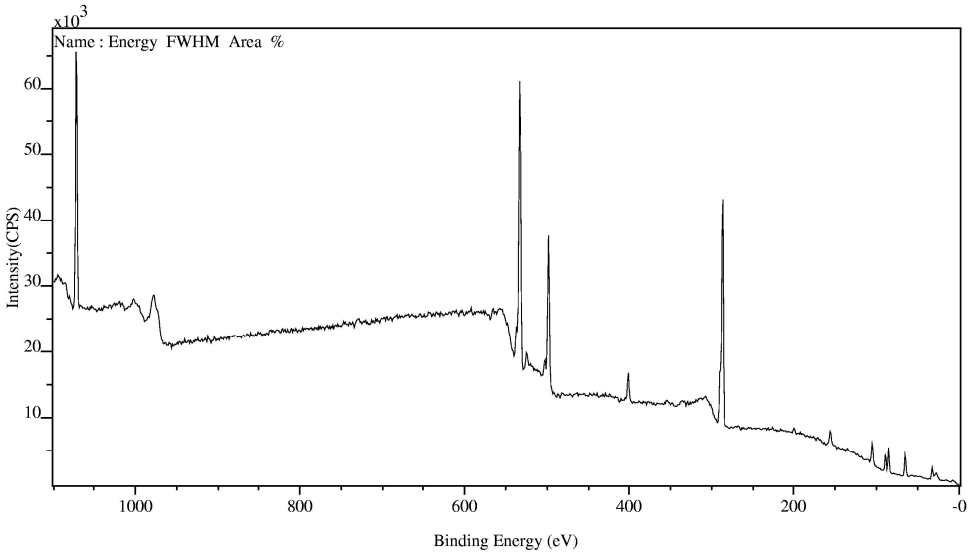

Figure 6.12 XPS spectrum of anti-GST modified Au surfaces. Lens mode: hybrid Resolution: Pass Energy 80 Anode; Mono (Al) (300 W) Step(meV); 1000.0 Dwell(ms): 100 Sweeps: 3 Acquisition Time (s): 330

γ-tubulin Immobilization and Verification

Figure 6.13 describes the fluorescent results of the verification of γ-tubulin binding on the anti-GST modified surfaces via coupling of fluorescent tagged antibodies.

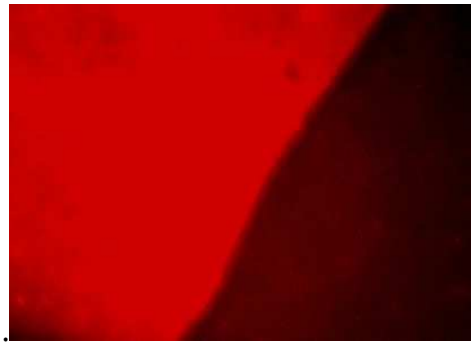

Figure 6.13 Fluorescent image obtained after binding of Cy3 tagged anti-γ-tubulin onto GST-γ-tubulin modified Au surfaces. The exposure times used were 1 s. The specimens were excited at λex ~545 nm and monitored at λem ~610 nm.

From Figure 6.13, it can be seen that the red fluorescence was observed only on the gold region and not on silicon dioxide region. That means that a GST-γ-tubulin monolayer was formed on the gold surface. The fusion protein (GST-γ-tubulin) is genetically similar to the γ-tubulin and to the glutathione S-transferase. The nucleotide binding site of γ-tubulin is on the opposite side of the juncture of the GST moiety. And the GST moiety can be attached to the antibody of the anti-GST monolayer covalently coupled to the reactive SAMs on the gold. So this GST-γ-tubulin layer has a good orientation with respect to γ-tubulin because the GST portion is at the bottom of the molecule in order to anchor with the anti-GST layer. The nucleotide binding sites of the γ-tubulin are accessible to free α/β dimers of MTs in the solution and the γ-tubulin layer can be functionalized as a nucleation center for microtubule growth. The MTs now in this

way could be prepared using this approach for possible self assembling of bio-nanoconnectors.

Conclusions

Different organothiol SAMs were investigated and the long chain MHA SAM system shows the capability of long term stability in water solutions making it a good surface modification reagent for biomolecule immobilization. The SAM formation time for MHA SAMs is apparently a slow process that arrives to a maximum plateau only after 48 hours of surface interaction in aqueous solution. The ethanol and water were compared as solvents and the aqueous solution showed to form more dense and stable SAMs, however slower.

By covalent attachment of the anti-GST protein to the best MHA SAM modified gold surface, a γ-tubulin modified surface was obtained which can serve as a nucleation center for MT growth. The fluorescent microscopy and the XPS analysis provides a definite confirmation of protein and antibody immobilization on the produced SAMs. Experiments of MT growth from the γ-tubulin modified surface will now be possible and will be explored under similar binding schemes.

CHAPTER 7 MICROTUBULE NUCLEATION AND GROWTH ON γ-TUBULIN FUNCTIONALIZED GOLD SURFACES

Abstract

Microtubules (MTs) are protein filaments that are emerging as potential building blocks in manufacturing nano-scale structures and systems such as interconnecting nano wires. Future development in using microtubules necessitates control of their nucleation and growth. We report the controlled nucleation and growth of microtubules from functionalized gold on a hydrophilic oxidized silicon wafer. The gold substrate is functionalized with γ-tubulin, a natural nucleating agent for microtubule growth. We show that the attached γ-tubulin retains its biological functionality and leads to nucleation and assembly of microtubules from the functionalized gold surface. We also analyze the interplay between the geometry of the nucleating substrates and the morphology of microtubule arrays and networks grown from them. We consider two geometrical arrangements of the substrates: (a) a square lattice of small gold pads on a hydrophilic oxidized silicon wafer and (b) a large flat surface. Fluorescence microscopy and scanning electron microscopy are employed to provide a detailed characterization of the length and morphology of the nucleated and grown microtubules. The observed microtubule morphologies are modeled, analyzed and discussed within the context of reaction-diffusion and nucleation controlled processes

Introduction

Microtubules (MTs) are naturally formed tubular structures with a 24 nm outer diameter and up to many microns in length. MTs are biopolymers assembled from protein heterodimers containing both α-and β-tubulin. MTs are polarized with a slow-growing end (so-called minus end exposing α-tubulin) and fast-growing end (β-tubulin terminated plus end). The plus end of a MT typically grows at a rate 5-10 times faster than the minus end. Tubulin dimers polymerize into MTs for tubulin concentrations above a critical value, C_C. At concentrations of tubulin dimmers near C_C, individual MTs exhibit dynamic instability (Mitchisona and Kirschner, 1984) and undergo apparently random successive periods of disassembly (catastrophe) and assembly (rescue). Although the process of MT growth is reasonably well understood, in vivo and in vitro MT nucleation is, however, still poorly understood. Within the cell, the minus end is tethered to microtubule-organizing centers (MTOC) such as centrosomes, and the plus end extends into the cytoplasm (Job et al., 2003). MT assembly is believed to nucleate from the MTOC through interaction with a tubulin isoform, γ-tubulin (Moritz et al., 1998; Gunawardane et al., 2000). Research in vitro has shown that γ-tubulin is an essential component in the centrosomes for microtubule nucleation (Felix et al., 1994; Stearns and Kirschner, 1994). Monomeric γ-tubulin and γ-tubulin protein complexes can both nucleate MT. The nucleation time of MTs has been shown to be shorter in the presence of monomeric γ-tubulin (Leguy et al., 2000). In vitro, monomeric γ-tubulin behaves as a minus-end-specific protein, with very high binding specificity to the microtubule end. It caps microtubule minus ends and catalyzes microtubule nucleation (Leguy et al., 2000; Li

and Joshi, 1995). Specific peptides and/ or complexes of γ-tubulin have also been identified to serve as binding sites to interact with tubulin heterodimers (Llanos et al., 1999; Moritz et al., 1998; Oegema et al., 1999; Wiese and Zheng, 2000).

The applicability of using MTs as templates for interconnecting devices on microchips necessitates the development of a protocol where MTs can be nucleated and directionally grown from specific sites on the microchip toward some target site elsewhere on that chip. Toward the goal of manufacturing MT-based nanostructures on a silicon wafer, we report here an "in situ" approach consisting of a starting metal pad functionalized with a derivatized MT nucleating complex and surface-driven growth of MTs from the pad. The advantage of this approach lies not only in the immobilization of MTs on the surface of a substrate but more importantly on the unique ability to initiate MT growth from desired sites. In addition, we also report on the effect of the geometry of the substrate on the morphology of the MTs. Based on the premise that MT growth may be influenced by the geometry of the environment, we have conducted additional experiments of MT growth from γ-tubulin functionalized surfaces with two geometrical arrangements of the substrates, namely, a square lattice of small gold pads (10 μm ×10 μm) on a hydrophilic oxidized silicon wafer and a large flat surface (nearly semi-infinite with respect to the scale of MTs). Fluorescence microscopy and scanning electron microscopy are employed to provide a detailed characterization of the morphology of the nucleated and grown microtubules.

Material and Methods

MT Nucleating Complex

We have generated a fusion protein consisting of glutathione *S*-transferase (GST) and γ-tubulin to be used as the nucleating agent for the initiation of microtubule growth. The GST-γ-tubulin was developed by first extracting RNA from human cells and using RT-PCR to obtain γ-tubulin. The primers that we used introduced restriction sites at both ends. Additionally, one of the primers created slight changes in codon sequence at the 5′ end; this particular clone could then be used to generate a fusion protein in pGEX-KG. This vector, containing GST followed by a glycine link, was used to generate our fusion protein GST-γ-tubulin. The recombinant protein was then produced in *E. coli* containing the expression construct and it was initially grown in 1.0 L of LB media in the presence of 100 μg/mL ampicillin. When the culture reached an absorbance of 0.9 at 600 nm, 1 mM isopropyl-D-thiogalactopyranoside (IPTG) was added to induce the expression of the GST-γ-tubulin. After 3 hours, the *E. coli* was concentrated by pelleting method using centrifugation for 10 min at 15,000 ×*g*. The pellet was then resuspended in 10 mL of PBST and was then placed on ice for 30 min in the presence of lysozyme. Cells were then ruptured using a Polytron three times for 10 s at maximum setting. Centrifugation at 10,000 ×*g* for 10 min at 4 °C provided supernatant that was passed through a 1 mL GSTtrap FF column (Amersham Biosciences). A standard protocol was then used to wash unbound proteins from the column and then to elute GST-γ-tubulin using free glutathione. Purity of the final product was analyzed using SDS-PAGE and specific antibody recognition. The final purification contained greater than 80% of an 85 kDa

protein, the size estimated to be the fusion protein. The recombinant protein was then verified using ELISA with antibodies that recognized specifically either GST or γ-tubulin. The final concentration of GST-γ-tubulin was estimated to be between 4 and 5 μM. (0.3-0.4 mg/mL)

Gold Surface Functionalization

A protein nucleation method for MT growth from gold substrates has been developed based on the self assembly of reactive alkanethiols together with the engineered fusion protein. Oxidized silicon wafers were patterned with gold electrodes, followed by treatment with piranha solution to clean organic contaminants and to activate the gold surface. An anti-GST antibody was bound to a SAM of carboxylic acid terminated alkanethiols on the gold surface through the carboxylic acid group at the end of the alkyl chains and it is presented in Figure 7.1a. Anti-GST is a specific antibody for selective binding of GST attached to recombinant proteins, in our case, the microtubule nucleating fusion protein, GST-γ-tubulin. Additionally, a specific antibody that binds γ-tubulin is then recognized by a secondary antibody that has a fluorescent tag (IgG-Cy3) and is used to quantify the extent of the formation of the protein assembly. Strong fluorescence from a functionalized gold surface on a SiO_2 substrate coated with the fusion protein indicates that the approach we have developed gives a uniform coverage of the electrode. The Fluorescence image is presented in Figure 7.1b.

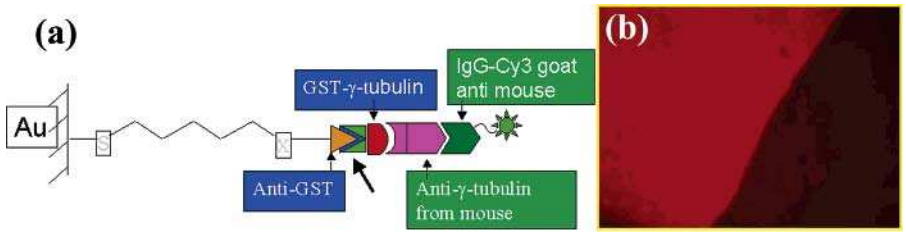

Figure 7.1 (a) Schematic of functionalization gold surface with GST-γ-tubulin. (b) Fluorescent image obtained after GST-γ-tubulin modification on Au surface

We have also characterized the morphology of the functionalized gold substrate by atomic force microscopy (AFM). Figure 7.2 reports AFM data of the initial localization of a γ-tubulin functionalized gold surface and of a pure gold surface. Prior to imaging, the pure gold surface was treated with piranha solution. The gold substrate exhibits some roughness with feature sizes of approximately 80-100 nm. The γ-tubulin localized surface appears to be morphologically similar to that of the gold substrate, indicating that the nucleating fusion protein film binds the substrate.

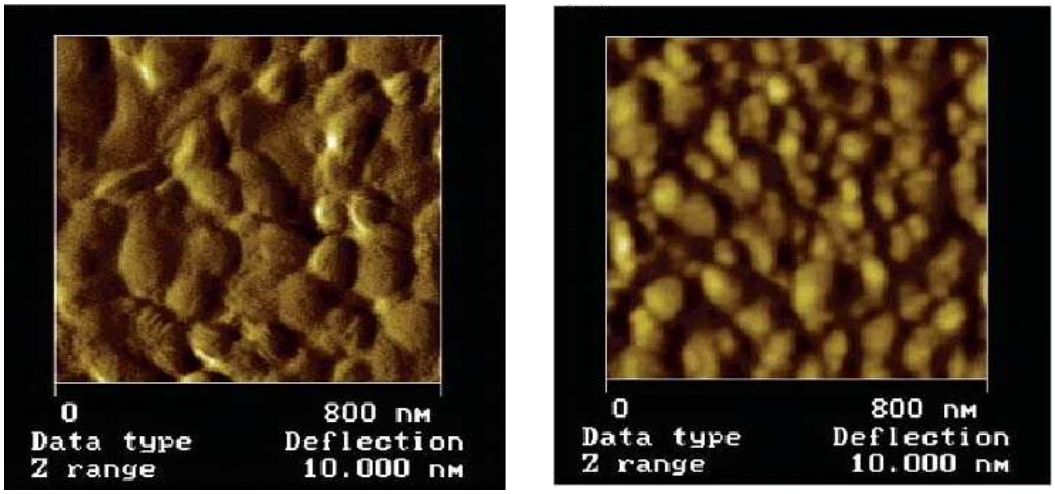

Figure 7.2 Surface morphology of (a) functionalized gold surface and (b) pure gold surface taken by atomic force microscopy (AFM)

MT Growth.

For this study, we used tubulin (>99% pure) prepared from bovine brain extracts modified with covalently linked fluorescein (Cytoskeleton Inc). The fluorescein modified tubulin was stored at -70 °C in storage buffer (pH 6.8; 80 mM piperazine-*N*,*N*′-bis(2-ethanesulfonic acid) sequi sodium salt (PIPES), 1 mM magnesium chloride ($MgCl_2$); 1 mM ethylene glycol-bis(α-amino-ethyl ether) *N*,*N*,*N*′,*N*′-tetraacetic acid (EGTA), and 1 mM guanosine 5′-triphosphate (GTP)).

In vitro MT assembly was performed in PEM 80 buffer (80 mM PIPES, 1 mM EGTA, 4 mM magnesium chloride ($MgCl_2$), using KOH to adjust PH to 6.9) using a final concentration of tubulin at 0.25 mg/mL (2.3×10^{-6} M). Polymerization was initiated by the addition of GTP (final concentration is 0.25 mM) in the presence of taxol (final concentration is 10 μM).

To test the specificity of the interaction between MTs and the γ-tubulin functionalized substrates, we have conducted experiments in which MTs were grown in the presence or absence of the functionalized Au surfaces. In the first case, patterned silicon substrates with functionalized Au pads were immersed into the solution during the polymerization process. The solutions, both with and without substrates, were transferred from an ice bath to a heat bath at 37 °C to promote polymerization for some predetermined amount of time. Because the MT concentration is very high in the solution, we have analyzed the MT growth dynamics in the solution by diluting it 50-fold into PEM 80 buffer and immediately fixing the MTs using the same amount of solution of 3% glutaradehyde for at least 3 min. The solution containing the fixed MTs was transferred

onto a poly-L-lysine coated slide for observation. The microchips were pulled out after polymerization, rinsed with PBS buffer for approximately 10 s, and fixed using methanol (-20 °C) for 3 min. The microtubules both on the glass slide and on the microchips were examined using immuno fluorescent microscopy. Detailed structural information was also obtained by scanning electron microscopy (SEM). The samples were prepared by supercritical CO_2 drying after fixing the MTs with glutaradehyde (3%) followed by sputtering a thin film of gold.

Gold Substrates.

Two different geometries of gold substrates were used in the study of the effect of the substrate on MT morphology. The gold substrates were patterned on a hydrophilic oxidized silicon wafer. The first substrate is nearly semi-infinite compared to the scale of MTs with dimensions 1.9 ×3.8 mm^2. The second geometry consists of a square lattice of small gold square pads (10 µm ×10 µm) on a hydrophilic oxidized silicon wafer. The periodicity of the lattice was also 10 µm. The cross sections of the two types of geometries are illustrated in Figure 7.3.

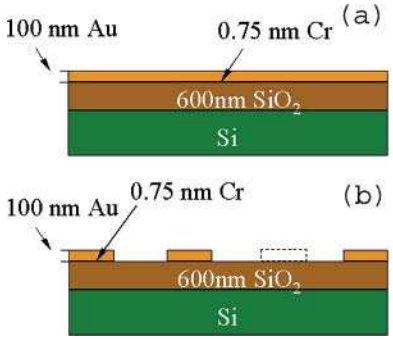

Figure 7.3 Cross sections of the oxidized silicon substrate patterned with (a) a large gold electrode (1.9 ×3.8 mm^2) and (b) an array of small gold pads (10 ×10 μm^2).

Results and Discussion

Microtubules were grown in the presence of two different gold surfaces prepared on hydrophilic oxidized silicon wafers. The gold pads on the first sample were functionalized with the GST-γ-tubulin as a nucleation protein. The gold pads on the second sample were not functionalized, and their immersion in a solution of γ-tubulin served as a control experiment. In Figure 7.4 we report Fluorescent microscopy images of typical pads on both samples. Sampling of the solution in which the non-functionalized sample was immersed indicated the presence of numerous MTs in suspension; however, none are seen on the surface of the non-functionalized substrate. In contrast the functionalized gold pad appears to be covered with MTs. To rule out direct nonspecific interaction between MTs self assembled in the solution and the functionalized gold electrodes, we have compared the growth dynamics of MTs grown in solution and of MTs that appear to cover the γ-tubulin functionalized gold surfaces.

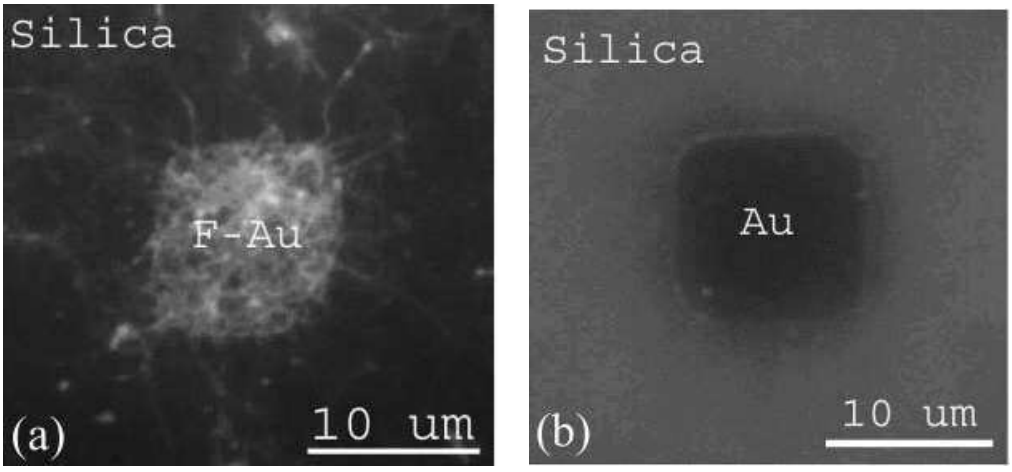

Figure 7.4 Fluorescence microscopy images of a typical small gold electrode on silica in (a) a sample with functionalized gold electrodes (F-Au) and (b) a sample with non-functionalized electrodes (Au) (cleaned with piranha solution). The immersion time in the tubulin containing solution is 30 min.

Two series of experiments were conducted for different growth times. In the first series we investigated the growth dynamics of the MTs that appear to cover the functionalized gold electrodes. The second series consisted of a study of the growth dynamics of MTs in the absence of functionalized substrate under the same growth conditions. Two polymerization time periods were considered: 5 and 10 min. The length distributions of MTs grown in the presence of a substrate that appear to cover the gold electrodes and the length distribution of MTs nucleated and grown in solution were measured. We report in Figure 7.5 the length distribution after 5 and 10 min of polymerization. The experiments that lasted 5 min show trends similar to those that lasted twice as much but of course lower values of the average MT lengths. Figures 7.5a and 7.5b show that the functionalized gold pad has a strong influence on the growth dynamics of MTs. The average lengths of MTs grown in solution are approximately 0.62 and 1.11 μm after 5 and 10 min of polymerization, respectively. In the presence of functionalized microchips, the average lengths of MTs on the functionalized gold surfaces increased significantly. Comparing the results of the polymerization with and without functionalized microchips, the average MT length increased from 0.62 to 1.68 μm for 5 min of polymerization and increased from 1.11 to 3.47 μm for the longer experiments. This result indicates that the γ-tubulin functionalized gold surface interacts specifically with MTs by promoting the nucleation of MTs and their subsequent growth.

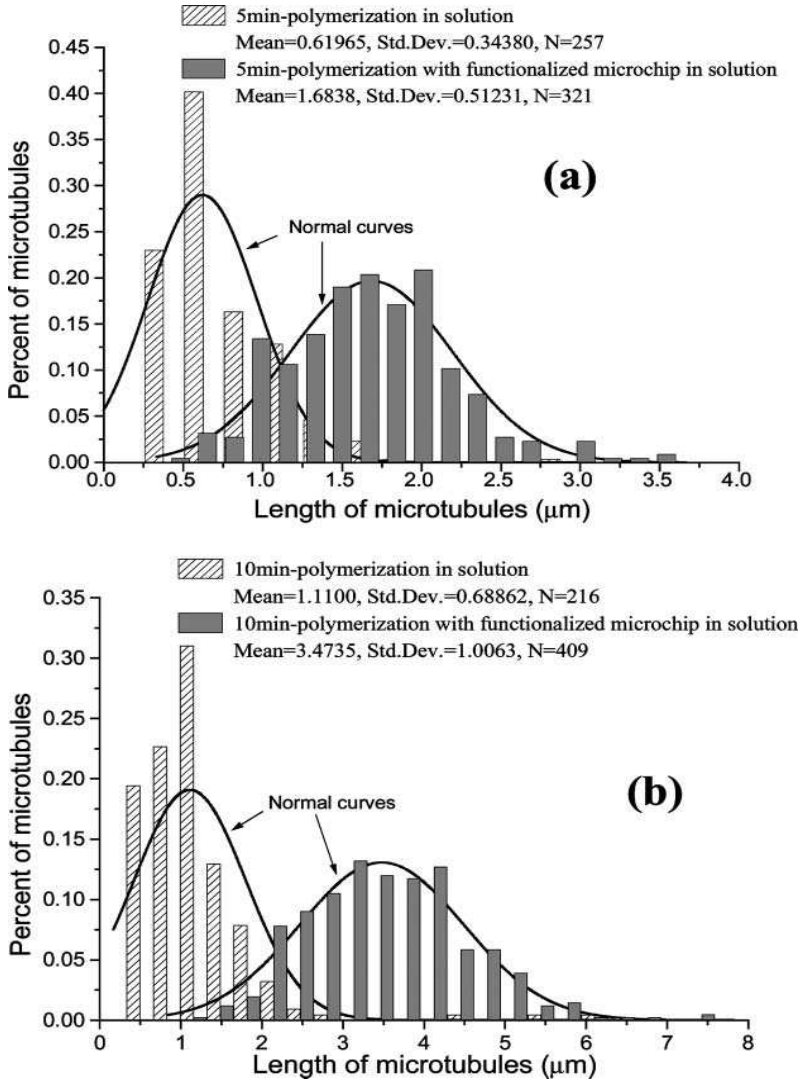

Figure 7.5 Length distribution of MT polymerized for 5 min (a) and 10 min (b) in solution and from a square array of γ-tubulin functionalized gold pads.

To verify that MTs growing from the functionalized gold pads are tethered to the γ-tubulin coated surface, we have conducted real time observations of MT growth under a Fluorescence microscope. For this experiment we have used a large flat functionalized gold substrate. A droplet of solution containing fluorescent tubulin was placed directly onto the functionalized gold surface for MT assembly and observed using Fluorescence microscopy. By using different focal planes, MTs were found both on the gold surface

and in the solution above the surface. The MTs observed in the proximity of the substrate are anchored by one end to the surface. We show in Figure 7.6 that a single MT that appears to be attached by one end to the surface. The microscope is focused on the pad surface thus the segment of the MT nearest to the substrate is in focus. The other end of the MT is blurred and out of focus, indicating that the MT is pointing into the solution. By applying pressure onto the cover slip of the microscope slide, we have induced a shear flow of the solution that drags and aligns the pointing end of the MT in its direction. The end of the MT closest to the substrate does not undergo any displacement showing that the MT is indeed bound to the functionalized gold pad. MTs nucleated and grown from a functionalized surface are shown to be amenable to orientation by fluid flow. Additional post nucleation and growth observations of flow-aligned MTs are presented in Figure 7.7. MTs were grown from a large functionalized gold pad for 30 min. Orientation of the MTs results from fluid passing over the surface during the immersion of the sample into the solution containing methanol used for fixing them. All MTs are aligned in the same direction and appear to be bound by one end to the substrate. It can be assumed that these MTs are bound by their (-) end as it is a known fact that γ-tubulin interacts only with that end (Lodish et al., 2003; Leguy et al., 2000).

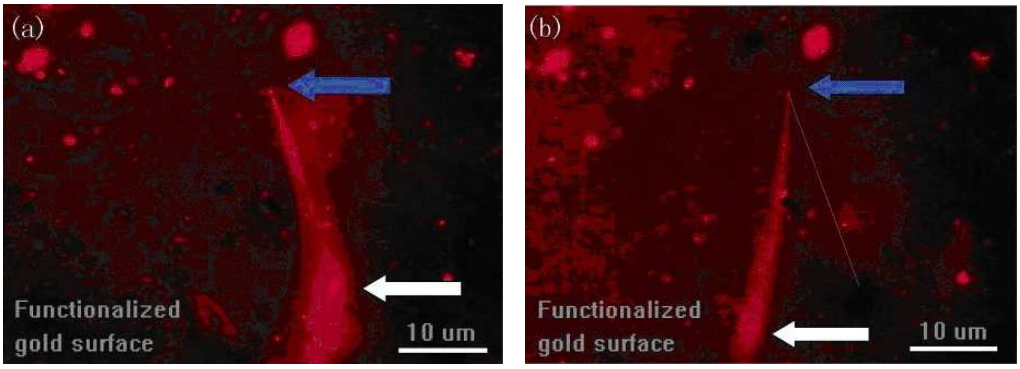

Figure 7.6 Fluorescence microscope images of a single MT polymerized from a γ-tubulin functionalized gold surface subjected to a fluid flow. Both images show that the MT has one end anchored to the surface (indicated by the blue arrow) with its other end out of focus pointing into the solution (marked by the white arrow). The dotted line in (b) marks the initial position of the MT prior to fluid flow. Bright spots on the surface are believed to be unstructured clusters of fluorescent tubulin.

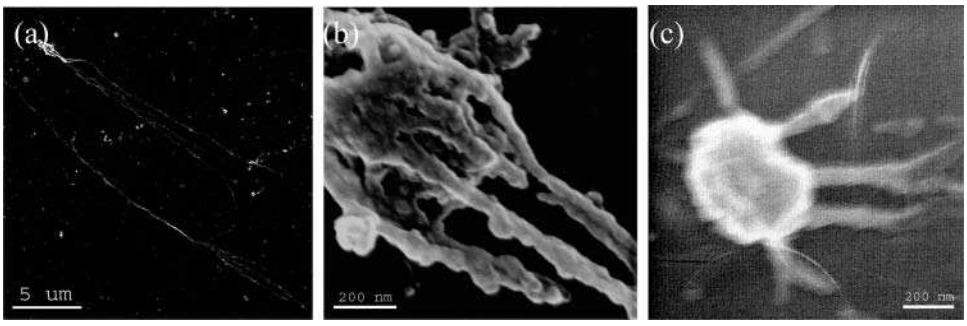

Figure 7.7 (a) Scanning electron microscopy (SEM) picture of MTs nucleated and aligned on the large functionalized gold substrate, (b) magnified SEM picture of the nucleation center in (a), (c) magnified SEM picture of a nucleation center that gave rise to only short MTs.

Quantitative analysis of images such as that of Figure 7.7a gives a low surface density of surface nucleation centers originating MTs of approximately 0.92 per 100 μm^2. This is a lower bound since we did not account for MTs shorter than 1 μmin when estimating this density. This density gives an estimated area per center nucleating MTs of approximately 108 μm^2, yielding a mean distance between MT originating nucleating centers of approximately 12 μm. Figure 7.7b shows that some of the MTs grown from the

surface are very long with a very wide distribution which is presented in Figure 7.8. The average length of the MTs is 22 μm and numerous bright fluorescent dots are observed on the functionalized gold surface. These must be composed of tubulin dimers clustered on the γ-tubulin functionalized surface. Some of these clusters appear to serve as centers from which one to several MTs originate. We note however that other MTs do not originate from a cluster and appear to have nucleated directly from the functionalized surface (as was also seen in Figure 7.6). Figure 7.7 also shows several clusters that are not associated with grown MTs. Figure 7.8 reports two SEM images of MTs nucleated on the large gold surface with different magnification. In Figure 7.8a one sees several very long MTs extending out from a cluster. The cluster is magnified in Figure 7.8b, showing that it contains several short MTs in addition to the very long one observed in Figure 7.4a. The cluster therefore appears to have the characteristics of a centrosome-like MT nucleation center, which enables the initiation and growth of numerous MTs (Bornens, 2002). In Figure 7.4c we show a nucleation center (cluster) that does not lead to the growth of long MTs but from which only short MTs (submicron in length) have emerged.

We have aligned the MTs by Marangoni fluid flow (Velarde, 1998) of the buffer solution over their surface. We start with a microchip covered with a droplet of buffer solution. The volume of the aqueous buffer solution droplet covering the sample was 3 μL at room temperature. When added at one side of the microchip, methanol at -20 °C quickly spreads into the solution (see Figure 7.9). The surface tension increases from the side where methanol was added to the opposite side. Marangoni flow occurs from the region with the lowest surface tension to the region with the highest surface tension. The

hydrostatic pressure increase in the region with higher surface tension induces a flow along the solution-substrate interface in the direction opposite to the Marangoni flow, orienting the surface bound MTs in the direction opposite to the direction of spread of the methanol. Once covered by methanol (-20 °C), the MTs are fixed on the functionalized surface.

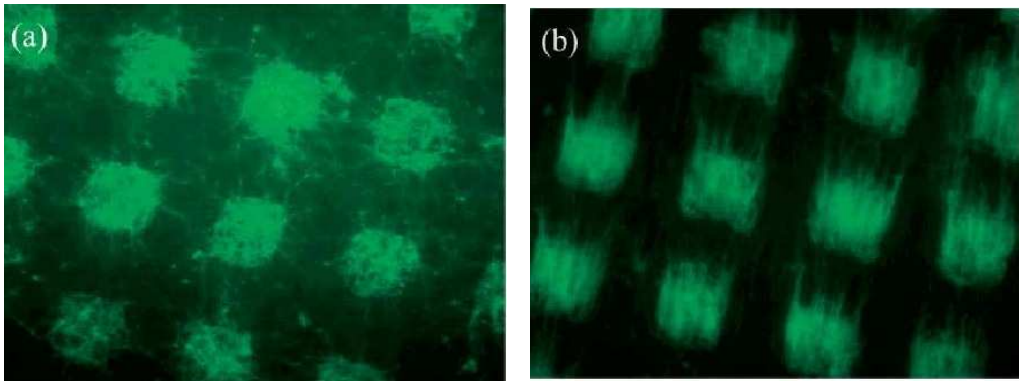

Figure 7.8 (a) Fluorescent microscope images of MTs grown from the square array of functionalized gold pads after 30 min of polymerization at 37 °C; (b) same as (a) but after alignment of the MTs by flowing fluid over the substrate.

The Fluorescent microscopy image of oriented MTs shown in Figure 7.8b appears to exhibit slightly brighter contrast near the edges of the square pads that are parallel to the direction of flow compared to the edges perpendicular to the flow. This observation suggests that more MTs may have nucleated near the edges of the pads or that more MTs have been able to grow from the edges of the pads than from the center.

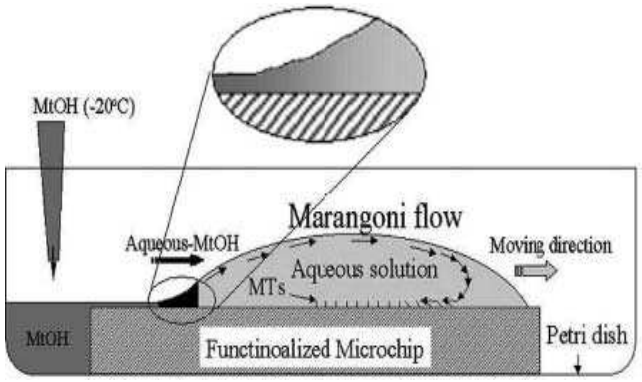

Figure 7.9 Experimental configuration for aligning MTs using Marangoni flow. Marangoni flow is induced by a gradient in surface tension at the solution-air interface (see text for details). The size of the substrate is exaggerated. Its actual size is 3 mm x 3 mm.

Our experiments show that surface bound γ-tubulin promotes MT nucleation. The difference in the growth behavior of MTs from the surface of the large functionalized gold pad and from the small pads (with strong edge effect) may then be the result of a non-uniform distribution of active nucleating fusion protein. As was stated in the Introduction, the arrangement of γ-tubulin proteins within a nucleation center is critical for effectively initiating nucleation. More favorable arrangements of the γ-tubulin coating may occur at the edge of the pads. A higher density of active nucleation sites at the edge of the gold pads may lead to a higher density of growing microtubules. On the other hand, the existence of nucleation centers on the large gold pad from which only very short MTs have grown (see Figure 7.7c) suggests that other processes may be involved for this geometry. For instance, a reaction diffusion process may play a role in the growth morphology of MTs from the extended functionalized surfaces (nearly semi-infinite geometry).

Conclusions

We have been able to functionalize gold surfaces with a MT nucleating protein, namely, γ-tubulin. We have also shown that the surface bound γ-tubulin retains its biological ability to nucleate MTs using fluorescent microscopy.

The dynamics of MTs grown from a γ-tubulin functionalized surface is drastically different from that of MTs grown from a solution, showing that the functionalized surface interacts specifically with the MTs. MTs grown in the presence of functionalized substrates have a longer length than those without functionalized substrate presence. MTs grown in the presence of functionalized substrates are tethered to the surface by one end which is believed to be the minus end of the MTs. This is proven by SEM images and MT aligning experiments using Marangoni flow.

CHAPTER 8 HETEROGENEOUS MICRO PATTERNING OF BIOMOLECULES ON GOLD SURFACE PLATFORMS WITH PHOTOREACTIVE COMPOUNDS

Abstract

For numerous applications such as biological sensing, biological activation of inorganic substrates, it is very important to develop a technology to precisely immobilize biomolecules in well defined patterns while retaining their native functionality.

In this work, self assembled monolayers (SAMs) of a photoreactive derivative were incorporated onto two adjacent gold coated pads on a silicon dioxide substrate. A successive photoreaction allowed the formation of a heterogeneous patterning of two specific functional biomolecules (antibodies).

With the incorporation of a photoreactive compound monolayer (4-[p-azidosalicylamido] butyl amine, ASBA) to carboxylic SAM functionalized gold pads, two different antibodies were successively immobilized onto the pads by using a photolithographic approach to form functional micro-scale dual protein pattern structures.

We have verified by fluorescent microscopy, that we can form micro-scale heterogeneous biomolecular patterns with two or more antibodies.

Introduction

A major challenge in the fabrication and development of biological devices has shown the ability to design advanced surfaces with controlled interaction with the biological world. Bio-interactions can be improved through surface functionalization, i.e.,

modifying the surface with chemical groups that trigger the proper interaction with biomolecules and cells. The protein based biosensoring platforms must provide optimal conditions in terms of protein orientation, binding capacity and activity in order to guarantee optimum performance (Frederix et al., 2003).

Submicron patterned surfaces can provide a big enhancement as compared with non-patterned surfaces in many applications (Valsesia et al, 2006; Lee et al., 2004; Agheli et al., 2006).

Many techniques are available to develop advanced platforms with controlled surface chemistry and well defined patterns at the nano-scale. These techniques can be classified as conventional or unconventional. Conventional techniques—projection lithography and scanning beam (or maskless) lithography — are highly developed and widely used for fabricating microelectronic circuits. The most common type of projection lithography is photolithography. A number of unconventional methods developed for nanofabrication enable new types of fabrication and circumvent limitations such as soft lithography (Gates et al., 2004; Falconnet et al., 2004; Xia et al., 1999), dip pen lithography (Lee et al., 2002) and scanning probe lithography (SPL) (Ginger et al., 2004; Kraemer et al., 2003).

Scanning beam lithographic techniques, such as electron beam and focused ion beam lithography, offer alternative approaches to patterning small features. These serial techniques are, however, slower than the parallel approach of projection lithography (Broers et al., 1976)

Soft lithography refers to a collection of techniques for creating microstructures and

nanostructures based on printing, moulding and embossing (Xia et al., 1998). The term soft refers to the stamp and/or to the substrate when they are composed of soft matter (e.g., polymers or self assembled monolayers). Soft lithography typically has features with lateral dimensions of 1–1000 μm and vertical dimensions between 100 nm and hundreds of microns (Quist et al., 2005; Delamarche, 2004; Weibel et al., 2005). This method has alignment difficulty during multiple step printing.

Scanning probe lithography (SPL) localizes modification of a surface by oxidation or by material transfer using a sharp probe in contact with the surface (Ginger et al., 2004; Kraemer et al., 2003). SPL is primarily serial process, so it is inherently slow.

In this work, a photolithographic method was used to form a heterogeneous protein pattern on micro-scale gold coated pads. The experiment involved using a photo reactive compound monolayer (ASBA), which was coated onto carboxylic SAM functionalized surfaces. Then different proteins were immobilized on the functionalized surfaces by the photochemical reaction between the amino groups on the proteins and the azide groups of ASBA. The structural formula of ASBA is shown in Figure 8.1. The micro-scale dual protein patterning was verified by fluorescent microscopy using two fluorescent tagged immunoglobins (IgG).

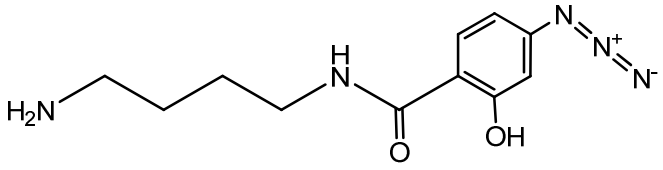

Figure 8.1 Structure formula of ASBA

Materials and Methods

Materials

16-mercaptohexadecanoic acid (MHA) ($HS(CH_2)_{15}COOH$, 90%), 1-ethyl-3-(3-dimethylaminopropyl) carbodiimide hydrochloride (EDAC), ethanol (200-proof) were obtained from Aldrich (Milwaukee, WI); sodium phosphate dibasic heptahydrate ($Na_2HPO_4 \cdot 7H_2O$, 98.0%), sulfuric acid (95%), and 30 % hydrogen peroxide from Fisher (Fairlawn, NJ) were used without further purification. FITC tagged mouse anti rabbit IgG, and rhodamine tagged mouse anti goat IgG were supplied from Sigma–Aldrich (St. Louis, MO). 4-(p-azidosalicylamido) butyl amine (ASBA) was purchased from Pierce Biotechnology (Rockford, IL). Gold-patterned silicon dioxide wafers were prepared at the Micro/nano Fabrication Center, University of Arizona (Tucson, AZ). Ultra pure water (18 MΩ·cm) produced by a Milli-Q system was used through all experiments.

Gold Substrates

The substrates were prepared from 2-inch silicon (111) wafers. A hydrophilic silicon dioxide layer of 600 nm was deposited on the wafer in a thermal furnace at a temperature of 950 ºC while feeding a 2% water vapor. Then a gold layer was patterned to the silicon oxide surface by photolithographic methods. The gold layer has a thickness of 100 nm with a layer of 0.75 nm Cr as an adhesive between the gold and the silicon dioxide.

The gold patterns have different micro-scale features that include a region of 4 small gold square pads (20 µm ×20 µm) on a hydrophilic silicon oxide, and these square pads are 20 μm apart. The 3-D illustration of this region is shown in Figure 8.2.

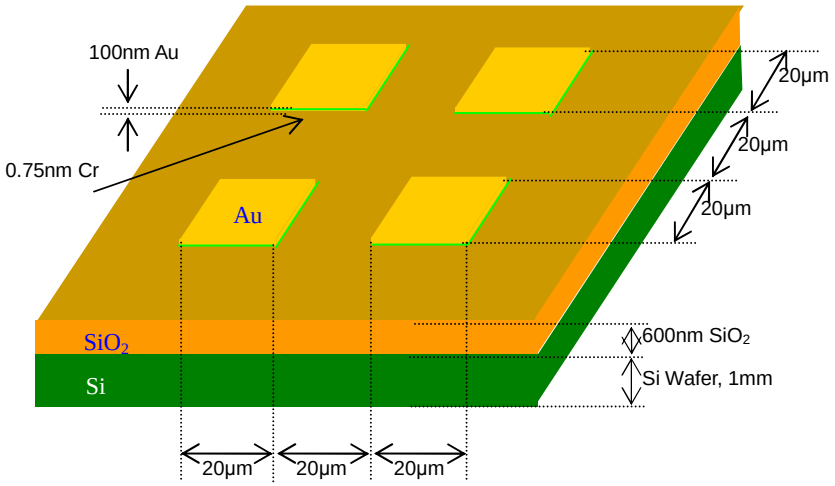

Figure 8.2 3-D view of the oxidized silicon substrate patterned with 4 small gold pads (20 ×20 µm^2), 20 µm apart; 0.75 nm Cr is used to attach the gold pads onto the silicon dioxide. The thickness of the gold pads is 100 nm.

Surface Functionalization

The functionalization of the gold pads with a photoreactive compound on the silicon dioxide surface is schematically described in Figure 8.3. The gold patterned silicon dioxide wafer was cleaned using a piranha solution (95% H_2SO_4/30% H_2O_2, 70:30, v/v). The wafer was immersed in a freshly prepared piranha solution for 30 min in an ultrasonic bath followed by washing thoroughly with water. Then the wafer was immersed into a saturated MHA aqueous solution containing 10% ethanol and left reacting for 48 hours to allow the SAMs of MHA to react to completion in the right orientation. After that, the wafer was rinsed with water.

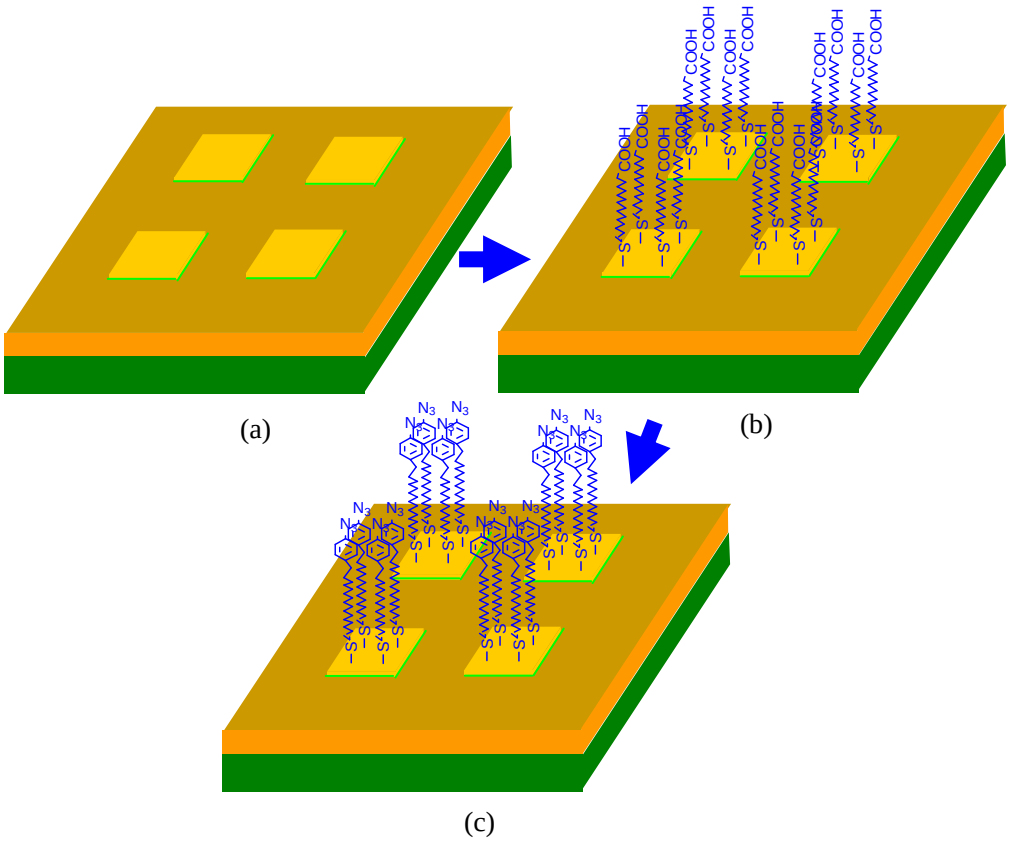

Figure 8.3 Schematic of functionalization of gold pad pattern: (a) gold patterned silicon dioxide substrate; (b) self assembling of bifunctional thiol compound; (c) activated surface with photoreactive compound

The MHA SAM coated surface was immersed into the 0.1 M MES buffer (pH 4.8) that included 1.0 mg/mL ASBA and 1.0 mg/mL EDAC. The wafer was gently shaken for 4.0 hours and then rinsed with water. In this step, a condensation reaction occurred between the carboxyl groups from the MHA SAMs and the amino groups from the ASBA. The carbodiimide, EDAC reacts with the carboxyl groups, first forming an active intermediate, and then the intermediate reacts with the amino group of the ASBA compound. This reaction is shown in Figure 8.4.

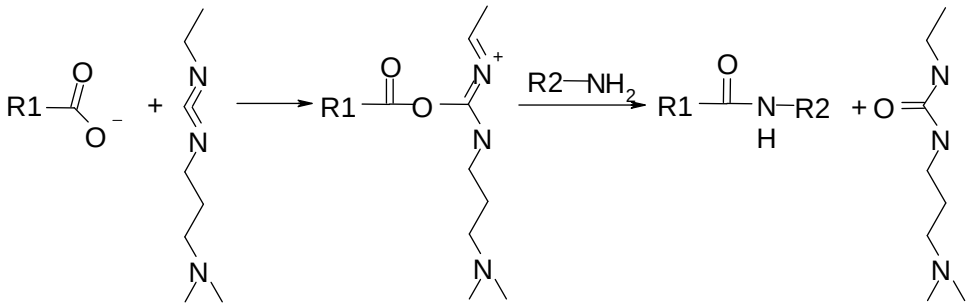

Figure 8.4 Chemical reaction mechanism of the condensation reaction between an amino group and a carboxyl group via the carbodiimide reagent, EDAC.

Protein Patterning

After rinsing with water, the wafer was loaded onto the ABM Alignment and Exposure System. Applying a designed chromium coated mask to the top of the wafer, 2 of the 4 gold pads were covered by the mask and the other 2 pads were exposed to the UV light. To this system, a 1.0 mg/mL of antibody (goat IgG) solution was added between the mask and the wafer, afterwards a long wavelength UV light (λ=365 nm) was applied to the mask. In this process, ASBA on the UV light exposed pads was activated by the UV light, forming a reactive nitrene intermediate that reacted immediately with the amino groups of the antibody. This reaction scheme is schematically shown in Figure 8.5. In the next step, the unbound antibody was removed by washing with PBS buffer for 30 seconds. To attach the second antibody (rabbit IgG), the above process was repeated, but this time the previously antibody functionalized pads were protected using a chromium coated mask so that now the previously non-exposed pads went through a similar activation and binding procedure. Once the process was complete, the wafer surface was

rinsed with buffer, and the dual protein patterned surface was obtained. The patterning process is schematically presented in Figure 8.6.

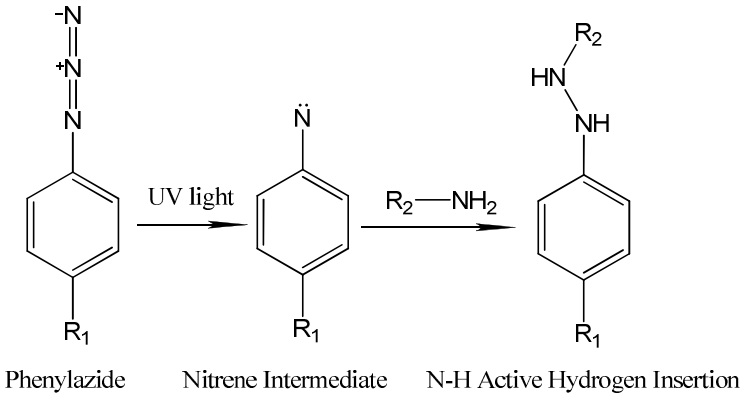

Figure 8.5 The photochemical reaction mechanism between an amino group and an azide group

Verification of Heterogeneous Protein Patterning

Prior to verifying the dual protein pattern by Fluorescent microscopy, we tested the specificity of the fluorescent tagged secondary antibodies to the background surface and the primary antibodies. In these background control experiments, the monoclonal mouse anti goat IgG-rhodamine and monoclonal mouse anti rabbit IgG-FITC were added to clean gold, MHA SAM modified, and ASBA modified surfaces, respectively.

To verify the specificity of the primary antibodies on the surfaces to the fluorescent tagged secondary antibodies, the goat IgG and rabbit IgG were directly bound to the ASBA coated surfaces covalently, respectively. Then a mixture of the secondary antibodies (rhodamine tagged monoclonal mouse anti goat IgG and FITC tagged monoclonal mouse anti rabbit IgG) was added to these surfaces to check the cross interaction between the primary and secondary antibodies by immuno fluorescent microscopy.

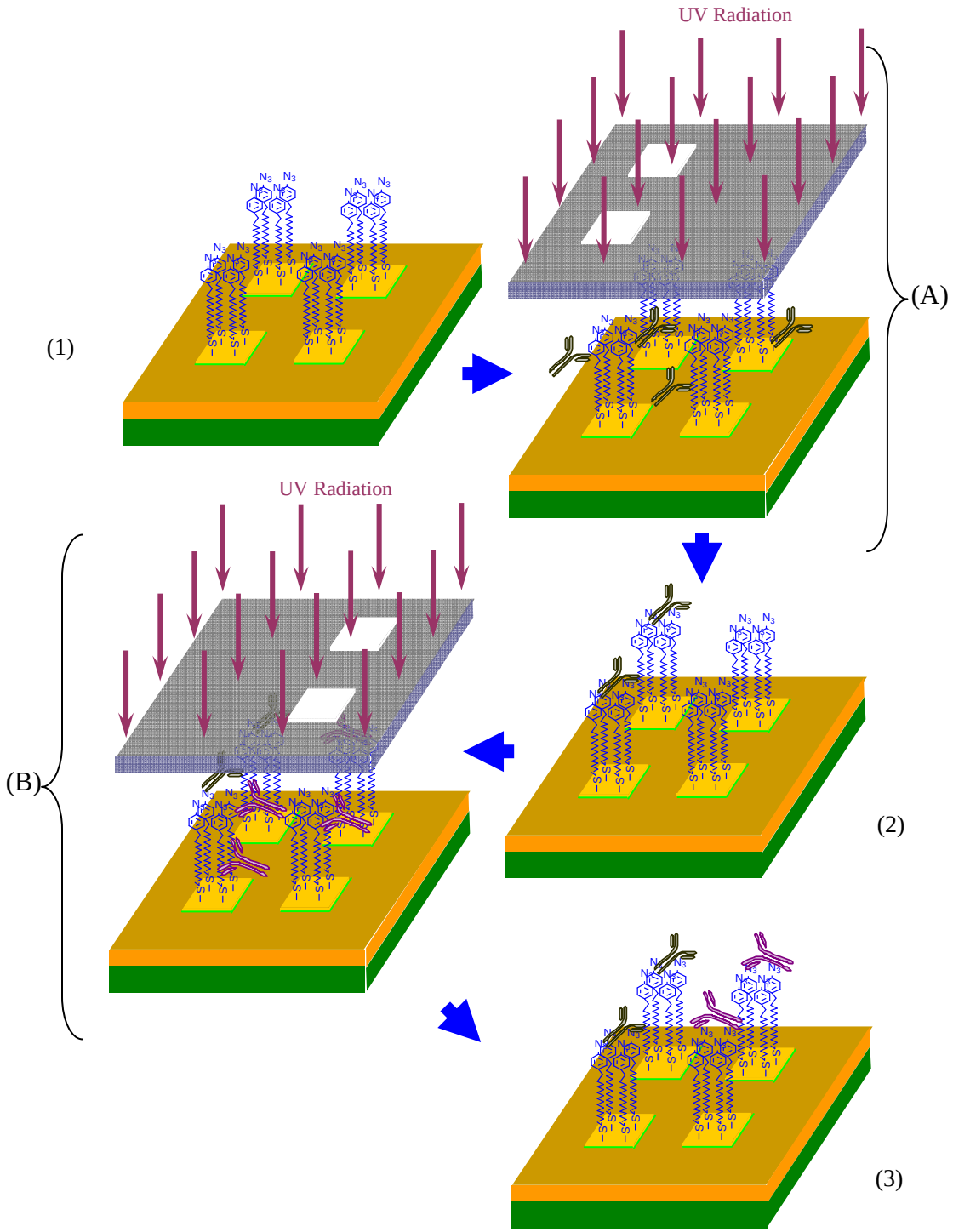

Figure 8.6 Schematic of protein micro patterning process: (A), (B) sequential photo activation steps; (1) initial surface coated with photoreactive compound; (2) functionalization with first antibody; (3) final heterogeneous functionalized surface.

To verify the heterogeneous protein patterned surface, a mixture consisting of both fluorescent tagged secondary antibodies that react with the immobilized goat IgG and rabbit IgG respectively was added to the heterogeneous patterned surface. Once the antibody-antigen interaction took place, the wafer was observed under a fluorescent microscope. The fluorescent dye labeling process is schematically presented in Figure 8.7.

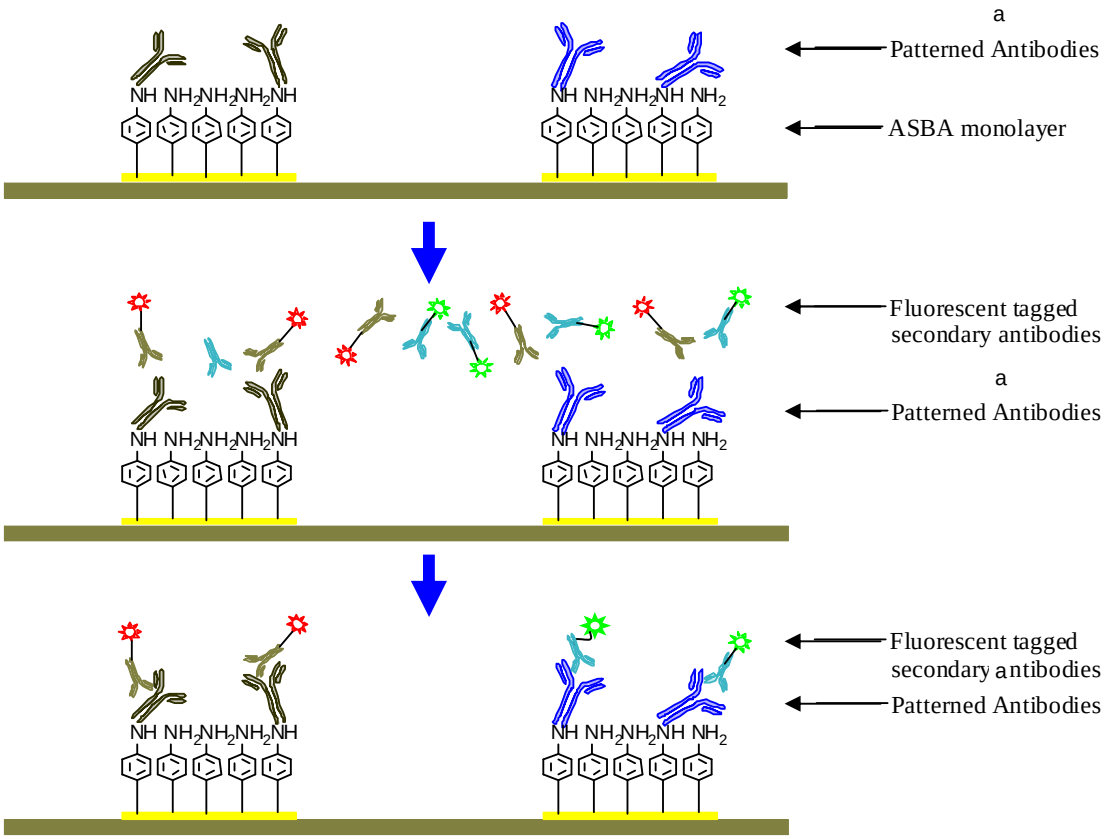

Figure 8.7 Schematic of fluorescent dye labeling process for verification of heterogeneity of patterned biomolecular structures.

Results and Discussion

From the background control experiments, there was no fluorescence on clean gold, MHA SAM modified, or ASBA modified surfaces, which means the fluorescent tagged secondary antibodies did not adsorb to such surfaces by nonspecific adsorption.

The high specificity of the primary antibodies to the secondary antibodies is shown in Figure 8.8. On the goat IgG coated surface, there was no green fluorescence which means the monoclonal anti rabbit IgG-FITC was not adsorbed onto the surface. The strong red fluorescence shows that the monoclonal anti goat IgG-rhodamine was adsorbed to the surface. Comparing the rabbit IgG coated surface, where only monoclonal anti rabbit IgG-FITC not monoclonal anti goat IgG-Rhodamine adsorbed to the surface, the control experiments show that the fluorescent tagged secondary antibodies bind to specific primary antibodies without cross interaction between the two complementary antibodies.

The fluorescent images taken from the heterogeneous protein patterned surfaces described in Figures 8.3, 8.6, and 8.7 are shown in Figure 8.9. These two images were taken at the same position on the same wafer but using different wavelength filters. The squares in the images have the dimensions of 20 μm and are 20 μm apart.

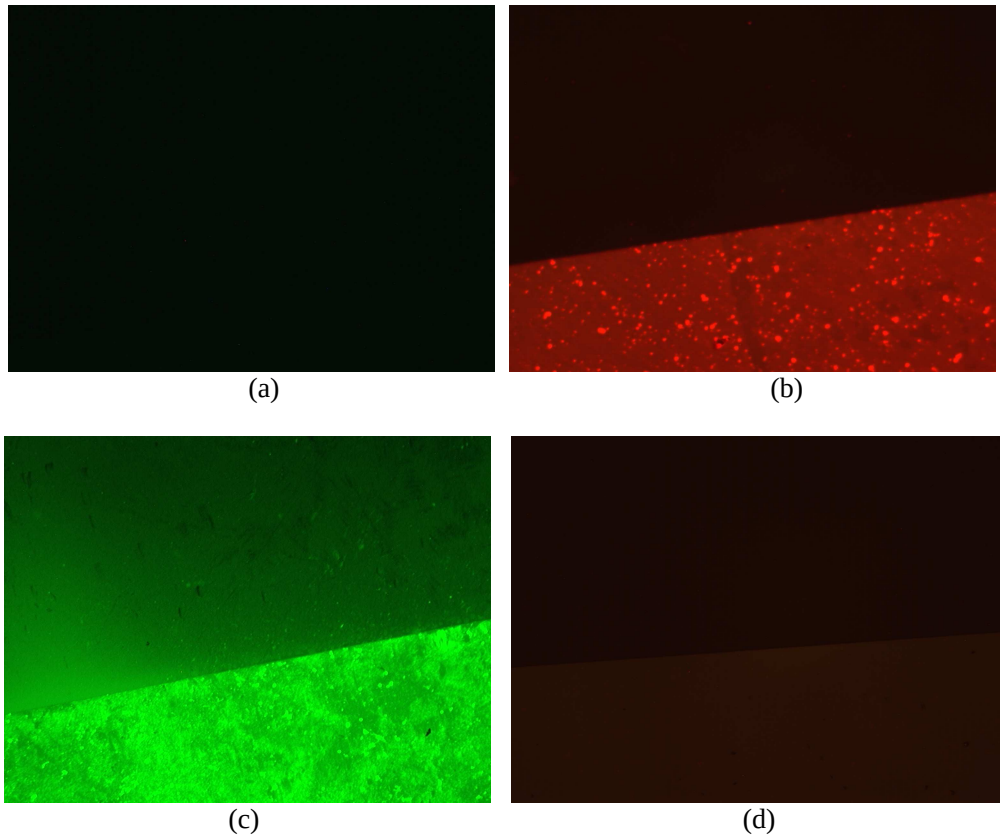

Figure 8.8 Fluorescent images were obtained after the attachment of mixture of monoclonal secondary antibodies to IgG surfaces. Image a) and b) were taken on goat IgG modified surface and a) the specimen was excited at λex ~495 nm and monitored at λem ~520 nm with the exposure time of 4 s; b) the specimen was excited at λex ~545 nm and monitored at λem ~610 nm with the exposure time of 1 s. Image c) and d) were taken on rabbit IgG surfaces and c) the specimen was excited at λex ~495 nm and monitored at λem ~520 nm with the exposure time of 4 s; d) the specimen was excited at λex ~545 nm and monitored at λem ~610 nm with the exposure time of 1 s.

In Figure 8.9a, the left 2 squares have red fluorescence only and no green fluorescence in the left squares of Figure 8.9b. This means that these 2 left squares only have the goat IgGs attached which only adsorb rhodamine tagged anti goat IgG (red). The right 2 squares have only rabbit IgGs which adsorb only FITC tagged anti rabbit IgG (green)

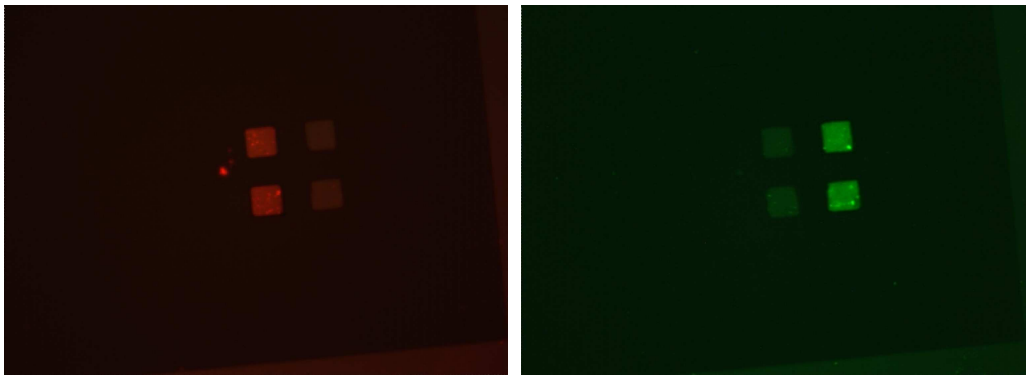

(a) (b)

Figure 8.9 Fluorescent images of heterogeneous protein patterned surface (a) the exposure times used were 1 s. The specimens were excited at λex ~545 nm and monitored at λem ~610 nm. (b) the exposure times used were 4 s. The specimens were excited at λex ~495 nm and monitored at λem ~520 nm.

From these images, one can verify that a dual protein pattern with goat IgG and rabbit IgG through a photolithographic method together with a photoreactive compound was successively functionalized onto micro sized gold surfaces. These surfaces can now be used to explore the growth of MTs with two cap proteins between at least two gold electrodes to form bio-nanointerconnectors.

Conclusions

The surface functionalization by ASBA through the MHA SAMs provides a useful approach of immobilization of multiple active biomolecules by photoreaction. By covalently attaching ASBA to the MHA SAM modified gold surface using a condensation reaction, different proteins can be bound to specific locations on a patterned substrate via photo lithographic methods.

The patterning of heterogeneous biomolecules on two micro-scale gold surfaces separated by a few microns was successfully obtained via photolithographic methods and

a photoreactive derivative. Each gold surface was modified with a different specific antibody. By repeating the masking and exposure steps, different proteins can be attached to gold surfaces to form heterogeneous protein patterns. The dual micro-scale protein patterns obtained in this work were verified by fluorescent microscopy.

The process reported in this work is amenable to patterning substrates with more than 2 different biomolecules. This method has extensive usefulness to the development of bio platforms for biosensors or biological applications in nanotechnology.

CHAPTER 9 CONCLUSIONS

This dissertation reports the work on the development of a novel bioseparation method for small proteins and peptides, namely size exclusion immobilized metal ion affinity chromatography (SEIMAC). These studies will help elucidate limits and potential application of the method as a viable alternative for affinity separation of proteins and peptides.

SEIMAC's features involve simultaneous specific adsorption with a chelator (IDA) and size exclusion control by the incorporation of permeating polymers, in our study using polyethylene glycol (PEG). SEIMAC hybrids were prepared with an agarose based matrix, Novarose, the chelator iminodiacetic acid (IDA) and the polyethylene glycol derivative, M-PEG-amine. Model proteins for this work included lysozyme, BSA, and myoglobin. To elucidate the effect of the permeation by the polymer, hybrid gels were prepared with different densities of PEG and a fixed density of the chelator. Metal ion capacities (for copper) remain constant in all these preparations. Once the metal was immobilized, binding studies with both BSA and lysozyme were performed. In all cases, a decrease of protein adsorption capacity was observed with BSA (a larger protein) being more pronounced as expected compared with lysozyme (a smaller protein). When a fixed density of PEG was bound to the gel with varying density of chelator, the results were similar with a BSA decrease in capacity again more evident.

The kinetics of chelator attachment on the matrices were also analyzed in this research, the objective and contribution of this analysis was to determine and control the

desired amount of a chelating ligand (ligand density) on a matrix, for a specific application. A mathematical model was derived that effectively explains the results and observations. Once specific experimental parameters were determined, the model helps predict apparently, very accurately, chelating loading density.

A similar analysis was performed on the kinetics of polymer (PEG) attachment to the chromatographic matrices to elucidate polymer density effects on the permeation of proteins.

Thus, this new methodology offers a potential tool as a peptide specific adsorbent. Studies with other metal ions, other chelators, and other polymers will help advance and prove the feasibility of this approach as a practical alternative for biomolecular separation.

A major task of this dissertation was also the preparation, functionalization, and characterization of smart platforms based on gold surfaces and self assembled monolayers (SAMs) to incorporate affinity ligands and biomolecules. The surfaces were effectively functionalized with proteins such as avidin, trypsin and immunoglobins (IgGs). In most of the studies, SAMs were prepared with MHA and then modified with affinity ligands via condensation reactions with carbodiimide derivatives.

The specifically functionalized SAMs (FSAMs) were used as linkers to attach and grow MTs, nano protein structures that could be used as biomolecular nanointerconnectors. This work effectively demonstrated the attachment (as linkers) of a tubulin protein, γ-tubulin, via an anti-GST coupling to the gold-SAM surface. Binding and growth of MTs on the γ-tubulin derivatized surfaces were observed under different conditions and demonstrated with the effectiveness of the functionalization.

Along the same line of research to effectively bind and use the MTs as nano-interconnectors, dual heterogeneous functionalization surfaces were prepared. This last effort was accomplished by incorporating photolithographic methods common in the semiconductor industry and a photoreactive derivative, 4-(p-azidosalicylamido) butylamine (ASBA). The patterning of heterogeneous biomolecules on two micro-scale gold surfaces separated by a few microns was successfully obtained. The dual micro-scale protein patterns obtained in this work were verified by fluorescent microscopy. This dual micro-scale protein patterns would be used for the idea that once one end of the MTs bind to one of the heterogeneous linkers, MTs will grow and attach to another different linker in a closed by location (another adjacent or opposite functionalized gold electrode).

The common theme in this dissertation was the effective preparation and functionalization of different surfaces with applications in biotechnology and bio-nano manufacturing of novel biomolecular nanostructures.

REFERENCES

Agheli, H.; Malmstroem J.; Larsson E. M.; Textor, M.; Sutherland, D. S. **Nanostructured biointerfaces.** *Nano Lett.* **2006**, 6 (6), 1165–1171

Aguilar, Z. P.; Vandaveer, W. R. I. V.; Fritsch, I. I. **Self-contained microelectrochemical immunoassay for small volumes using mouse IgG as a model system.** *Anal. Chem.* **2002**, 74, 3321-3329.

Antikainen, N. M.; Martin, S. F. **Altering protein specificity: techniques and applications.** *Bioorg. Med. Chem.* **2005**, 13 (8), 2701-2716.

Arakali, S. V.; Luft, J. R.; DeTitta, G. T. **Non-ideality of aqueous solutions of polyethylene glycol: consequences for its use as a macromolecular crystallizing agent in vapor-diffusion experiments.** *Acta Cryst.* **1995**, D51 (5),772-779

Ashby, P. D.; Chen, L. W.; Lieber, C. M. **Probing intermolecular forces and potentials with magnetic feedback chemical force microscopy.** *J. Am. Chem. Soc.* **2000**,122, 9467-9472.

Auer, F.; Scotti, M.; Ulman, A.; Jordan, R.; Sellergren, B.; Garno,J.; Liu, G. Y. **Nanocomposites by electrostatic interactions: 1. Impact of sublayer quality on the organization of functionalized nanoparticles on charged self-assembled layers.** *Langmuir* **2000**, 16, 7554-7557.

Bain, C. D.; Troughton, E. B.; Tao, Y. T.; Evall, J.; Whitesides, G. M.; Nuzzo, R. G. **Formation of monolayer films by the spontaneous assembly of organic thiols from solution onto gold.** *J. Am. Chem. Soc.* **1989**, 111, 321-335.

Ben-Dov, I.; Willner, I.; Zisman, E. **Piezoelectric immunosensors for urine specimens of chlamydia trachomatis employing quartz crystal microbalance microgravimetric analyses,** *Anal. Chem.* **1997**, 69, 3506-3512.

Benjamin J. H.; Ortiz-Vega, M. J.; Wang, L. N. H. **Adsorption of [N-(phosphonomethyl)imino]diacetic acid and iminodiacetic acid on poly(4-vinylpyridine),** *Ind. Eng. Chem. Res.* **1999**, 38, 2754-2764

Björling, M.; Karlström, G.; Linse, P. **Conformational adaption of poly(ethylene oxide): A carbon-13 NMR study.** *J. Phys. Chem.* **1991,** 95 (17), 6706–6709

Bonnerjea, J.; Hoare, S. O. M.; Dunnil, P. **Protein purification: the right step at the right time.** *Bio/Technology*, **1986**, 4, 955-958.

Bornens, M. **Centrosome composition and microtubule anchoring mechanisms.** *Curr. Opin. in Cell Biol.* **2002**, 14 (1), 25-34.

Boubour, E.; Lennox, R. B. **Insulating properties of self-assembled monolayers monitored by impedance spectroscopy.** *Langmuir* **2000**, 16, 4222-4228.

Broers, A. N.; Molzen, W. W.; Cuomo, J. J.; Wittels, N. D. **Electron-beam fabrication of 8-nm metal structures.** *Appl. Phys. Lett.* **1976**, 29,596–98

Bruice, P. Y. **Organic chemistry**, 4th edition, **2004,** Prentice Hall

Bushan, B. **Springer handbook of nanotechnology. 2004** 147–184, Springer-Verlag, New York

Caruso, F.; Rodda, E.; Furlong, D. N.; Niikura, K.; Okahata, Y. **Quartz crystal microbalance study of DNA immobilization and hybridization for nucleic acid sensor development.** *Anal. Chem.* **1997**, 69, 2043-2049.

Chaga, G. S, **Twenty-five years of immobilized metal ion affinity chromatography: past, present and future.** *J. of Biochem. Biophys. Methods*. **2001**, 49(1-3), 313-334.

Champluvier, B.; Kula, M. R. **Sequential membrane-based purification of proteins, applying the concept of multidimensional liquid chromatography (MDLC).** *Bioseparation* **1992**, 2(6), 343-51.

Chapman, R. G.; Ostuni, E.; Yan, L.; Whitesides, G. M. **Preparation of mixed self-assembled monolayers (SAMs) that resist adsorption of proteins using the reaction of amines with a SAM that presents interchain carboxylic anhydride groups.** *Langmuir* **2000**, 16, 6927-6936

Chase, H. A.; Draeger, N. M. **Affinity purification of proteins using expanded beds.** *Journal of Chromatography,* **1992,** 591, 129-145

Clemence, J. F.; Ranieri, J. P.; Aebischer, P. Sigrist, H.; **Photoimmobilization of a bioactive laminin fragment and pattern-guided selective neuronal cell attachment.** *Bioconjugate Chem* **1995,** 6 (4), 411–417.

Costello, B. A.; De, L.; Luckham, P. F.; Tadros, T. F. **Forces between adsorbed low-molecular-weight graft copolymers.** *J. Colloid Interface Sci.* **1993,** 156 (1),72–77.

CRC handbook of chemistry and physics. 88th edition. Lide, D. R. Ed., **2007-2008**, available at http://www.hbcpnetbase.com/.

Cuatrecasas, P.; Anfinsen, C. V. **Affinity chromatography.** *Ann. Rev. Biochemistry* **1971,** 40, 259-278.

Delamarche, E. **Microcontact printing of proteins.** *Nanobiotechnol.* **2004,** 31–52 .

Dubois L. H.; Zegarski B. R.; Nuzzo R. G. **Fundamental studies of microscopic wetting on organic surfaces. 2. Interaction of secondary adsorbates with chemically textured organic monolayers.** *J. Am. Chem. Soc*. **1990**, 112, 570-579

Duesman, K.; Chance, R. **Photolithographic processing using two photomasks to produce patter. 2004** U.S. Pat. Appl. Publ.

Elbert, D. L.; Hubbell, J. A. **Surface treatments of polymers for biocompatibility.** *Ann. Rev. Mater. Sci.* **1996**, 26, 365-394.

Enzelberger, M. M.; Minning, S.; Schmid, R. D. **Designing new metal affinity peptides by random mutagenesis of a natural metal-binding site**. *J. Chromatogr. A* **2000**, 898 (1), 83-94

Falconnet, D.; Pasqui, D.; Park, S.; Eckert, R.; Schift, H.;, Gobrecht, J.; Barbucci, R.; Textor, M. **A novel approach to produce protein nanopatterns by combining nanoimprint lithography and molecular self-assembly.** *Nano Lett*. **2004,** 4 1909–14

Fanou-Ayyi, L.; Vijayalaksmi, M. A. **Metal-chelate affinity chromatography as a separation tool, Annals of the New York Academy of Sciences.** *Ann. NY Acad. Sci.* **1983**, 413 (3), 300-306.

Felix, M. A.; Antony, C.; Wright, M.; Maro, B. *J.* **Centrosome assembly in vitro: role of γ-tubulin recruitment in Xenopus sperm aster formation.** *Cell Biol.* **1994**, *124*, 19-31.

Fisher, G. L.; Hooper, A. E.; Opila, R. L.; Allara, D. L.; Winograd, N. **The interaction of vapor-deposited Al atoms with CO_2H groups at the surface of a self-assembled alkanethiolate monolayer on gold.** *J. Phys. Chem. B* **2000**, 104 (14), 3267-3273.

Flaschel, E.; Friehs, K. **Improvement of downstream processing of recombinant proteins by means of genetic engineering methods.** *Biotechnol. Adv*. **1993,** 11 (1), 31-77

Franco, M.; Nealey, P. F.; Campbell, S.; Teixeira, A. I.; Murphy, C. J. **Adhesion and proliferation of corneal epithelial cells on self-assembled monolayers.** *J. Biomed. Mater. Res.* **2000**, 52 (2), 261-269.

Frederix, F.; Bonroy, K.; Laureyn, W.; Reekmans, G.; Campitelli, A.; Dehaen, W.; Maes, G. **Enhanced performance of an affinity biosensor interface based on mixed self-assembled monolayers of thiols on gold.** *Langmuir* **2003**, 19 (10), 4351-4357

Fung, Y. S.; Wong, Y.Y. **Self-assembled monolayers as the coating in a quartz piezoelectric crystal immunosensor to detect Salmonella in aqueous solution.** *Anal. Chem .* **2001**, 73 (21), 5302-5309.

Gates, B. D.; Xu, Q.; Christopher, J.; Wolfe, D. B.; Whitesides, G. M.; **Unconventional nanofabrication.** *Annu. Rev. Mater. Res*. **2004**, 34, 339-372.

Geankoplis, C. J.; **Transport processes and unit operations**, 2nd. ed. **1983**, Allyn and Bacon, Boston, MA

Ginger, D. S.; Zhang, H.; Mirkin, C. A. **The evolution of dip-pen nanolithography.** *Angew. Chem. Int. Ed. Engl*. **2004**, 43, 30–35

Gombotz, W. R.; Guanghui, W.; Horbett, T. A.; Hoffman,, A. S. in **Poly(ethylene glycol) chemistry: Biotechnical and biomedical applications**', Harris, J. M. Ed., **1992,** Plenum Press, New York

Goubran-Botros, H.; Vijayalaksmi, M. A. **Immobilized metal ion affinity electrophoresis: A preliminary report.** *Electrophoresis* **1991**, 12(12), 1028-32.

Groll, J.; Amirgoulova, E. V.; Ameringer, T.; Heyes, C. D.; Röcker, C.; Nienhaus, G. U.; Möller, M. **Biofunctionalized, ultrathin coatings of cross-linked star-shaped poly(ethylene oxide) allow reversible folding of immobilized proteins.** *J. Am. Chem. Soc.* **2004** 126 (13),4234–4239.

Gunawardane, R. N.; Lizarraga, S. B.; Wiese, C.; Wilde, A.; Zheng, Y. **γ-tubulin complexes and their role in microtubule nucleation.** *Curr. Top. De*V*. Biol.* **2000**, *49*, 55-73.

Harder, P.; Grunze, M.; Dabint, R.; Whitesides, G. M.; Laibinis, P. E. **Molecular conformation in oligo (ethylene glycol)-terminated self-assembled monolayers on gold and silver surfaces determines their ability to resist protein adsorption.** *J. Phys. Chem.* **1998**, *102 (2)*, 426-436.

Harris, J. M. Ed. **Introduction to biotechnical and biomedical applications of poly(ethylene glycol),** *Poly(ethyleneglycol) Chemistry, Biotechnical and Biomedical Applications. Harris, J. M., Ed.*; **1992,** Plenum Press, New York,

Harris, J. M.; Zalipsky, S. Ed. **Polyethylene glycol: Chemistry and biological applications.** *Proceedings of a Symposium at the 213th National Meeting of the American Chemical Society,* **1997,** American Chemical Society, Washington, DC.

Hermanson, G. T. **Bioconjugate techniques**, **1996** Academic Press, New York

Herrwerth, S.; Rosendahl, T.; Feng, C.; Fick, J.; Eck, W.; Himmelhaus, M.; Dahint, R.; Grunze, M. **Covalent coupling of antibodies to self-assembled monolayers of carboxy-functionalized poly(ethylene glycol): Protein resistance and specific binding of biomolecules.** *Langmuir* (2003), 19(5), 1880-1887.

Hickman, J. J.; Laibinis, P. E.; Auerbach, D. I.; Zou, C.; Gardner, T. J.; Whitesides, G. M.; Wrighton, M. S. **Orthogonal self-assembly of redox active molecules on platinum and gold: selective reaction of disulfide with gold and isonitrile with platinum.** *Langmuir,* **1992**, 8, 357-359

Himmelhaus, M.; Bastuck, T.; Tokumitsu, S.; Grunze, M.; Livadaru, L.; Kreuzer, H. J. **Growth of a dense polymer brush layer from solution.** *Europhys. Lett.* **2003,** 64 (3), 378–384.

Horstmann, B.J.; Chase, H.A.; **Modeling the affinity adsorption of immunoglobulin G to Protein A immobilized to agarose matrixes.** Chem. Eng. Res. Des. **1989**, 67(3), 243.

Huang, E.; Satjapipat, M.; Han, S.; Zhou, F. **Surface structure and coverage of an oligonucleotide probe tethered onto a gold substrate and its hybridization efficiency for a polynucleotide target.** *Langmuir* **2001**, 17 (4), 1215-1224

Huck, W. T. S.; Yan, L.; Stroock, A.; Haag, R.; Whitesides, G.M. **Patterned polymer multilayers as etch resists.** *Langmuir* **1999**, 15(20), 6862-6867.

Ito, Y.; **Surface micropatterning to regulate cell functions.** *Biomaterials* **1999**, 20 (23-24), 2333–2342.

Jacoby, W.; Wilcheck, M. Ed. **Affinity techniques, enzyme purification: Pt, B.** *Methods in Enzymology* 34, **1974**, Academic Press,

Jo, S.; Park, K. **Surface modification using silanated poly(ethylene glycol)s.** *Biomaterials* **2000**, *21 (6)*, 605-616

Job, D.; Valiron, O.; Oakley, B. **Microtubule nucleation.** *Curr. Opin. Cell Biol.* **2003**, *15* (1), 111-117.

Jung, L. S.; Campbell, C. T. **Sticking probabilities in adsorption of alkanethiols from liquid ethanol solution onto gold.** *J. Phys. Chem. B* **2000**, 104 (47), 11168-11178

Kane, R. S.; Takayama, S.; Ostuni, E.; Ingber, D.E.; Whitesides, G. M. **Patterning proteins and cells using soft lithography.** *Biomaterials* **1999**, 20 (23-24), 2363–2376.

Kingshott, P.; Griesser, H. J. **Surfaces that resist bioadhesion.** *Curr. Opin. Solid State Mater. Sci.* **1999**, *4 (4)*, 403-412.

Kjellander, R.; Florin, E. **Water structure and changes in thermal stability of the system polyethylene oxide-water.** *J. Chem. Soc. Faraday Trans. I.* **1981** 77 (9), 2053–2077.

Kokkoli, E.; Zukoski, C. F. **Interaction forces between hydrophobic and hydrophilic self-assembled monolayers.** *J. Colloid Interface Sci.* **2000**, 230 (1),176-180.

Kokkoli, E.; Zukoski, C. F. **Surface pattern recognition by a colloidal particle.** *Langmuir* **2001**, 17 (2), 369-376

König, B.; Gratzel, M. **Site of dopamine D1 receptor binding to Gs protein mapped with synthetic peptides**. *Biochimica et biophysica acta* **1994**, 1223(2), 261-266.

Kovacs, G. T. A.; Maluf, N. I.; Peterson, K. A. **Bulk micromachining of silicon***.* *Proc. IEEE* **1998,** 86 (80, 1536–1551

Kraemer, S.; Fuierer, R. R.; Gorman, C. B. **Scanning probe lithography using self-assembled monolayers.** *Chem. Rev.* **2003,** 103, 4367–4418

Labropoulos, K. C.; Niesz, D. E.; Danforth, S. C.; Kevrekidis, P. G. **Dynamic rheology of agar gels: theory and experiment. Part I. Development of a rheological model**, *Carbohydr. Polym.* **2002**, 50, 393-406

Lahiri, J.; Isaacs, L.; Tien, J.; Whitesides, G.M. **A Strategy for the generation of surfaces presenting ligands for studies of binding based on an active ester as a common reactive intermediate: A surface plasma resonance study.** *Anal. Chem*.**1999**, 71 (4), 777-790.

Lahiri, J.; Kalal, P.; Frutos, A. G.; Jonas, S. T.; Schaeffler, R. **Method for fabricating supported bilayer lipid membranes on gold.** *Langmuir* **2000**, 16 (20), 7805-7810.

Laibinis, P. E.; Whitesides, G. M. **ω-Terminated alkanethiolate monolayers on surfaces of copper, silver, and gold have similar wettabilities.** *J. Am. Chem. Soc.* **1992**, 114(6), 1990-1995

Lee, S.W.; Laibinis, P. E. **Protein-resistant coatings for glass and metal oxide surfaces derived from oligo(ethylene glycol)-terminated alkytrichlorosilanes.** *Biomaterials* **1998**, *19 (18)*, 1669-1675.

Lee, S. W.; Laibinis, P. E. **Directed movement of liquids on patterned surfaces using noncovalent molecular adsorption.** *J. Am. Chem. Soc*. **2000**, 122 (22), 5395-5396 (a)

Lee, S. W.; Laibinis, P. E. **Molecular adsorption of n-alkyl amines, carboxylic acids, and amides onto well-defined, polar organic surfaces.** *Isr. J. Chem.* **2000**, 40 (2), 99-106 (b)

Lee, K. B.; Park, S. J.; Mirkin, C. A.; Smith, J. C.; Mrksich, M. **Protein nanoarrays generated by dip-pen nanolithography.** *Science (New York, N.Y.),* **2002,** *295 (5560)*, 1702-1705.

Lee, K. B.; Kim, E. Y.; Mirkin, C. A.; Wolinsky, S. M. **The use of nanoarrays for highly sensitive and selective detection of human immunodeficiency virus type 1 in plasma.** *Nano Lett.* **2004,** 4(10), 1869-1872

Leguy, R.; Melki, R.; Pantaloni, D.; Carlier, M. F. **Monomeric gamma -tubulin nucleates microtubules**. *J. Biol. Chem.* **2000**, *275* (29), 21975-21980.

Levicky, R.; Herne, T. M.; Tarlov, M. J.; Satija, S. K. **Using self-assembly to control the structure of DNA monolayers on gold: A neutron reflectivity study.** *J. Am. Chem. Soc.* **1998**, 120 (38), 9787-9792.

Li, Q.; Joshi, H. C. **Gamma-tubulin is a minus end-specific microtubule binding protein.** *J. Cell Biol.* **1995**, 131 (1), 207-214.

Limberis, L.; Magda, J. J.; Stewart, R. J. **Polarized alignment and surface immobilization of microtubules for kinesin-powered nanodevices.** *Nano Lett.* **2001**, *1* (5), 277-280.

Liu, G. Y.; Amro, N. A. **Positioning protein molecules on surfaces: a nanoengineering approach to supramolecular chemistry.** *Proc. Natl. Acad. Sci. U.S.A.* **2002**, *99 (8)*, 5165-5170.

Llanos, R.; Chevrier, V.; Ronjat, M.; Meurer-Grob, P.; Martinez, P.; Frank, R.; Bornens, M.; Wade, R. H.; Wehland, J.; Job, D. **Tubulin binding sites on γ - tubulin: identification and molecular characterization.** *Biochemistry* **1999**, *38 (48)*, 15712-15720.

Lodish, H.; Berk, A.; Zipuski, S. L.; Matsudaira, P.; Baltimore, D.; Darnell, J. **Molecular cell biology, 5th ed., 2003**, Freeman, New York,.

Lom, B.; Healy, K. E.; Hockberger, P.E.; **A versatile technique for patterning biomolecules onto glass coverslips.** *J Neurosci Meth* **1994,** 50 (3), 385–397.

Losic, D.; Shapter, J. G.; Gooding, J. **Concentration dependence in microcontact printing of self-assembled monolayers (SAMs) of alkanethiols.** *Electrochemistry Communications* (2001), 3(12), 722-726.

Lowe, C.R.; Dean, P.D.G. **Affinity chromatography***,* **1974,** Wiley, NY.

Ma, H.; Hyun, J.; Stiller, P.; Chilkoti, A. **"Non-fouling" oligo(ethylene glycol)-functionalized polymer brushes synthesized by surface-initiated atom transfer radical polymerization.** *Adv. Mater.* **2004,** 16 (4), 338–341.

MacBeath, G.; Schreiber, S. L. **Printing proteins as microarrays for high-throughput function determination.** *Science (Washington, D. C.),* **2000**, *289 (5485)*, 1760-1763.

Maisano, G.; Majolino, D.; Migliardo, P.; Venuto, S.; Aliotta, F.; Magazu, S. **Sound velocity and hydration phenomena in aqueous polymeric solutions.** *Mol. Phys.* **1993,** 78 (2), 421–435.

Malmsten, M.; Emoto, K.; Van Alstine, J. M. **Effect of chain density on inhibition of protein adsorption by poly(ethylene glycol) based coatings.** *J. Coll. Interface Sci.* **1998**, *202 (2)*, 507-517.

Mertig, M.; Kirsch, R.; Pompe, W. **Biomolecular approach to nanotube fabrication.** *Appl. Phys. A* **1998**, *66*, S723-S727.

Mirsky, V.M.; Riepl, M.; Wolfbeis, O.S.; **Capacitive monitoring of protein immobilization and antigen-antibody reactions on monomolecular alkylthiol films on gold electrodes, Biosensors & Bioelectronics.** *Biosens. Bioelectron .***1997**, 12 (9-10), 977-989.

Mitchison, T.; Kirschner, M. **Dynamic instability of microtubule growth.** *Nature* **1984**, 312(5991*)*, 237-242.

Moritz, M.; Zheng, Y.; Alberts, B. M.; Oegema, K. **Recruitment of the γ -tubulin ring complex to Drosophila salt-stripped centrosome scaffolds.** *J. Cell Biol.* **1998**, *142 (3)*, 775-786.

Mrksich, M.; Whitesides, G. M. **Patterning self-assembled monolayers using microcontact printing: a new technology for biosensors.** *Trends Biotechnol* **1995,** 13 (6), 228–235.

Müller, E. A.; Rasmussen, P. **Densities and excess volumes in aqueous poly(ethylene glycol) solutions.** *Journal of Chemical Engineering Data.* **1991,** 36 (2), 214–217.

Nakanishi, K.; Muguruma, H.; Karube, I. **A novel method of immobilizing antibodies on a quartz crystal microbalance using plasma-polymerized films for immunosensors.** *Anal. Chem.* **1996**, 68 (10), 1695-1700.

Nealey P. F.; Black A. J.; Wilbur J. L.; Whitesides G. M. **Micro- and nanofabrication techniques based on self-assembled monolayers.** *Molecular Electronics,* **1997***, 343-367.*

Nicolau, D. V.; Taguchi, T.; Taniguchi, H.; Tanigawa, H.; Yoshikawa, S. **Patterning neuronal and glia cells on light-assisted functionalized photoresists.** *Biosensors Bioelectron* **1999,** 14(3), 317–325

Nuzzo, R. G.; Dubois, L. H.; Allara, D. A. A. **Fundamental studies of microscopic wetting on organic surfaces, 1, Formation and structural characterization of a self-consistent series of polyfunctional organic monolayers.** *J. Am. Chem. Soc.***1990**, 112 (2), 558-569.

Oegema, K.; Wiese, C.; Martin, O. C.; Milligan, R. A.; Iwamatsu, A.; Mitchison, T. J.; Zheng, Y. **Characterization of two related Drosophila gamma-tubulin complexes that differ in their ability to nucleate microtubules**. *J. Cell Biol.* **1999**, *144 (4)*, 721-733.

Papra, A.; Gadegraard, N.; Larsen, N. B. **Characterization of ultrathin poly(ethylene glycol) monolayers on silicon substrates.** *Langmuir* **2001**, *17 (5)*, 1457-1460.

Park, I.; Kim, N. **Thiolated Salmonella antibody immobilization onto the gold surface of piezoelectric quartz crystal.** *Biosens. Bioelectron.* **1998**, 13 (10), 1091-1097.

Patel, N.; Davies, M. C.; Hartshorne, M.; Heaton, R. J.; Roberts, C. J.; Tendler, S. J. B.; Williams, P. M. **Immobilization of protein molecules onto**

homogeneous and mixed carboxylate-terminated self-assembled monolayers. *Langmuir* **1997**, 13 (24), 6485-6490.

Pathirana, S.T.; Barbaree, J.; Chin, B.A.; Hartell, M.G.; Neely, W.C.; Vodyanoy, V. **Rapid and sensitive biosensor for Salmonella.** *Biosens. Bioelectron.* **2000**, 15 (3-4), 135-141.

Pearson, R. G. **Benchmark papers in inorganic chemistry, hard and soft acids and bases. 1973**

Porath, J.; Carlsson, J.; Olsson, I.; Belfrage, G. **Metal chelate affinity chromatography, a new approach to protein fractionation.** *Nature* **1975**, 258(5536), 598-599.

Porath, J. **High-performance immobilized-metal-ion affinity chromatography of peptides and proteins.** *Journal of chromatography* **1988**, 443, 3-11 (a).

Porath, J. **IMAC - immobilized metal ion affinity based chromatography.** *Trends Anal. Chem*. **1988,** 7 (7), 254-259 (b).

Porath, J. **Immobilized metal ion affinity chromatography.** *Protein Expression and Purification*. **1992**, 3(4), 263-81.

Prime, K. L.; Whitesides, G. M. **Adsorption of proteins onto surfaces containing end-attached oligo(ethylene oxide): a model system using self-assembled monolayers.** *J. Am. Chem. Soc.* **1993**, *115 (23)*, 10714-10721.

Qian, X.; Metallo, S. J.; Choi, I. S.; Wu, H.; Liang, M. N.; Whitesides, G. M.; **Arrays of self-assembled monolayers for studying inhibition of bacterial adhesion.** *Anal. Chem.* **2002**, 74 (8), 1805-1810.

Quist, A. P.; Pavlovic, E.; Oscarsson, S. **Recent advances in microcontact printing.** *Anal. Bioanal. Chem*. **2005**, 381, 591–600

Sarikaya, M.; Tamerler, C.; Jen, A. K. Y.; Schulten, K.; Baneyx, F. **Molecular biomimetics: nanotechnology through biology.** *Nat. Mater.* **2003**, *2* (9), 577-585.

Schuyler,S. C.; Pellman, D. **Microtubule "plus-end-tracking proteins": the end is just the beginning.** *Cell* **2001**, *105* (4), 421-424.

Scouten, W. H. **Affinity chromatography. Bioselective adsorption on Inert matrices. 1981**, John Wiley & Sons, NY.

Shen, M. S.; Hoffman, A. S.; Ratner, B. D.; Feijen, J.; Harris, J. M. **Immobilization of polyethylene oxide surfactants for non-fouling**

biomaterial surfaces using an argon glow-discharge treatment. *J Adhes Sci Technol* **1993**, 7 (10), 1065–1076

Singhvi, R.; Kumar, A.; Lopez, G. P.; Stephanopoulos, G. N.; Wang, D. I. C.; Whitesides, G. M.; Ingber, D. E. **Engineering cell shape and function.** *Science (Washington, DC, United States),* **1994**, *264 (5159)*, 696-698.

Smith, D. A.; Wallwork, M. L.; Zhang, J.; Kirkham, J.; Robinson,C.; Marsh, A.; Wong, M. **The effect of electrolyte concentration on the chemical force titration behavior of functionalized SAMs: Evidence for the formation of strong ionic hydrogen bonds.** *J. Phys. Chem. B* **2000**, 104 (37), 8862-8870.

Sofia, S. J.; Merrill, E. W. **Grafting of PEO to polymer surfaces using electron beam irradiation**. *Journal of biomed.l mater. research,* **1998**, 40(1), 153-163 (a)

Sofia, S. J.; Premnath, V.; Merrill, E. W. **Poly(ethylene oxide) grafted to silicon surfaces: Grafting density and protein adsorption.** *Macromolecules* **1998**, 31 (15), 5059 –5070 (b)

Sorribas, H.; Padeste, C.; Tiefenauer, L. **Photolithographic generation of protein micropatterns for neuron culture applications.** *Biomaterials* **2002,** 23 (3), 893–900

Stearns, T.; Kirschner, M. **In vitro reconstitution of centrosome assembly and function:The central role of γ -tubulin.** *Cell* **1994**, *76 (4)*, 623-637.

Stolnik, S.; Illum, L.; Davis, S. S. **Long circulating microparticulate drug carriers.** *Adv Drug Delivery Rev* **1995**, 16 (2–3), 195–214.

Stolnik, S.; Felumb,N. C.; Heald, C. R.; Garnett, M. C.; Illum, L.; Davis, S. S. **Adsorption behavior and conformation of selected poly-(ethylene oxide) copolymers on the surface of a model colloidal drug carrier.** *Colloid Surf A* **1997**, 122 (1–3), 151–159.

Sugihara, K.; Shimazu, K.; Uosaki, K. **Electrode potential effect on the surface pKa of a self-assembled 15-mercaptohexadecanoic acid monolayer on a gold/quartz crystal microbalance electrode.** *Langmuir* **2000**, 16 (18), 7101-7105

Sulkowski, E. **In protein purification, micro to macro. 1987,** Alan R. Liss, NY, pp. 149-162

Sulkowski, E. **The saga of IMAC and MIT.** *BioEssays,* **1989***,* 10 (5), 170-175

Szleifer, I. **Polymers and proteins: interactions at interfaces.** *Curr. Opin. Colloid Interface Sci.* **1997,** 2 (3), 337–344.

Tirosh, O.; Barenholz, Y.; Katzhendler, J.; Priev A. **Hydration of polyethylene glycol-grafted liposomes.** *Biophys. J.* **1998,** 74 (3), 1371–1379.

Turkova, J. **Affinity chromatography. 1978**, Elsevier, Amsterdam.

Valsesia, A.; Colpo, P.; Lisboa, P.; Lejeune, M.; Meziani, T.; Rossi, F. **Immobilization of antibodies on biosensing devices by nanoarrayed self-assembled monolayers.** *Langmuir* **2006**, 22 (4), 1763–1767

Veiseh, M.; Zhang, Y.; Hinkley, K.; Zhang, M. **Two-dimensional protein micropatterning for sensor applications through chemical selectivity technique.** *Biomed. Microdevices* **2001,** 3 (1), 45–51

Velarde, M. G. **Drops, liquid layers and the Marangoni effect.** *Philos. Trans. R. Soc. London, Ser. A* **1998**, *356* (1739), 829-844.

Vijayalaksmi, M.A. **Pseudobiospecific ligand affinity chromatography, Trends in Biotechnology.** *Trends in Biotechnol,* **1989,** 7 (3), 71-76.

Walczak, M. M.; Chung, C.; Stole, S. M.; Widrig, C. A.; Porter, M. D. **Structure and interfacial properties of spontaneously adsorbed n-alkanethiolate monolayers on evaporated silver surfaces.** *J. Am. Chem. Soc.* **1991**, 113 (7), 2370-2378

Weibel, D. B.; **Bacterial printing press that regenerates its ink: Contact-printing bacteria using hydrogel stamps.** *Langmuir,* **2005**, 21, 6436–6442

Whitesides G. M.; Gorman C. B. **Self-assembled monolayers, models for organic surface chemistry. 1995**, Boca Raton, FL

Whitesides, G. M.; Ostuni, E.; Takayama1, S.; Jiang, X. and Ingber, D. E. **Soft lithography in biology and biochemistry.** *Annu. Rev. Biomed. Eng.* **2001**, 3, 335-373

Whitesides, G. M.; Jiang, X.; Ostuni, E.; Chapman, R. G.; Grunze, M. **SAMS and biofunctional surfaces, The "inert surface" problem.** *Polymer Preprints.* **2004**, 45(1), 90-91.

Wiese, C.; Zheng, Y. **A new function for the γ -tubulin ring complex as a microtubule minus-end cap.** *Nat. Cell Biol.* **2000**, 2 (6), 358-364.

Williams, R. A.; Blanch, H. W. **Covalent immobilization of protein monolayers for biosensor applications.** *Biosens. Bioelectron.* **1994**, 9 (2), 159-167

Winzerling, J. J.; Berna, P.; Porath, J. **How to use immobilized metal ion affinity chromatography.** *Methods (San Diego, CA, United States),* **1992**, 4(1), 4-13.

Wolfe, D. B.; Whitesides, G. M. **Rapid prototyping of functional microfabricated devices by soft lithography.** *Nanolithography and Patterning Techniques in Microelectronics*, **2005,** 76-119.

Wong, J. W.; Albright, R. L.; Wang, N. H. L. **Immobilized metal ion affinity chromatography (IMAC) - chemistry and bioseparation applications.** *Separation and Purification Methods,* **1991**, 20(1), 49-106.

Wong, Y. Y.; Ng, S. P.; Ng, M. H.; Si, S. H.; Yao, S. Z.; Fung, Y. S. **Immunosensor for the differentiation and detection of Salmonella species based on a quartz crystal microbalance.** *Biosens. Bioelectron.* **2002**, 17, 676-684.

Xia, Y.; Whitesides, G. M. **Soft lithography.** *Angewandte Chemie, International Edition* **1998**, 37, 550–575

Xia, Y.; Rogers, J. A.; Paul, K. E.; Whitesides, G. M. **Unconventional methods for fabricating and patterning nanostructures.** *Chem. Rev.* **1999**, 99,1823–48

Xu, S.; Miller, S.; Laibinis, P. E.; Liu, G. Y. **Fabrication of nanometer scale patterns within self-assembled monolayers by nanografting.** *Langmuir* **1999**, 15, 7244-7251.

Yang, Y.; Constance, B. H.; Deymier, P. A.; Hoying, J.; Raghavan, S.; Zelinski, B. J. J. **Electroless metal plating of microtubules: Effect of microtubule-associated proteins.** *J. Mater. Sci.* **2004**, *39*, 1927-1933.